NASA TM X-170

TECHNICAL MEMORANDUM
X-170

SOME EFFECTS OF CONTROL PROFILE AND CONTROL TRAILING-EDGE ANGLE ON THE OSCILLATING HINGE-MOMENT AND FLUTTER CHARACTERISTICS OF FLAP-TYPE CONTROLS AT TRANSONIC SPEEDS

By William C. Moseley, Jr., and Thomas G. Gainer

Langley Research Center
Langley Field, Va.

NATIONAL AERONAUTICS AND SPACE ADMINISTRATION
WASHINGTON
January 1960

NATIONAL AERONAUTICS AND SPACE ADMINISTRATION

TECHNICAL MEMORANDUM X-170

SOME EFFECTS OF CONTROL PROFILE AND CONTROL TRAILING-EDGE ANGLE ON THE OSCILLATING HINGE-MOMENT AND FLUTTER CHARACTERISTICS OF FLAP-TYPE CONTROLS AT TRANSONIC SPEEDS*

By William C. Moseley, Jr., and Thomas G. Gainer

SUMMARY

12695 ow

Free-oscillation tests were made in the Langley high-speed 7- by 10-foot tunnel to determine some effects of control profile and control trailing-edge angle on the dynamic hinge-moment characteristics of a trailing-edge, flap-type control. The unswept, untapered semispan-wing-control models had aspect ratios of 3 and NACA 65A-series airfoil sections. The essentially full-span control was 30 percent of the wing chord and was hinged at the 0.765 wing-chord line. Tests at Mach numbers from 0.60 to 1.02 were made for a range of oscillation reduced frequency at an angle of attack of 0°.

Increasing the wing maximum thickness-to-chord ratio while retaining the control trailing-edge angle constant at 13.33° had little effect on the variation of aerodynamic damping with amplitude for most test conditions but did have a stabilizing effect on the unstable damping which occurred at the high reduced frequencies at Mach numbers from 0.88 to 0.96. Increasing the control trailing-edge angle to 19.75° had a stabilizing effect on the unstable aerodynamic damping which was present for the control with trailing-edge angle equal to 5.25° in the Mach number range from 0.90 to 1.02 (maximum for these tests). The damping for the "splitter-plate" control on the 6-percent-thick wing-control model was unstable at Mach numbers from about 0.94 to 1.02. Increasing the wing thickness to 10 percent had a stabilizing effect on the unstable damping in this Mach number range (0.94 to 1.02). Both the serrated and full wedge control modifications resulted in slight decreases in the magnitude of the unstable damping which occurred for the conventional control at Mach numbers from about 0.98 to 1.02. Changes in maximum wing thickness-to-chord ratio while holding the control trailing-edge angle

*Title, Unclassified.

constant had little effect on the variation of static hinge moment with control deflection. Increasing the control trailing-edge angle from 5.25° to 19.75° resulted in the static hinge moments becoming overbalanced at low deflections throughout the Mach number range.

INTRODUCTION

Dynamic hinge-moment information on flap-type controls at transonic speeds are useful in flutter studies and in the design of control servo-systems. A program to obtain oscillating hinge-moment data on flap-type controls at transonic speeds is being carried out at the Langley high-speed 7- by 10-foot tunnel using small low-aspect-ratio wings and a reflection plane test technique. Included in this program have been the effects of control hinge-line position (ref. 1), some control profile modifications (refs. 2 and 3), control wedge angle and control aspect ratio or span (ref. 4), and wing thickness and sweep (ref. 5). Additional dynamic hinge-moment information can be found in reference 6 which is the report of an investigation made on a low-aspect-ratio, delta-wing-control model with a conventional control and a thickened trailing-edge control and in reference 7 in which several control-surface configurations were tested.

Previous investigations have generally shown the aerodynamic damping in the control rotational mode to be unstable at transonic speeds (for example, ref. 8), and a single-degree-of-freedom flutter can exist if this unstable aerodynamic damping exceeds the stable damping from other sources in the control system. Usually some form of artificial damping must be added to the control system for dynamic stability. Since this addition generally leads to mechanical complexities, it is desirable to stabilize the control aerodynamically by some relatively simple geometric change, provided overall control efficiency can be maintained.

The present investigation was made using the unswept models of reference 5 and the same control hinge-line location. Several control profiles were investigated including a "serrated wedge" (wherein triangular wedges both in plan form and profile are superimposed on the control surfaces), a full wedge, "splitter-plate" controls, and controls having a range of trailing-edge angles. Altogether ten control-profile modifications were studied.

A free-oscillation test technique was used and oscillating hinge moments together with associated flutter characteristics were determined at an angle of attack of 0° for the following conditions: a range of control reduced frequencies, initial oscillation amplitudes up to 12°, and a Mach number range from 0.60 to 1.02. In addition, static hinge moments and rolling moments were obtained.

SYMBOLS

b	twice span of semispan model, ft
c	wing chord, ft
c_a	control chord (distance from hinge line rearward to trailing edge of control), ft
c_b	balance chord (distance from hinge line forward to leading edge of control), ft
c_t	total control chord, $c_b + c_a$, ft
C_h	control hinge-moment coefficient, $\frac{\text{Hinge moment}}{2M'q}$
$C_{h_\delta} = \frac{\partial C_h}{\partial \delta}$	
$C_{h_{\delta,\omega}} = \frac{\text{Real part of } M_\delta}{2M'q}$, per radian $C_{h_{\dot{\delta},\omega}} = \frac{\text{Imaginary part of } M_\delta}{2M'qk}$, per radian	} subscript ω indicates an oscillatory coefficient
C_l	rolling-moment coefficient, $\frac{\text{Wing bending moment}}{qSb}$
f	frequency of control oscillation, cps
f_o	control wind-off natural frequency, cps
I	moment of inertia of control system, slug-ft^2
k	control reduced frequency, $\frac{\omega c_t}{2V}$
M	effective test Mach number over span of model, $\frac{2}{S}\int_0^{b/2} cM_a\, dy$
M_a	average chordwise Mach number
M'	area moment of control area rearward of and about hinge line, cu ft

[redacted]

M_δ	aerodynamic hinge moment on control per unit deflection, positive when it tends to push the trailing edge down, ft-lb/radian
q	free-stream dynamic pressure, lb/sq ft
S	twice wing area of semispan model, sq ft
t/c	ratio of wing thickness to chord
t_s	splitter-plate thickness, in.
V	free-stream velocity, ft/sec
y	spanwise distance from plane of symmetry, ft
δ	control-surface deflection, measured in a plane perpendicular to control-surface hinge line, positive when control-surface trailing edge is below wing-chord plane, radians except as noted otherwise
δ_1	amplitude of control oscillation, deg to each side of mean control deflection
λ	logarithmic decrement, $\frac{d(\log_{10} \delta_1)}{d(\text{time})}$, per second
ϕ	control trailing-edge angle included between sides which form trailing edge (positive when trailing-edge thickness is less than thickness at hinge line, negative when trailing-edge thickness is greater than thickness at hinge line), deg
ω	circular frequency of oscillation, $2\pi f$, radians/sec

MODEL AND APPARATUS

The models each consisted of a semispan wing with tip store, a trailing-edge flap-type control, and a control-system spring deflector mechanism. A schematic drawing of the test installation is shown in figure 1, and general dimensions of the model with various cross sections are given in figure 2. The control system was designed so that its moment of inertia could be varied in order to measure the dynamic hinge moments and flutter characteristics for a range of control reduced frequency.

Wing Details

The wings were unswept and untapered, with a full-span aspect ratio of 3.0 and NACA 65A series airfoil sections. Thickness-chord ratios investigated were 0.04, 0.06, 0.08, and 0.10.

The wings were constructed of solid steel. All tests were made with a tip store attached to the wings, and tip stores of different weight were used to vary the wing natural frequencies. The natural first bending and torsion frequencies of the wing with the two tip stores are given in table I. The frequencies were obtained with the control system spring clamped as shown in figure 1.

Control-Surface Details

The essentially full-span controls had a total chord c_t equal to 30 percent of the wing chord and were hinged at the 76.5-percent-wing-chord line. The controls had a $0.277c_a$ blunt overhang balance and the gap between the control and the wing was unsealed.

Cross sections of the models tested in this investigation are shown in figure 2(b). The wings with $t/c = 0.04$, 0.06, and 0.08 were tested with controls having the trailing edge beveled to an angle of 13.33° (the true-contour trailing-edge angle of a 65A010 airfoil section). The wing with $t/c = 0.10$ was tested with a beveled control having a trailing-edge angle of 19.75° and a straight-contour control having a trailing-edge angle of 5.25°. The beveled controls were of constant thickness from the nose radius back to the juncture with the trailing-edge bevel. All of these controls had a steel spar and a spruce afterportion. In order to mass balance the controls, tungsten inserts were distributed in the nose overhang. The entire control surface was wrapped with silk.

The second group of controls had splitter-plate type of modifications wherein the rearward 50 percent of the control chord c_a consisted of a flat plate (fig. 2(b)). Three splitter-plate configurations were tested: the wing with $t/c = 0.06$ was tested with a control having a splitter-plate thickness t_s of 0.013 in. and the wing with $t/c = 0.10$ was tested with controls having $t_s = 0.013$ in. and $t_s = 0.031$ in. Each control was constructed with five chordwise stiffeners equally spaced across the span. Since these controls were made of steel it was necessary to drill holes rearward of the hinge line, in addition to the tungsten inserts, in order to mass balance them completely. These holes were filled with balsa before the control was covered with silk.

The wing with $t/c = 0.06$ was also equipped with two wedge-type controls, with the thickness at the trailing edge of the wedge section being twice the thickness of the control at the hinge line ($\phi = -7.96^\circ$). The first of these was a serrated wedge control, consisting of triangular wedges or tetrahedra superimposed on a conventional profile control similar to a control previously tested in reference 7 (fig. 2(b)). The triangular wedges extended from the point of maximum thickness to the trailing edge, and the included angle between the adjacent wedges was about 28°. The second was a conventional or full wedge control; that is, the wedge section extended along the complete span of the control. Both of these controls had a steel spar and a spruce afterportion and were mass balanced about the control hinge line by the tungsten inserts.

A tang on the inboard end of the control extended through the reflection plane to the outside of the tunnel (fig. 1). The tang extension consisted of a rod and a torsion spring. The control was mounted by two ball bearings on the rod extension outside the tunnel and a plain bearing at the wing tip. Control-system alinement was carefully checked to keep friction to a minimum. Attached to the rod was a deflector arm used to apply a step deflection to the control system. The natural frequency of the control system was varied by changing the moments of inertia of the control system by clamping weights of different size and inertia to the rod. The moments of inertia of the control system for the controls tested are given in table II.

INSTRUMENTATION

Electric strain gages were located near the root of the wing to indicate the wing bending and torsion responses. A static calibration was made of the wing-bending gage in order to measure wing bending moments and obtain an indication of control effectiveness. Control position was measured by the reluctance-type pickup located near the inboard end of the control. (See fig. 1.) Outputs of the strain gages and of the position indicator were recorded against time by a recording oscillograph. Dynamic calibration of the recording system indicated accurate response to a frequency of about 500 cycles per second.

TESTS

The tests were made in the Langley high-speed 7- by 10-foot tunnel utilizing the sidewall reflection-plate test technique. This technique involves the mounting of a relatively small model on a reflection plate spaced out from the tunnel wall to bypass the tunnel boundary layer. Local

velocities over the surface plate allow testing to a Mach number of about 1.02 without choking the tunnel.

The variation of Reynolds number based on the wing mean aerodynamic chord with test Mach number is presented in figure 3. The width of the cross-hatched area represents, for these tests at a given Mach number, the maximum variation of Reynolds number with atmospheric conditions.

Oscillating hinge moments were obtained for amplitudes up to about 12° through a Mach number range of 0.60 to 1.02 at an angle of attack of 0°. The control-reduced-frequency range varied with Mach number and was generally in the range from 0.04 to 0.16. In addition, static hinge-moment and rolling-moment data were obtained at $\alpha = 0^{\circ}$.

These tests were made transition free, that is, with no roughness added to the wing surface, to insure boundary-layer transition from laminar to turbulent-flow conditions. The results of reference 5 indicate that no major trend effects would be expected because of fixing transition for these tests.

TEST TECHNIQUE AND REDUCTION OF DATA

The control system was designed so that at the test frequencies the torsional response of the control about the hinge line was essentially that of a single-degree-of-freedom system. The wing response characteristics were varied relative to the control oscillation frequency by the choice of tip-store weight so that the physical response of the model for the various test conditions was predominantly control rotation. Therefore, the aerodynamic moment resulting from angular deflection of the control about the hinge line could be determined from the free-oscillation characteristics of the control system subsequent to known starting conditions. Typical oscillograph records of the time response of a model tested by the free oscillation test technique used are shown in figure 4. For all models tested in this investigation, the wing motions were small relative to the control motions and the mean deflection during oscillation was near 0° in all cases.

The test technique used to initiate the free oscillations depended on the total (aerodynamic plus nonaerodynamic) damping of the control system for the particular test condition. When the total damping was unstable at low deflections, the hinge moments were determined from the unstable oscillation following release of the control at $\delta \approx 0^{\circ}$ (fig. 4(c)). This type of oscillation was initiated by random tunnel disturbances and in all cases was self-limiting. When the total damping was stable or varied from stable to unstable within the test oscillation amplitude range, the free oscillation was initiated by releasing the

control at some deflection angle (fig. 4(b)) with the ensuing oscillation being either a buildup or a decay.

Evaluation of Spring Moments

The aerodynamic inphase or spring moment was determined from the natural frequency of oscillation of the control system. Since the variation of inphase moment with amplitude is not necessarily linear and the test method was not sufficiently accurate to determine the variation in natural frequency with amplitude, the values of $C_{h_{\delta,\omega}}$ presented are effective values averaged over the amplitude range of the oscillation. In this investigation, the effect of the values of damping on the natural frequency was considered negligible, and the aerodynamic spring-moment derivative was determined from the relationship

$$C_{h_{\delta,\omega}} = \frac{I\left(\omega_o^2 - \omega^2\right)}{2M'q} \tag{1}$$

where the subscript o signifies a wind-off condition. A negative value of $C_{h_{\delta,\omega}}$ opposes the control displacement and acts as an aerodynamic spring which increases the stiffness or natural frequency of the control system.

Evaluation of Damping Moments

The aerodynamic out-of-phase or damping moment was determined from the rate of buildup or decay of the free oscillation of the control system. The damping moment is not necessarily linear with amplitude; however, the damping results were analyzed on the basis of an equivalent linear system. It was assumed that the damping forces were adequately described by an equivalent viscous damping and that the time response of the actual system was simulated by a linear system having the appropriate damping constant at each oscillation amplitude for a given frequency. The variation of damping-moment derivative with oscillation amplitude was obtained by plotting the logarithm of the amplitude of successive cycles of the oscillation against time and taking the slope at any given amplitude of the faired curves as the value of the logarithmic decrement $\lambda = \frac{d\left(\log_{10} \delta_1\right)}{d(\text{time})}$ of the oscillation. The aerodynamic damping derivative was determined from the relationship

$$C_{h_{\dot{\delta},\omega}} = \frac{4.6IV}{qM'c_t}(\lambda - \lambda_o)$$

where the subscript o refers to wind-off values taken at approximately the same frequency and amplitude as the wind-on values.

Tare or wind-off damping values were determined before and after each test and average values were used in reducing the test data. Although care was taken to check the alinement of the control system, some difficulties were encountered in keeping the tare or friction damping constant in the bearing system that was made necessary by the relatively large amplitudes studied in these tests. As a result, some scatter or erratic variations of $C_{h_{\dot{\delta},\omega}}$ can be expected for this type of test technique. Expressed in terms of the aerodynamic damping coefficient $C_{h_{\dot{\delta},\omega}}$ for a representative Mach number of 1.00, essentially all tare damping values for the models tested were in the range from about -2 to about -5 for the minimum inertia condition (the condition giving the highest values of control reduced frequency) and from about -5 to about -11 for the maximum inertia condition (the condition giving the lowest values of control reduced frequency). Even so, the data are indicative of the general trends with amplitude and Mach number which are considered the most important results of the tests.

Determination of Static Moments

Static hinge moments were measured by restraining the control system in torsion with a calibrated electric strain-gage beam which measured the torque or moment about the control hinge line for various control deflections. The static hinge-moment coefficient C_h was determined from the relationship

$$C_h = \frac{\text{Hinge moment}}{2M'q}$$

Wing bending moments were measured for various control deflections with a calibrated electric strain gage located at the wing root. Wing rolling-moment coefficients were then approximated by the relationship

$$C_l = \frac{\text{Wing bending moment}}{qSb}$$

CORRECTIONS

No corrections have been applied to the data for the chordwise and spanwise velocity gradients or the effects of the tunnel walls. It is shown in reference 9 that a tunnel resonance phenomenon can appreciably

[redacted]

decrease the magnitude of forces and moments measured in oscillation tests. However, it is believed that this phenomenon had no appreciable effect on the results of the present investigation. In general, most of the test frequencies were well removed from the calculated resonant frequencies, and there was no apparent decrease in moments for the test frequencies that were close to resonant frequencies. It is possible that the magnitude of the resonant effects would be relieved by the model tip effects and the nonuniformity of the velocity field in the test section.

Control-deflection corrections determined from static calibrations have been applied to the output of the position pickup to give the deflection at the midspan of the control surface for the static data. No corrections were applied to the oscillating data to account for the twist of the control system outboard of the position pickup since, for the physical constants and frequencies involved, this was generally negligible.

RESULTS AND DISCUSSION

Damping Moments and Flutter Characteristics

The variation of aerodynamic damping coefficient $C_{h_{\dot{\delta},\omega}}$ with oscillation amplitude for various Mach number and reduced frequencies together with the associated flutter characteristics are presented in figure 5 for the $\phi = 13.33^\circ$ control models. Figure 6 was cross plotted from figure 5 and shows the variation of $C_{h_{\dot{\delta},\omega}}$ with Mach number at representative amplitudes of approximately 1° and 8° and reduced frequencies of approximately 0.08 and 0.04. Similarly, aerodynamic damping results are shown for the models with $\phi = 5.25^\circ$ control and $\phi = 19.75^\circ$ control in figures 7 and 8, for the three splitter-plate-control models in figures 9 and 10, and for the full-wedge and serrated-wedge-control models in figures 11 and 12. For purposes of comparison, data from reference 5 showing the variation of $C_{h_{\dot{\delta},\omega}}$ with Mach number for conventional profile control models having thickness-to-chord ratios of 0.06 (fig. 12) and 0.10 (figs. 6 and 8) are also presented.

For these tests it was not feasible to maintain a constant value of reduced frequency; therefore, values of reduced frequency k are tabulated on the plots of $C_{h_{\dot{\delta},\omega}}$ against amplitude (figs. 5, 7, 9, and 11). Also given are flutter amplitudes and frequencies for all conditions where flutter occurred.

Models with $\phi = 13.33^{\circ}$ control.- In general, the aerodynamic damping results for the various models show a nonlinear variation of $C_{h_{\dot{\delta},\omega}}$ with oscillation amplitude, particularly at Mach numbers above M = 0.80. Aerodynamic results for the models with $\phi = 13.33^{\circ}$ control (fig. 5) indicate that for each of the models the damping was stable for all amplitudes and reduced frequencies investigated at Mach numbers from 0.60 to about 0.85 and was either stable or slightly unstable in the Mach number range from about 0.98 to 1.02, the maximum Mach number tested. In the Mach number range from about 0.88 to about 0.96, the damping was generally stable at the lower reduced frequencies, but became unstable for the models with t/c = 0.04 and 0.06 at the high reduced frequencies (corresponding to $f_o = 288.0$ and $f_o = 325.0$). In general, $C_{h_{\dot{\delta},\omega}}$ tended to increase with increasing amplitude in the low amplitude range (below about 3°) and was fairly constant at a relatively low level of stable damping through the remaining amplitude range. For the unstable damping conditions which existed at the intermediate Mach numbers, however, values of $C_{h_{\dot{\delta},\omega}}$ tended to decrease with increasing amplitude with maximum unstable values of $C_{h_{\dot{\delta},\omega}}$ occurring at the low oscillation amplitudes, thus leading to the limited amplitude type of flutter response obtained. The cross plots of figure 6 further illustrate these points. Also included in figure 6 are cross plots of the data for the conventional controls of reference 5. These data are included to show the stabilizing effect of control trailing-edge angle on the unstable damping which occurred for the conventional controls at transonic Mach numbers, and indicate that control trailing-edge angle is an important parameter to be considered when evaluating results previously reported showing the effects of wing thickness on control aerodynamic damping.

When comparing the flutter characteristics with the aerodynamic damping values (fig. 5), it should be remembered that the control system had a certain level of nonaerodynamic damping. Flutter involved the degree of freedom of control rotation about the hinge line and for these models generally had to be initiated by deflecting the control to an initial amplitude (usually about 12°) and then releasing it. There was then a decay in the resulting oscillation until a steady-state condition was reached, wherein the aerodynamic damping fed into the control oscillation over a complete cycle was equal to the energy dissipated by the nonaerodynamic damping of the control system. The flutter frequencies given are for the steady-state oscillatory conditions for these models.

Increasing the thickness-to-chord ratio while holding the trailing-edge angle constant at 13.33° had little effect on the variation of $C_{h_{\dot{\delta},\omega}}$ with amplitude for most test conditions, but did have a stabilizing effect on the unstable damping which occurred in the intermediate Mach number range at the high reduced frequencies. For example, the t/c = 0.04 model

at M = 0.88, unstable damping occurred but was delayed to about M = 0.90 for the t/c = 0.06 model and increasing the thickness-to-chord ratio to 0.08 completely eliminated unstable damping in the intermediate Mach number range.

Models with $\phi = 5.25^\circ$ and $\phi = 19.75^\circ$ controls.- The data of figure 7 indicate that increasing the control trailing-edge angle from 5.25° to 19.75° on the t/c = 0.10 wing-control combination had a stabilizing effect on the $C_{h_{\dot{\delta},\omega}}$ variation with oscillation amplitude in the Mach number range from about 0.90 to 1.02 while having only a small effect on the damping at lower Mach numbers. Values of $C_{h_{\dot{\delta},\omega}}$ for both of these models were stable and fairly constant through the range of test amplitudes in the low Mach number range (from 0.60 to about 0.88). At the higher Mach numbers, the $C_{h_{\dot{\delta},\omega}}$ variation for the model with $\phi = 5.25^\circ$ control was of the type which might result in limited amplitude flutter; that is, maximum unstable values of $C_{h_{\dot{\delta},\omega}}$ occurred at the low oscillation amplitudes and $C_{h_{\dot{\delta},\omega}}$ tended to decrease with increasing amplitude. Flutter did not occur for this model, however, since the nonaerodynamic damping present in the system was greater than the unstable aerodynamic damping present. For the model with $\phi = 19.75^\circ$ control, on the other hand, large stable values of $C_{h_{\dot{\delta},\omega}}$ were obtained at the low amplitudes such that, although $C_{h_{\dot{\delta},\omega}}$ tended to become less stable with increasing amplitude, the damping remained stable for most of the amplitude and Mach number range, with only small unstable values of $C_{h_{\dot{\delta},\omega}}$ occurring at M = 1.02.

In general, changes in reduced frequency resulted in only small changes in the magnitude of $C_{h_{\dot{\delta},\omega}}$ throughout the amplitude and Mach number ranges investigated. It should be noted, however, that at Mach numbers of 0.92 and 0.94, unstable damping for the model with $\phi = 5.25^\circ$ control occurred only at the high reduced frequencies (corresponding to $f_o = 263.0$ cps).

Control trailing-edge angle effects are also illustrated in figure 8 which shows a definite trend toward more stable damping as the trailing-edge angle is increased at transonic Mach numbers.

Splitter-plate-control models.- The aerodynamic results for the splitter-plate-control model with t/c = 0.06 and $t_s = 0.013$ tested in this investigation (fig. 9) show generally stable damping at Mach numbers from 0.60 to about 0.92, and generally unstable damping at transonic Mach numbers from 0.94 to 1.02. At a Mach number of 0.92,

unstable damping occurred only at the higher amplitudes, but as the Mach number was increased above 0.94, the damping became unstable throughout the amplitude range for all reduced frequencies with maximum unstable values occurring at the lower amplitudes. The limited-amplitude type of flutter response obtained for this model was in all cases self-starting; that is, upon release of the control the oscillation built up to a steady-state condition.

By increasing the maximum thickness-to-chord ratio of the $t_s = 0.013$ model to 0.10, a stable $C_{h_{\dot{\delta},\omega}}$ variation was obtained at Mach numbers up to about 0.98, with $C_{h_{\dot{\delta},\omega}}$ becoming slightly unstable for some test conditions above $M = 0.98$. This trend toward more stable damping with increasing maximum thickness-to-chord ratio at transonic Mach numbers is clearly illustrated by the data presented in figure 10. Figure 10 also shows that increasing the splitter-plate thickness from 0.013 to 0.031 on the model with $t/c = 0.10$ generally tended to make the damping slightly less stable at the higher test Mach numbers, and that there was generally little difference in the variation of $C_{h_{\dot{\delta},\omega}}$ with Mach number for the three splitter-plate models at Mach numbers below about 0.85.

Wedge-control models.- The damping for the full-wedge control model tested in this investigation (fig. 11(b)) was stable at the low oscillation amplitudes at Mach numbers from 0.60 to about 0.98 while generally becoming unstable at the higher amplitudes in the Mach number range from about 0.85 to about 0.98. At Mach numbers of 1.00 and 1.02, a low level of unstable damping generally existed for the complete range of amplitudes and reduced frequencies. For the serrated-wedge-control model (fig. 11(a)) the damping remained stable throughout the amplitude range at Mach numbers up to about 0.98. At Mach numbers above about 0.98, however, the unstable damping variation which occurred resulted in limited amplitude flutter at the high reduced frequencies. For these models, decreasing the reduced frequency at the intermediate Mach numbers (from about 0.90 to 0.98) had a stabilizing effect on the damping but otherwise variation within the reduced-frequency range produced no definite trends in the damping variation.

A comparison of the damping for the full- and serrated-wedge control models with that for the basic $t/c = 0.06$ wing-control combination (having a conventional control) of reference 5 is given by the cross plots of figure 12. The full-wedge modification to the conventional control made the damping more stable in the subsonic Mach number region ($M = 0.60$ to about 0.88), and generally less stable in the intermediate Mach number region (0.90 to 0.96). The main effect resulting from the serrated-wedge modification was a highly stable shift in the damping variation with Mach number at Mach numbers from about 0.85 to about 0.98. Both the full-wedge and

serrated-wedge modifications resulted in slight decreases in the magnitude of the unstable values of $C_{h_{\delta,\omega}}$ which occurred for the conventional control model at Mach numbers from about 0.98 to 1.02. The flutter occurring for the serrated-wedge model at the low amplitudes in this region was probably associated with the marked amplitude effect on damping at frequencies above those presented in figure 12.

Spring Moments

Static hinge-moment or spring-moment coefficients are plotted against control deflection in figures 13 to 16 for the various models tested. The variations of the static and dynamic spring-moment derivative C_{h_δ} and $C_{h_{\delta,\omega}}$ with Mach number are shown in figure 17, together with comparative results from reference 5.

For the models with $\phi = 13.33^\circ$ control, changes in the thickness-to-chord ratio from 0.04 to 0.08 had very little effect on the static hinge-moment variation with control deflection throughout the Mach number range investigated (fig. 13). Values of C_h for these models were either underbalanced or close to balance at the low deflections and became more underbalanced at the higher deflections. At Mach numbers of 1.00 and 1.02, the variation of C_h with δ was nearly linear and the aerodynamic center shifted rearward so that C_h for these models became considerably underbalanced.

In agreement with previously indicated control trailing-edge-angle effects (for example, ref. 10), the $\phi = 5.25^\circ$ control was more underbalanced than any of the $\phi = 13.33^\circ$ models including the basic $t/c = 0.10$ wing model of reference 5 (which also had a true contour trailing-edge angle of 13.33°). Increasing the control trailing-edge angle from 5.25° to 19.75° resulted in a decrease in the underbalance of the control, especially at the lower control deflections, such that the 19.75° control became overbalanced at the lower deflections throughout the range of test Mach numbers.

For the splitter-plate-control model with $t/c = 0.06$ and $t_s = 0.013$ (fig. 15) the variation of C_h with δ was fairly linear and underbalanced over the entire range of control deflections throughout the Mach number range. For the model with $t/c = 0.10$ and $t_s = 0.013$, C_h varied with δ in a similar manner, but was considerably less underbalanced at the lower control deflections at Mach numbers in the vicinity of $M = 0.95$. Increasing the splitter-plate thickness from 0.013 to 0.031 for the 10-percent-wing control model had no appreciable effect on the static hinge-moment variations. (Compare figs. 15(b) and 15(c).)

The static hinge-moment data of reference 5 show that the variation of C_h with δ for the basic model with $t/c = 0.06$ was generally linear and close to balance at the lower control deflections in the Mach number range from 0.60 to 0.90. At Mach numbers from 0.95 to 1.02 the variation of C_h with δ remained linear but became more underbalanced as the loading shifted rearward. The serrated-wedge modification to the conventional control (fig. 16) had little effect on this variation, except at a Mach number of 0.95 where the serrated-wedge control became overbalanced at the lower control deflections. The full-wedge modification, on the other hand, resulted in a static hinge-moment variation which was more linear and considerably more underbalanced than for the conventional control for the complete test range.

The spring-moment derivatives measured from static C_{h_δ} and dynamic $C_{h_{\delta,\omega}}$ data were generally in qualitative agreement for each of the models tested in this investigation (fig. 17). Direct comparison of the static and dynamic results to determine the effects of oscillating frequency is not feasible since the derivatives could not be evaluated for the same amplitude range. For the test technique used, the dynamic derivatives in some cases were evaluated for an amplitude range where the static hinge-moment data became nonlinear with amplitude.

Rolling Moments

Rolling-moment coefficients, as determined from the wing bending response to an airload under nonoscillatory conditions, are plotted as a function of control deflection for the various models in figures 18 to 21. In general, the variation of C_l with δ was fairly linear over the deflection range presented, with little effect on the variation being produced by changes in test Mach number. It can be seen by comparing these figures that the effectiveness of each of the controls in producing roll was essentially the same for all models, with the exception of the $\phi = 5.25^\circ$ and the two 10-percent splitter-plate-control models which produced a higher C_l per degree control deflection than any of the other controls. Also, figure 21 shows that the serrated-wedge control gained an increase in effectiveness at the higher deflections and the full-wedge control increased in effectiveness with Mach number.

CONCLUSIONS

Results of oscillating hinge-moment tests at Mach numbers from 0.60 to 1.02 to determine some effects of control profile and control trailing-edge angle indicate the following conclusions:

1. Increasing the wing maximum thickness-to-chord ratio while retaining the control trailing-edge angle constant at 13.33° had little effect on the variation of $C_{h_{\dot{\delta},\omega}}$ with amplitude for most test conditions but did have a stabilizing effect on the unstable damping which occurred at the high reduced frequencies at Mach numbers from 0.88 to 0.96.

2. Increasing the control trailing-edge angle to 19.75° had a stabilizing effect on the unstable aerodynamic damping which was present for the control with trailing-edge angle equal to 5.25° in the Mach number range from 0.90 to 1.02 (maximum for these tests).

3. The damping for the splitter-plate control on the 6-percent-thick wing-control model was unstable at Mach numbers from about 0.94 to 1.02. Increasing the wing thickness to 10 percent had a stabilizing effect on the unstable damping in this Mach number range (0.94 to 1.02).

4. Both the serrated- and full-wedge control modifications resulted in slight decreases in the magnitude of the unstable damping which occurred for the conventional control at Mach numbers from about 0.98 to 1.02.

5. Changes in maximum wing thickness-to-chord ratio while holding the control trailing-edge angle constant had little effect on the variation of static hinge moment with control deflection. Increasing the control trailing-edge angle from 5.25° to 19.75° resulted in the static hinge moments becoming overbalanced at low deflections throughout the Mach number range.

Langley Research Center,
National Aeronautics and Space Administration,
Langley Field, Va., August 19, 1959.

REFERENCES

1. Thompson, Robert F., and Moseley, William C., Jr.: Effect of Hinge-Line Position on the Oscillating Hinge Moments and Flutter Characteristics of a Flap-Type Control at Transonic Speeds. NACA RM L57C11, 1957.

2. Thompson, Robert F., and Moseley, William C., Jr.: Oscillating Hinge Moments and Flutter Characteristics of a Flap-Type Control Surface on a 4-Percent-Thick Unswept Wing With Low Aspect Ratio at Transonic Speeds. NACA RM L55K17, 1956.

3. Moseley, William C., Jr., and Price, George W., Jr.: Effects of Control Profile on the Oscillating Hinge-Moment and Flutter Characteristics of a Flap-Type Control at Transonic Speeds. NACA RM L57E27, 1957.

4. Moseley, William C., Jr., and Thompson, Robert F.: Effect of Control Trailing-Edge Thickness or Aspect Ratio on the Oscillating Hinge-Moment and Flutter Characteristics of a Flap-Type Control at Transonic Speeds. NACA RM L58B25, 1958.

5. Moseley, William C., Jr., and Gainer, Thomas G.: Effect of Wing Thickness and Sweep on the Oscillating Hinge-Moment and Flutter Characteristics of a Flap-Type Control at Transonic Speeds. NASA TM X-123, 1959.

6. Martz, C. William: Experimental Hinge Moments on Freely Oscillating Flap-Type Control Surfaces. NACA RM L56G20, 1956.

7. Wyss, John A., Sorenson, Robert M., and Gambucci, Bruno J.: Effects of Modifications to a Control Surface on a 6-Percent-Thick Unswept Wing on the Transonic Control-Surface Flutter Derivatives. NACA RM A58B04, 1958.

8. Martin, Dennis J., Thompson, Robert F., and Martz, C. William: Exploratory Investigation of the Moments on Oscillating Control Surfaces at Transonic Speeds. NACA RM L55E31b, 1955.

9. Runyan, Harry L., and Watkins, Charles E.: Considerations on the Effect of Wind-Tunnel Walls on Oscillating Air Forces for Two-Dimensional Subsonic Compressible Flow. NACA Rep. 1150, 1953. (Supersedes NACA TN 2552.)

10. Thompson, Robert F.: Investigation of a 42.7° Sweptback Wing Model to Determine the Effects of Trailing-Edge Thickness on the Aileron Hinge-Moment and Flutter Characteristics at Transonic Speeds. NACA RM L50J06, 1950.

TABLE I.- NATURAL FIRST BENDING AND TORSION FREQUENCIES OF WINGS

Configuration	Tip store	Bending, cps	Torsion, cps
t/c = 0.04 wing, ϕ = 13.33° control	Light	108	480
	Heavy	80	317
t/c = 0.06 wing, ϕ = 13.33° control	Light	157	695
	Heavy	121	499
t/c = 0.08 wing, ϕ = 13.33° control	Light	194	980
	Heavy	162	770
t/c = 0.10 wing, ϕ = 5.25° control	Light	238	---
	Heavy	210	---
t/c = 0.10 wing, ϕ = 19.75° control	Light	244	---
	Heavy	222	---
t/c = 0.06 wing, serrated-wedge control	Light	165	610
	Heavy	118	465
t/c = 0.06 wing, full-wedge control	Light	157	670
	Heavy	122	500
t/c = 0.06 wing, splitter-plate control	Light	155	693
	Heavy	119	495
t/c = 0.10 wing, thin splitter-plate control	Light	236	---
	Heavy	216	---
t/c = 0.10 wing, thick splitter-plate control	Light	240	---
	Heavy	220	---

TABLE II.- MOMENTS OF INERTIA AND WIND-OFF NATURAL FREQUENCIES OF CONTROL SYSTEMS

Configuration	Inertia, weight	I, slug-ft^2	f_o, cps
t/c = 0.04 wing, ϕ = 13.33° control	None	0.99×10^{-5}	288.0
	Small	2.31	188.0
	Large	6.53	111.0
t/c = 0.06 wing, ϕ = 13.33° control	None	1.00	325.0
	Small	2.32	218.0
	Large	6.55	128.5
t/c = 0.08 wing, ϕ = 13.33° control	None	1.00	283.5
	Small	2.32	184.0
	Large	6.55	109.8
t/c = 0.10 wing, ϕ = 5.25° control	None	1.10	263.0
	Small	2.42	178.0
	Large	6.65	107.5
t/c = 0.10 wing, ϕ = 19.75° control	None	1.02	320.0
	Small	2.34	211.0
	Large	6.57	126.8
t/c = 0.06 wing, serrated-wedge control	None	1.08	333.0
	Small	2.39	215.3
	Large	6.63	128.5
t/c = 0.06 wing, full-wedge control	None	1.16	293.5
	Small	2.47	202.0
	Large	6.71	124.3
t/c = 0.06 wing, splitter-plate control	None	1.13	299.5
	Small	2.44	205.0
	Large	6.67	125.5
t/c = 0.10 wing, thin splitter-plate control	None	1.20	268.0
	Small	2.51	182.0
	Large	6.75	111.0
t/c = 0.10 wing, thick splitter-plate control	None	1.35	238.0
	Small	2.66	189.0
	Large	6.90	106.0

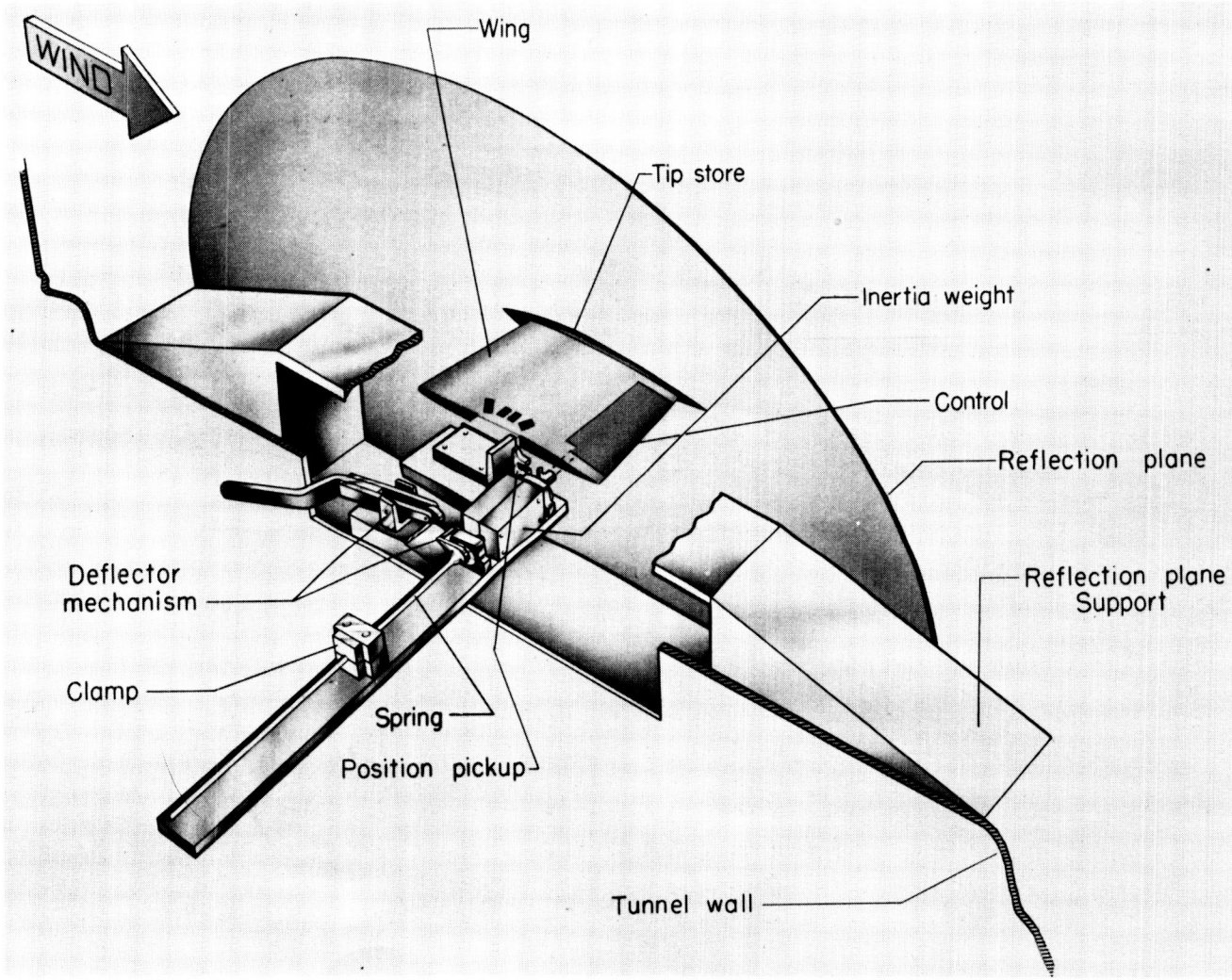

Figure 1.- Schematic drawing of test installation. L-90563.2

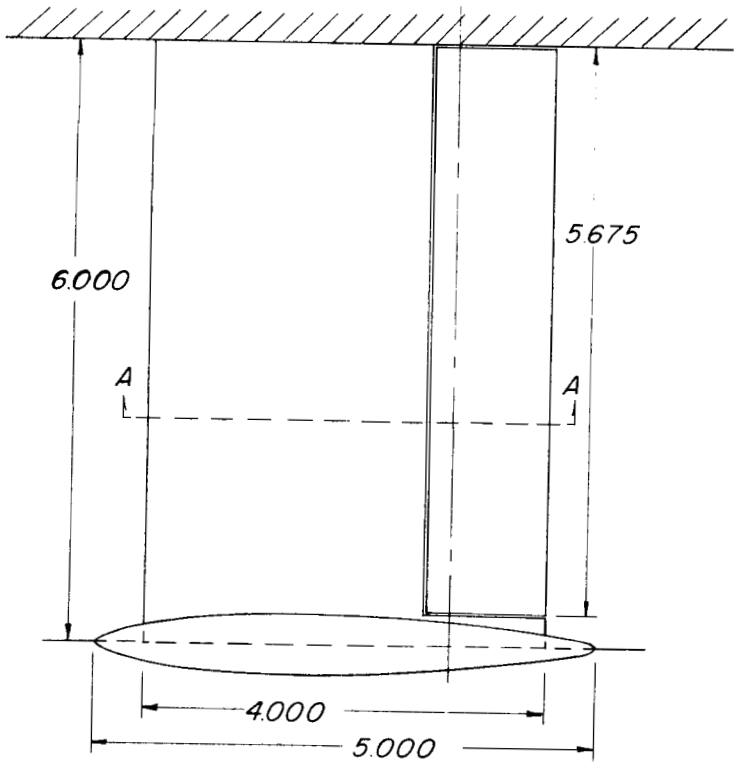

Wing Data

Area	0.333 sq ft
Aspect ratio	3.0
Mean aerodynamic chord	0.333 sq ft
Airfoil sections parallel to free stream	NACA 65A-series

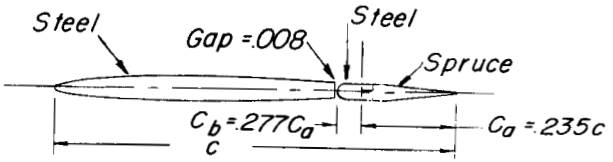

Section A-A

(a) Model arrangement.

Figure 2.- General dimensions of model. All dimensions are in inches unless otherwise noted.

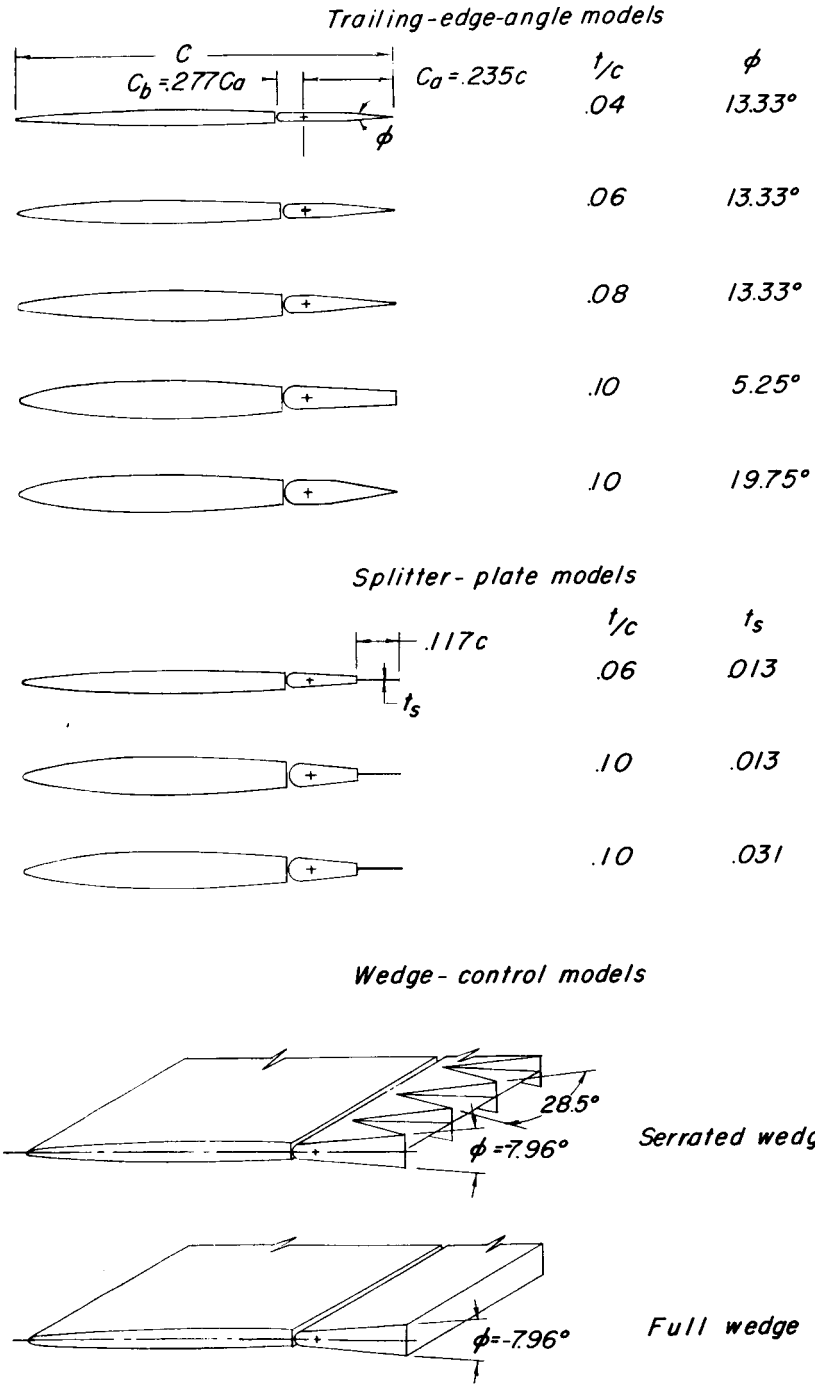

(b) Cross sections of models tested.

Figure 2.- Concluded.

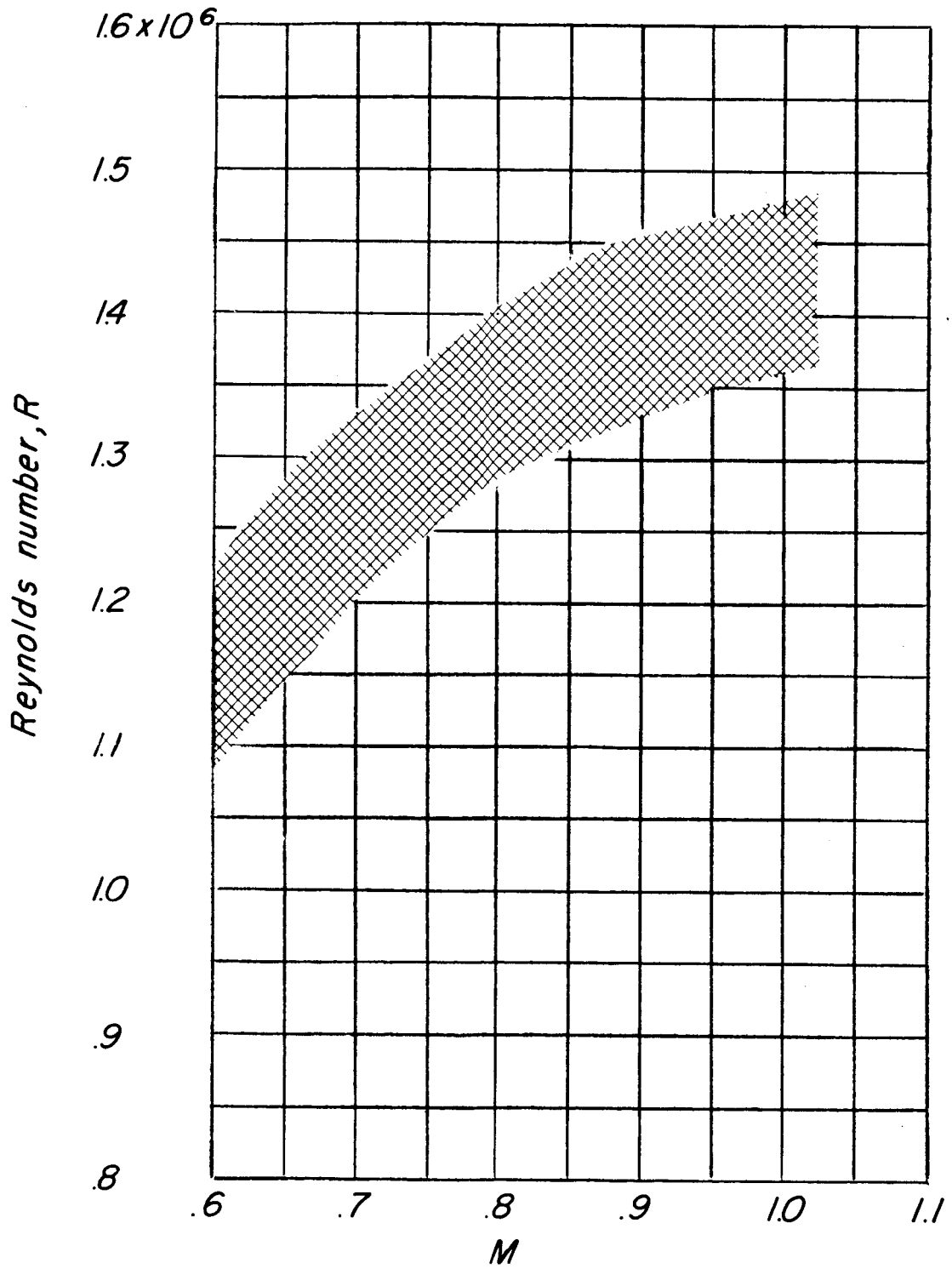

Figure 3.- Variation of Reynolds number with Mach number.

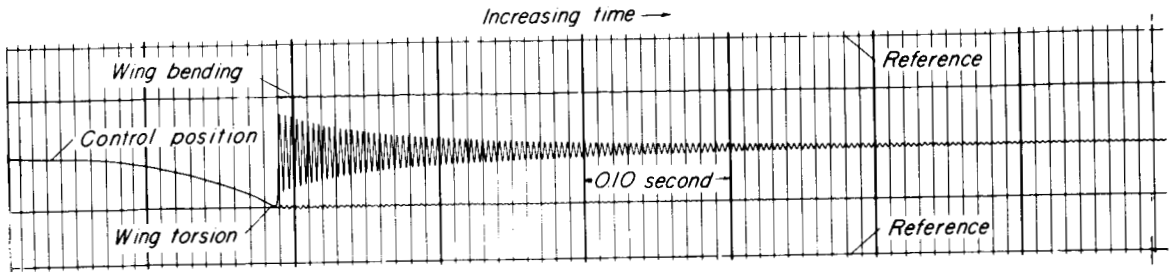

(a) Wind off; control released at $\delta \approx 12^{\circ}$.

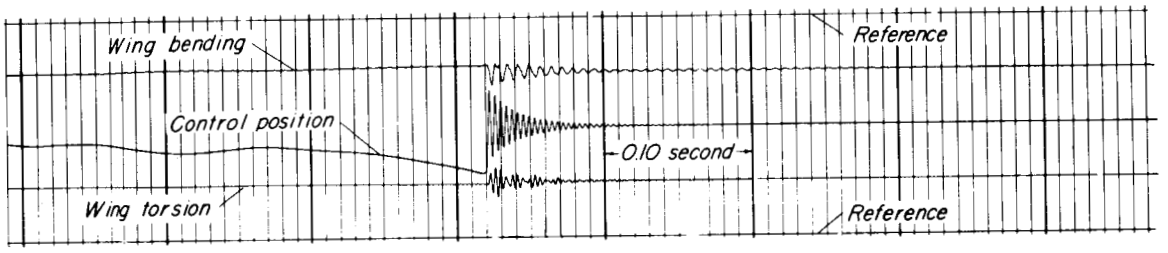

(b) M = 0.70; control released at $\delta \approx 12^{\circ}$.

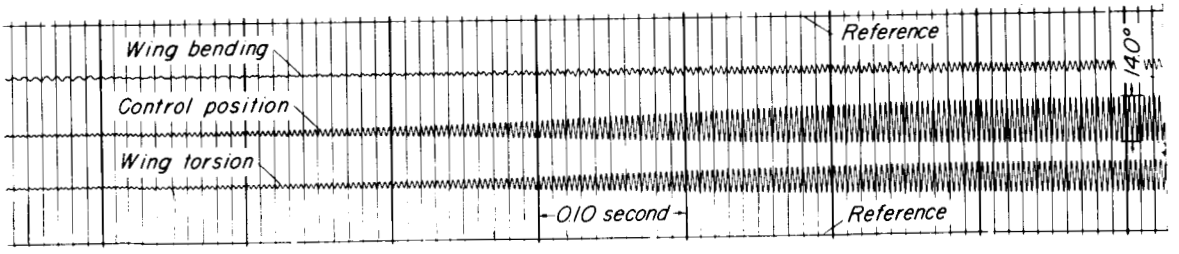

(c) M = 1.01; control released at $\delta \approx 0^{\circ}$.

Figure 4.- Oscillograph records typical for the free-oscillation test technique used.

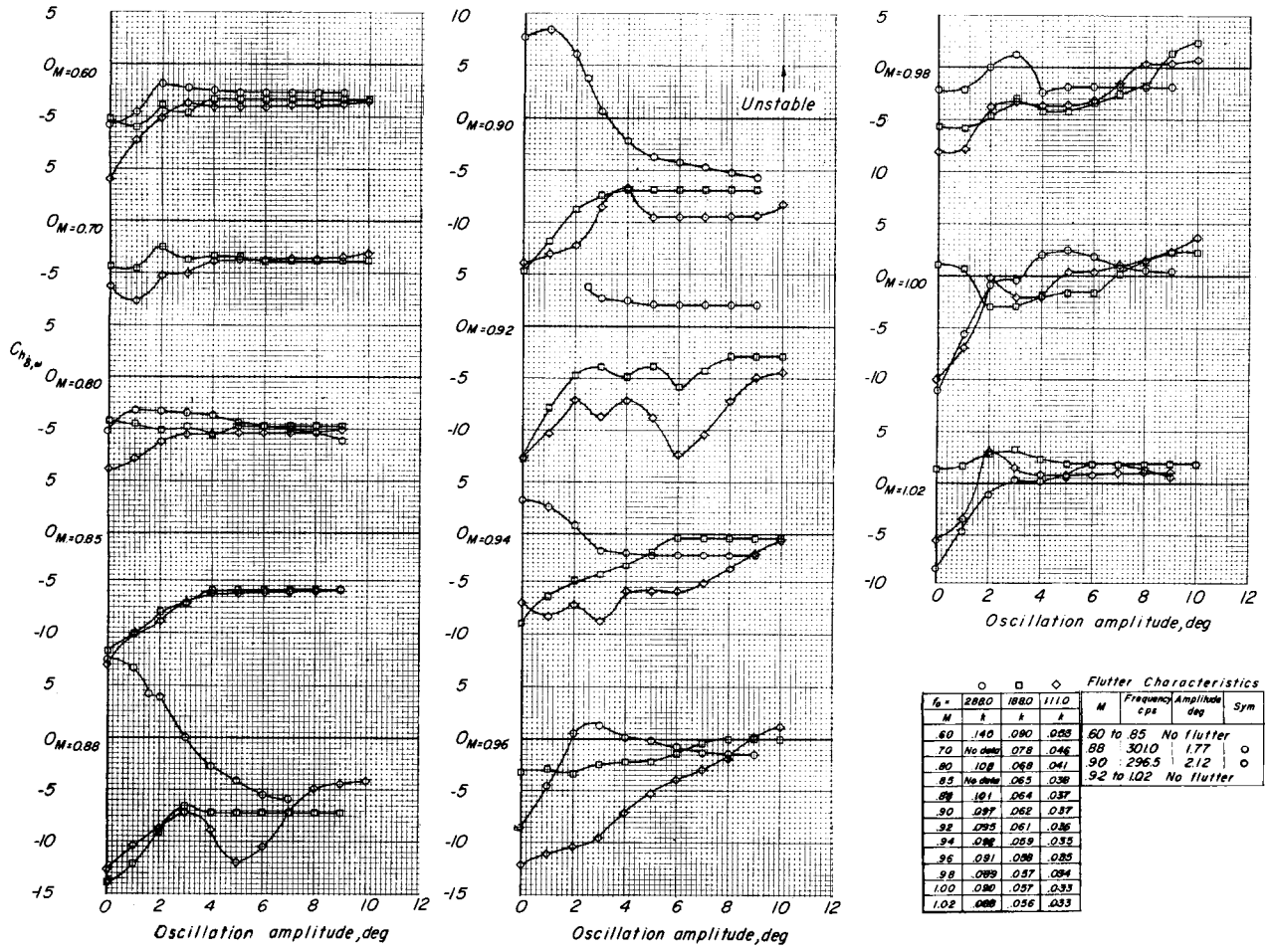

f_o =	288.0	188.0	111.0
M	k	k	k
.60	.140	.090	.065
.70	No data	.078	.046
.80	.108	.068	.041
.85	No data	.065	.038
.88	.101	.064	.037
.90	.097	.062	.037
.92	.095	.061	.036
.94	.093	.059	.035
.96	.091	.058	.035
.98	.089	.057	.034
1.00	.090	.057	.033
1.02	.088	.056	.033

(a) The t/c = 0.04 wing-control model.

Figure 5.- Variation of damping derivative with oscillation amplitude for various Mach numbers and reduced frequencies. ϕ = 13.33° control.

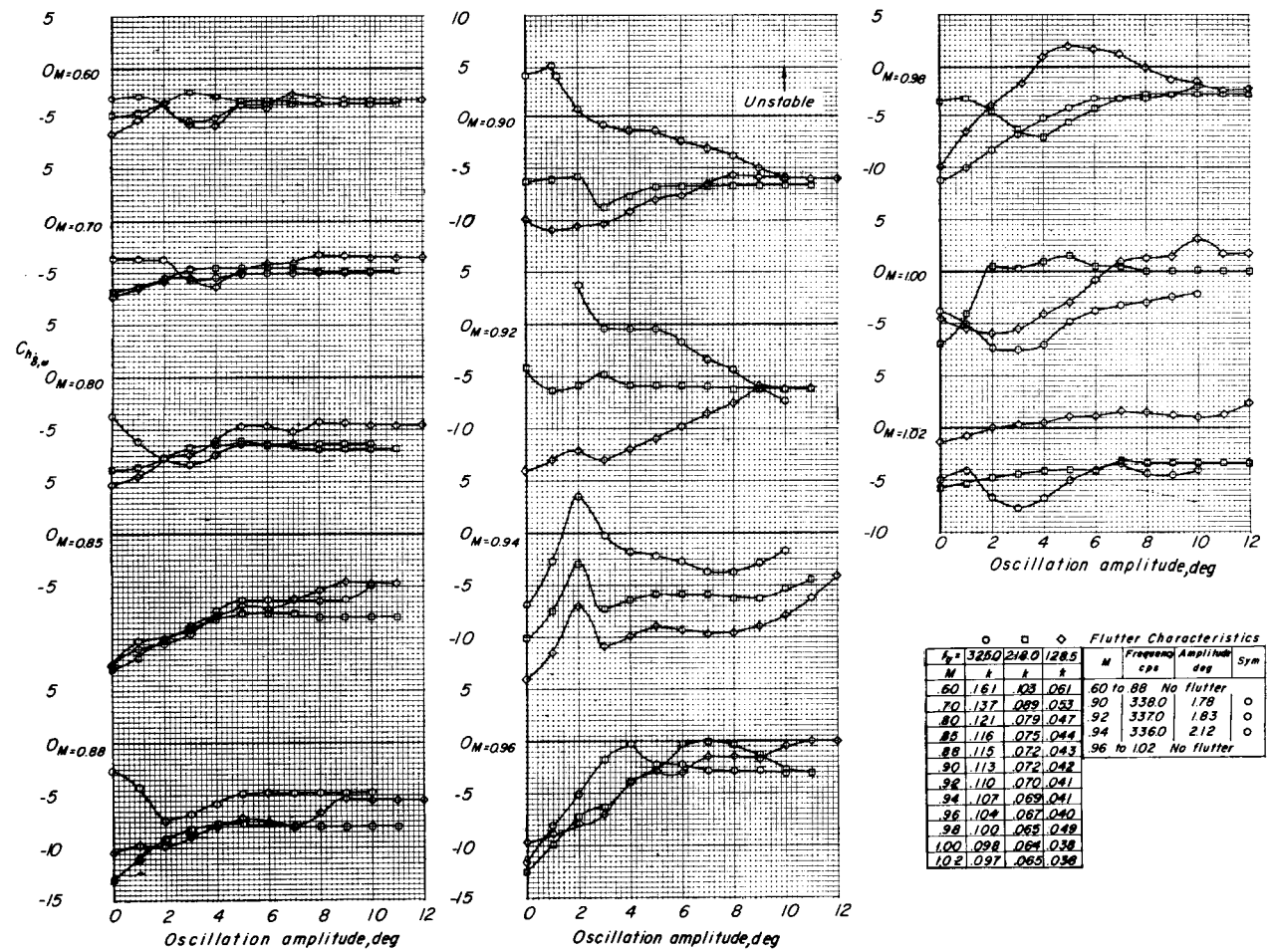

f_α =	328.0	218.0	128.5
M	k	k	k
.60	.161	.103	.061
.70	.137	.089	.053
.80	.121	.079	.047
.85	.116	.075	.044
.88	.115	.072	.043
.90	.113	.072	.042
.92	.110	.070	.041
.94	.107	.069	.041
.96	.104	.067	.040
.98	.100	.065	.039
1.00	.098	.064	.038
1.02	.097	.065	.038

M	Frequency cps	Amplitude deg	Sym
.60 to .88	No flutter		
.90	338.0	1.78	○
.92	337.0	1.83	○
.94	336.0	2.12	○
.96 to 1.02	No flutter		

(b) The t/c = 0.06 wing-control model.

Figure 5.- Continued.

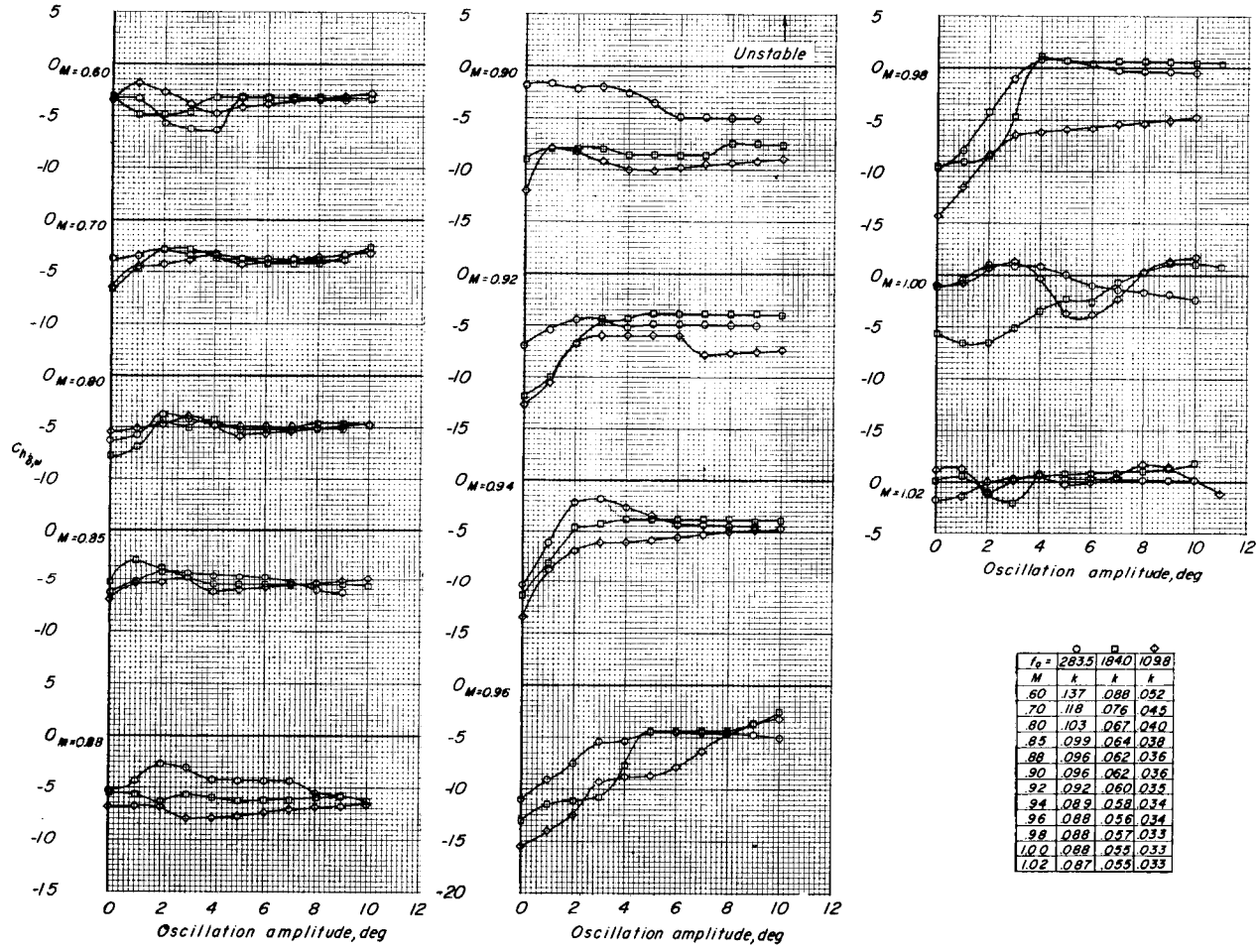

f_0 =	○ 2835	□ 1840	◇ 1098
M	k	k	k
.60	.137	.088	.052
.70	.118	.076	.045
.80	.103	.067	.040
.85	.099	.064	.038
.88	.096	.062	.036
.90	.096	.062	.036
.92	.092	.060	.035
.94	.089	.058	.034
.96	.088	.056	.034
.98	.088	.057	.033
1.00	.088	.055	.033
1.02	.087	.055	.033

(c) The t/c = 0.08 wing-control model.

Figure 5.- Concluded.

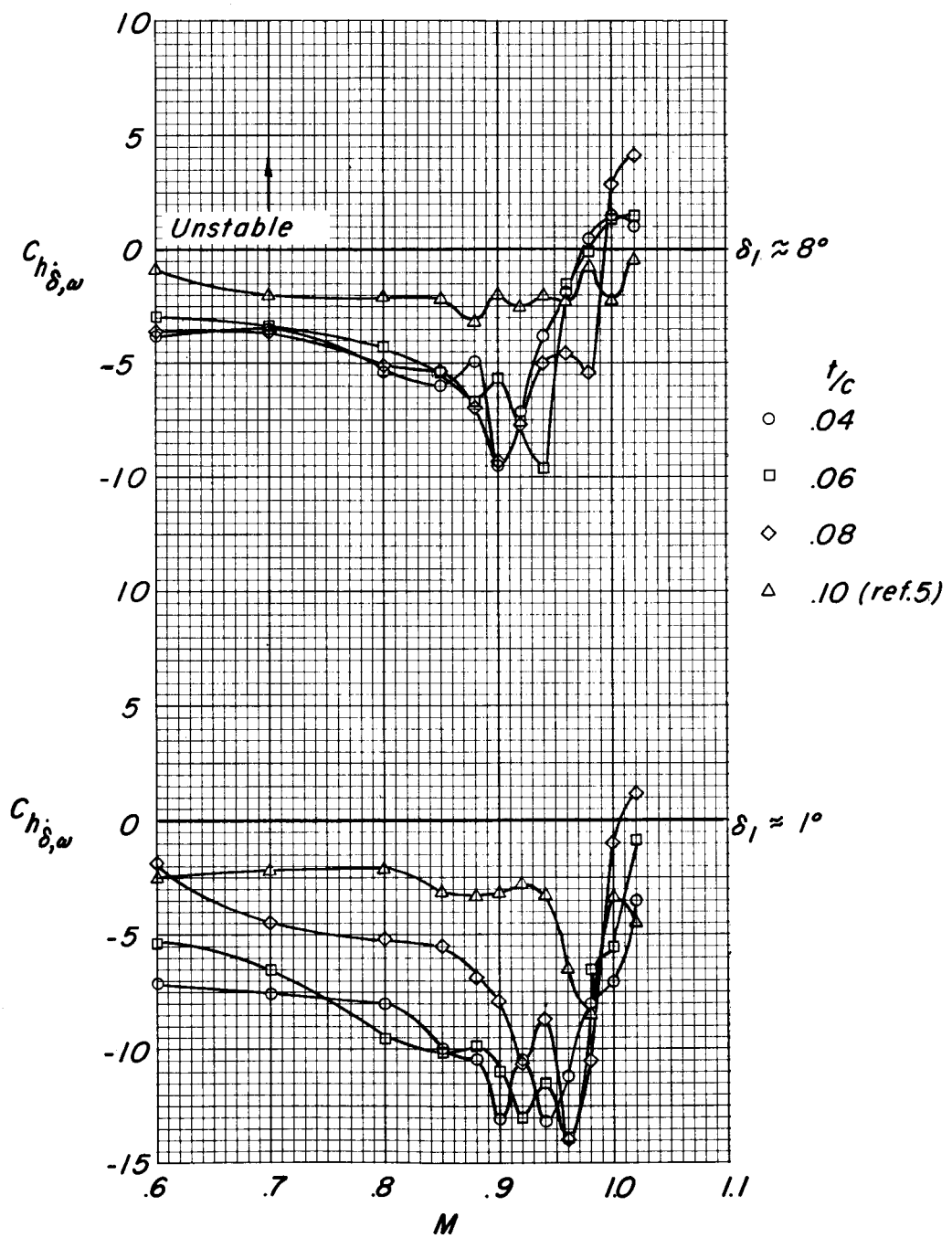

(a) $k \approx 0.04$.

Figure 6.- Variation of damping derivative with Mach number for oscillation amplitudes of approximately 1° and 8°. Models with $\phi = 13.33°$ control and conventional control from reference 5.

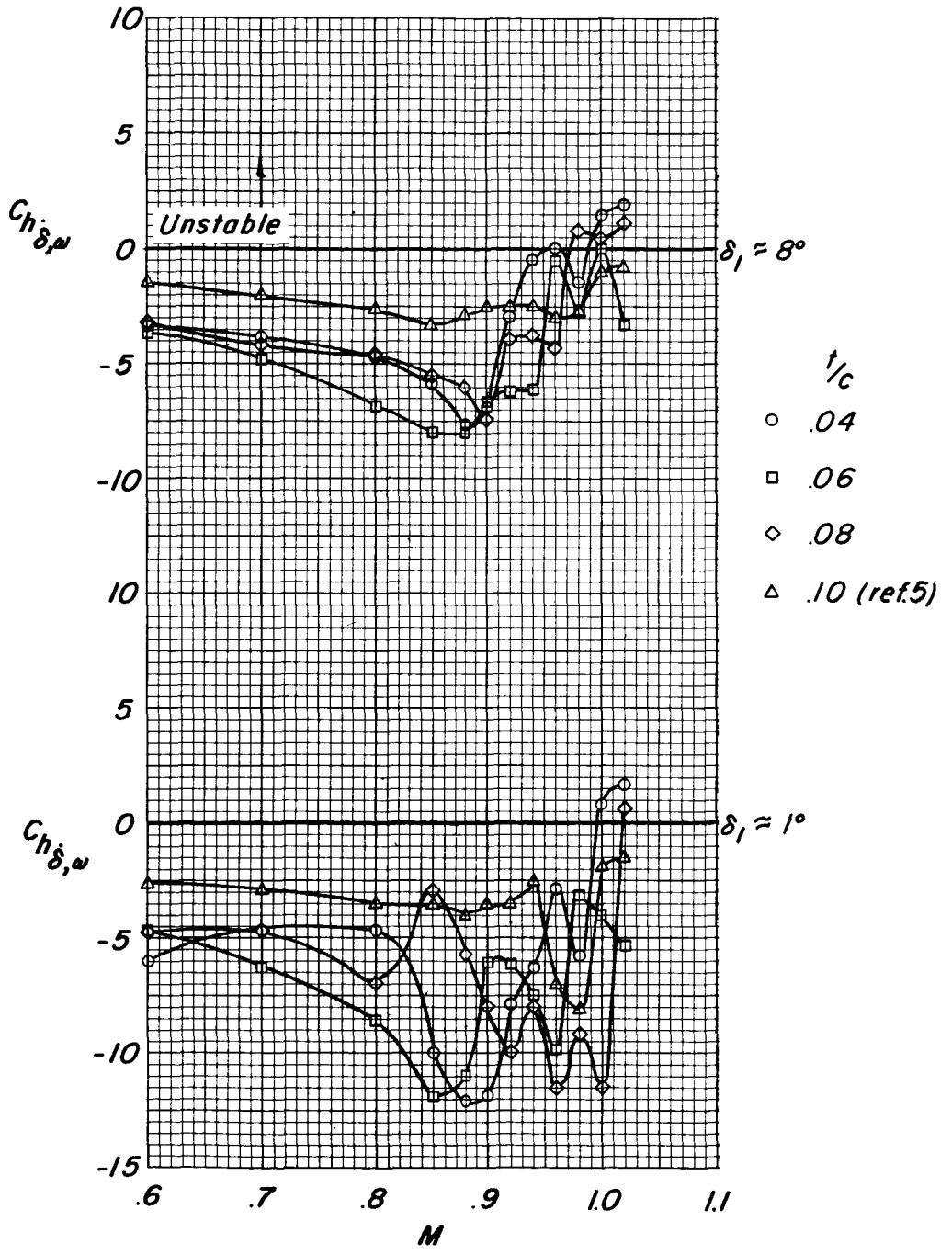

(b) $k \approx 0.08$.

Figure 6.- Continued.

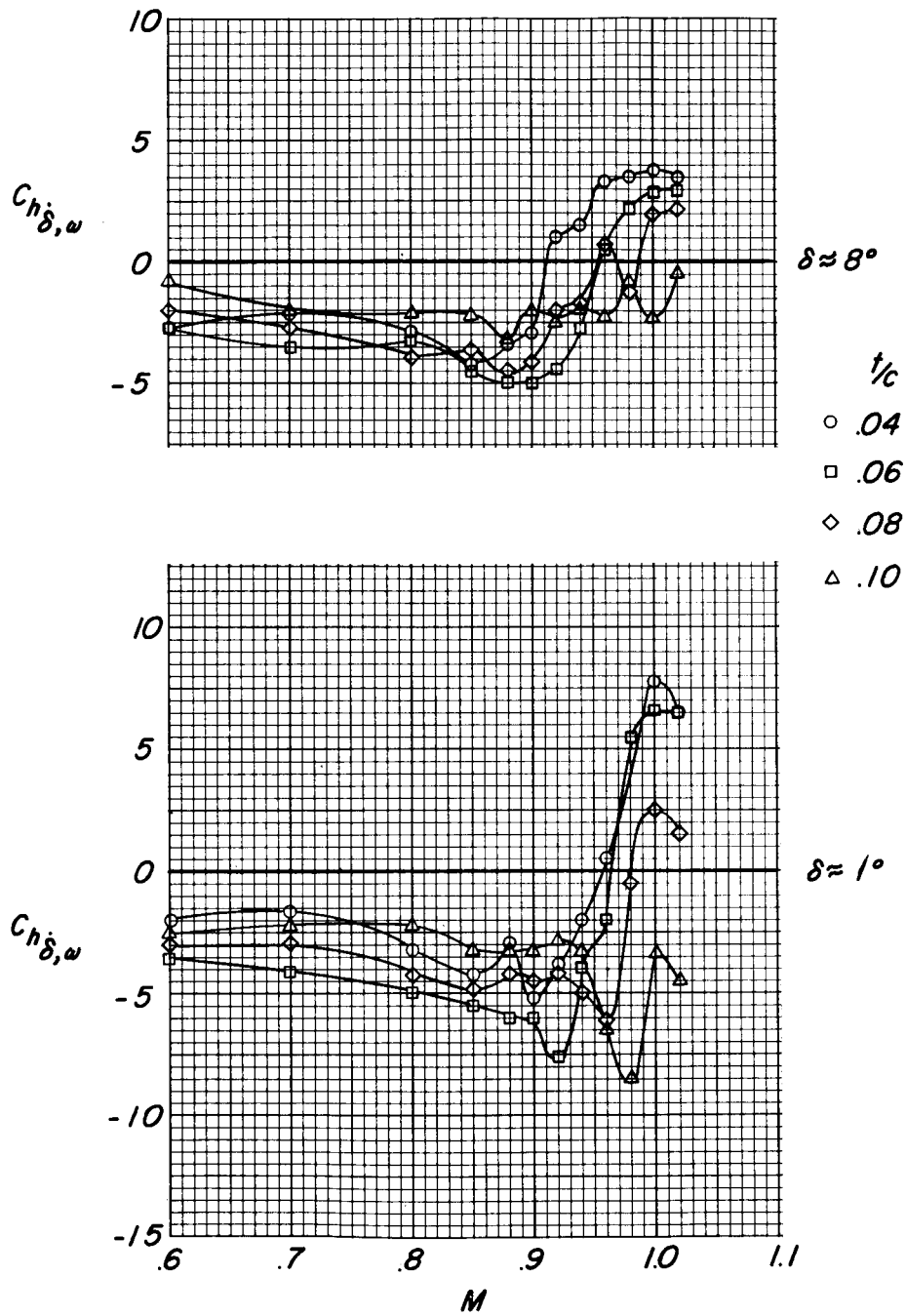

(c) k ≈ 0.04 (ref. 5).

Figure 6.- Continued.

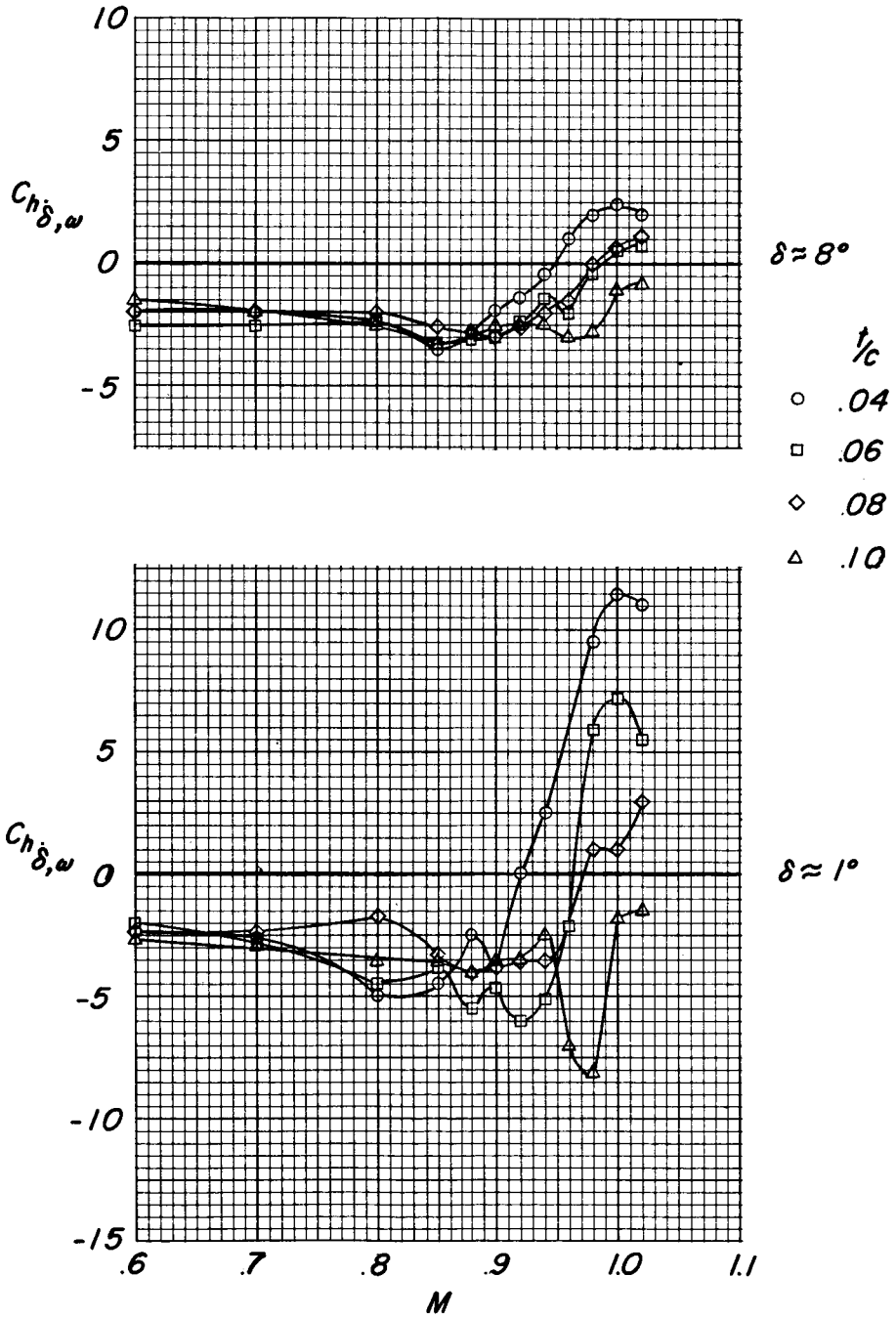

(d) $k \approx 0.08$ (ref. 6).

Figure 6.- Concluded.

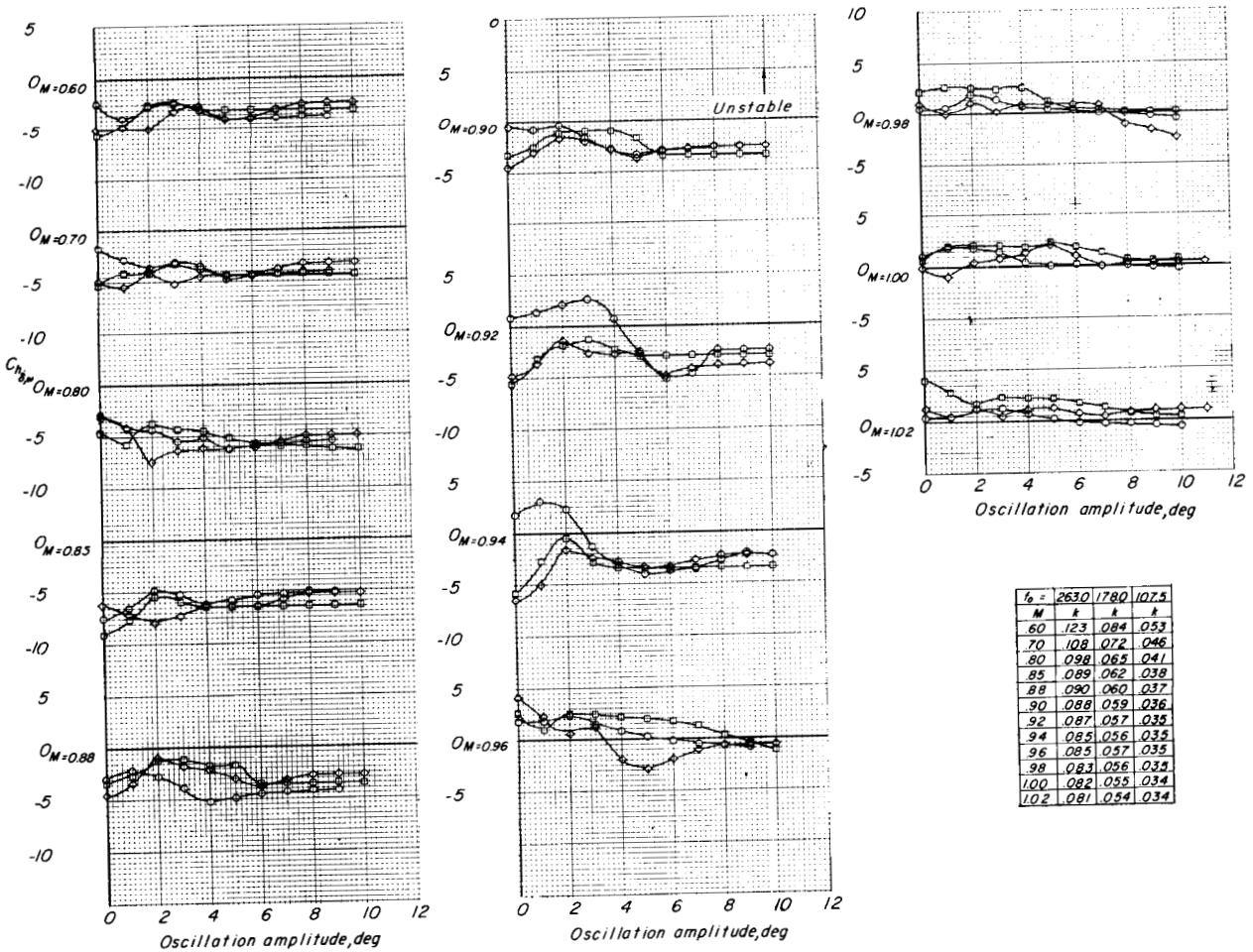

f_0 =	2630	1780	1075
M	k	k	k
.60	.123	.084	.053
.70	.108	.072	.046
.80	.098	.065	.041
.85	.089	.062	.038
.88	.090	.060	.037
.90	.088	.059	.036
.92	.087	.057	.035
.94	.085	.056	.035
.96	.085	.057	.035
.98	.083	.056	.035
1.00	.082	.055	.034
1.02	.081	.054	.034

(a) The $\phi = 5.25^{\circ}$ control.

Figure 7.- Variation of damping derivative with oscillation amplitude for various Mach numbers and reduced frequencies. t/c = 0.10 wing-control model.

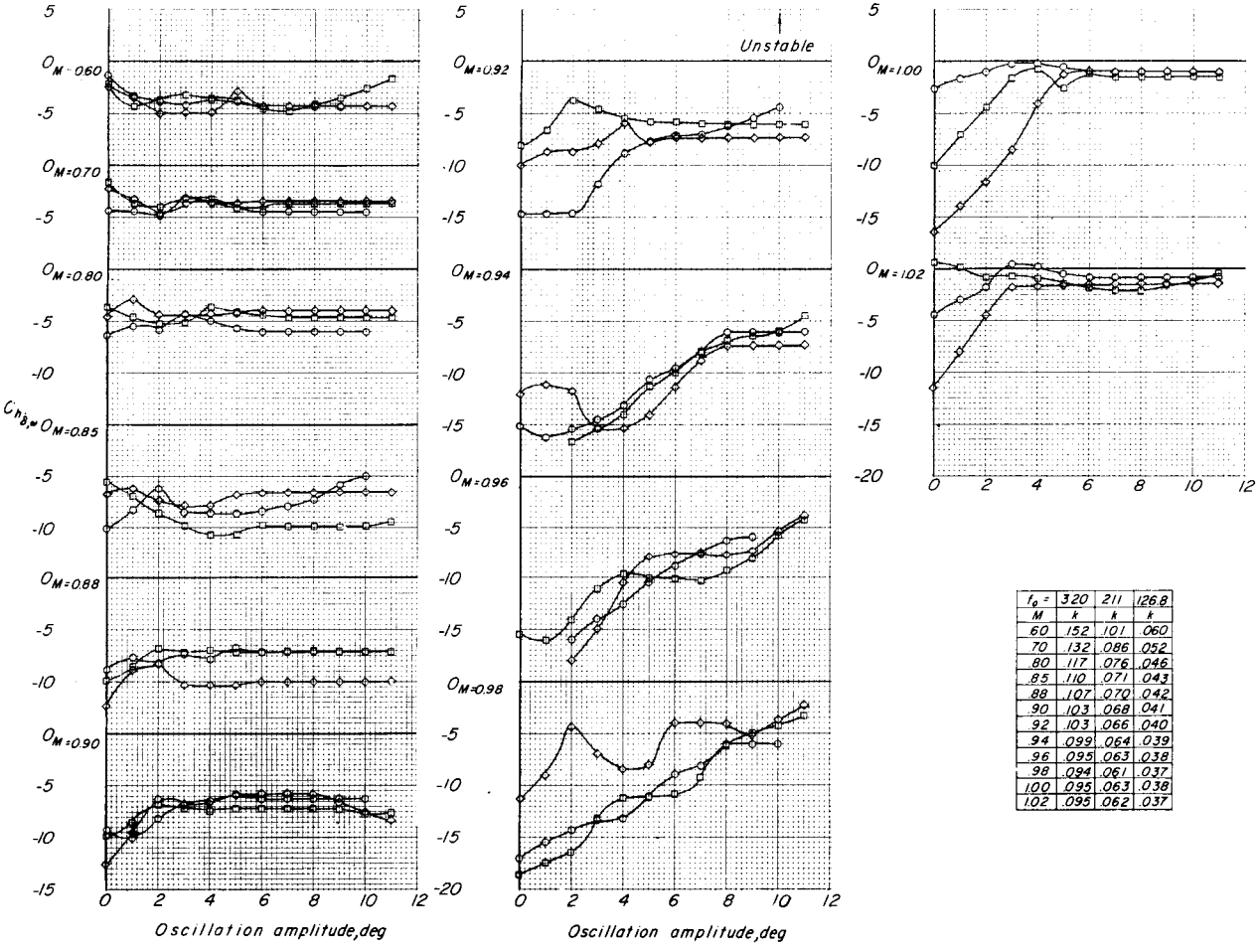

t_0 =	320	211	126.8
M	k	k	k
.60	.152	.101	.060
.70	.132	.086	.052
.80	.117	.076	.046
.85	.110	.071	.043
.88	.107	.070	.042
.90	.103	.068	.041
.92	.103	.066	.040
.94	.099	.064	.039
.96	.095	.063	.038
.98	.094	.061	.037
1.00	.095	.063	.038
1.02	.095	.062	.037

(b) The $\phi = 19.75^{\circ}$ control.

Figure 7.- Concluded.

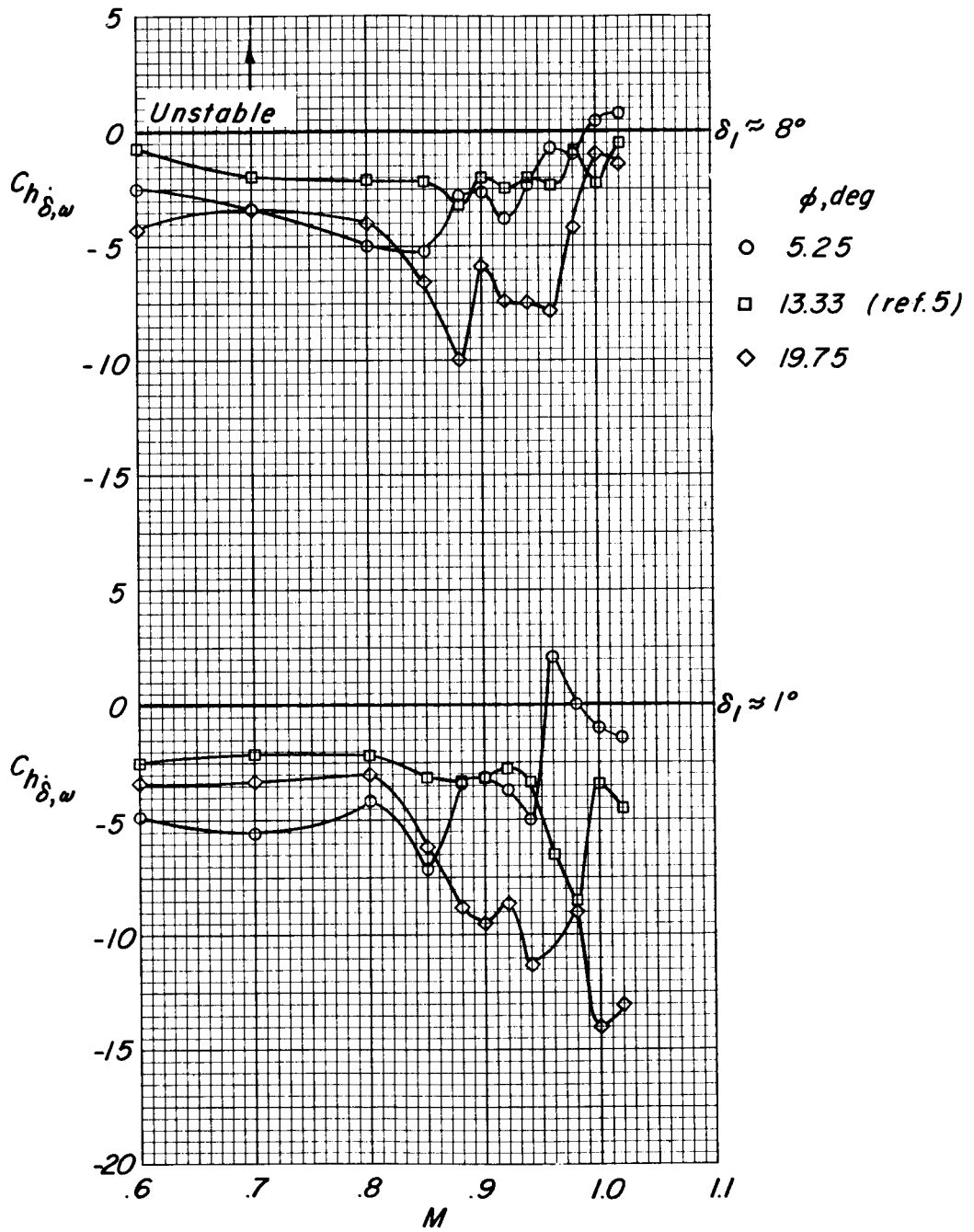

(a) $k \approx 0.04$.

Figure 8.- Variation of damping derivative with Mach number for oscillation amplitudes of approximately 1^o and 8^o. t/c = 0.10 wing-control model.

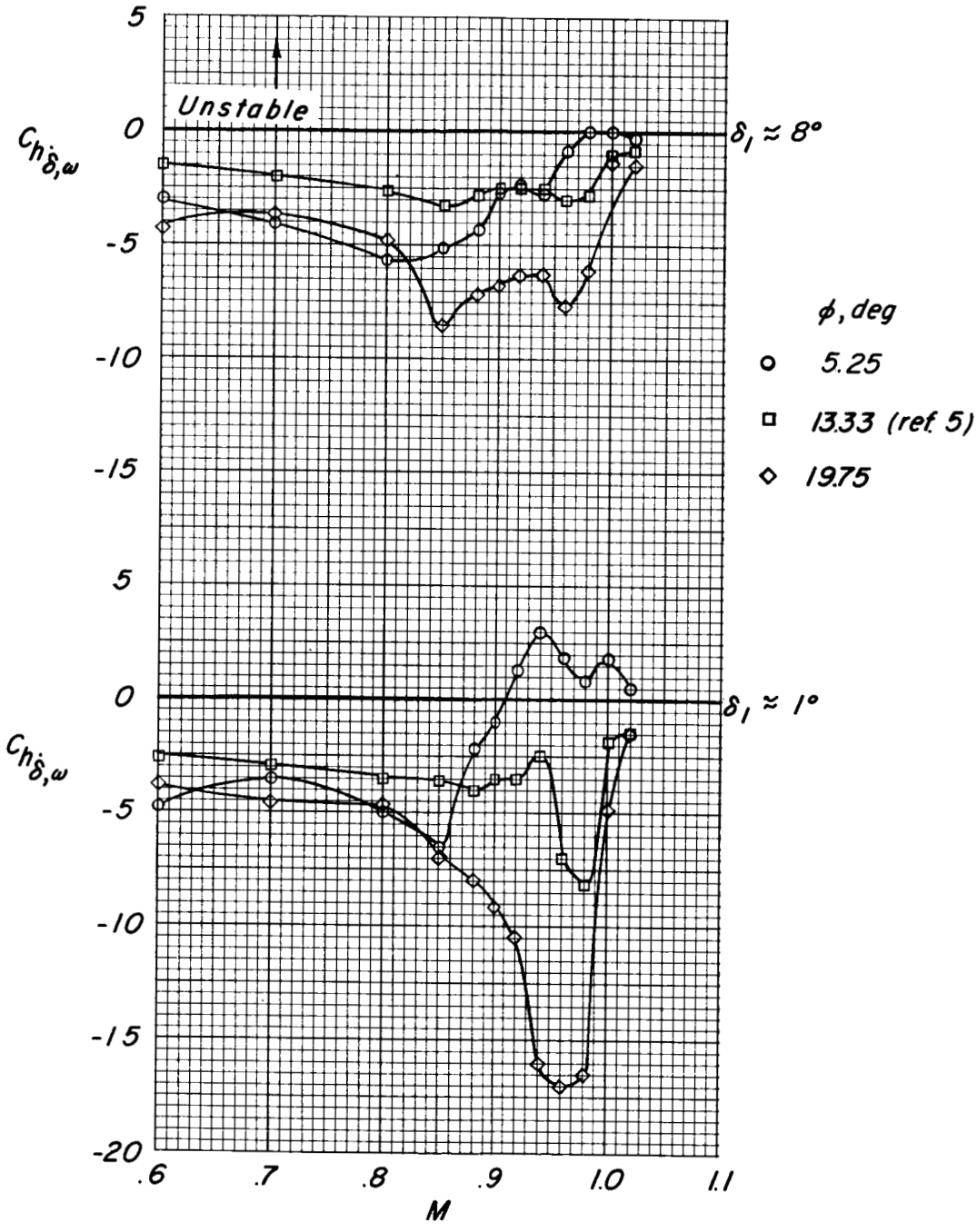

(b) $k \approx 0.08$.

Figure 8.- Concluded.

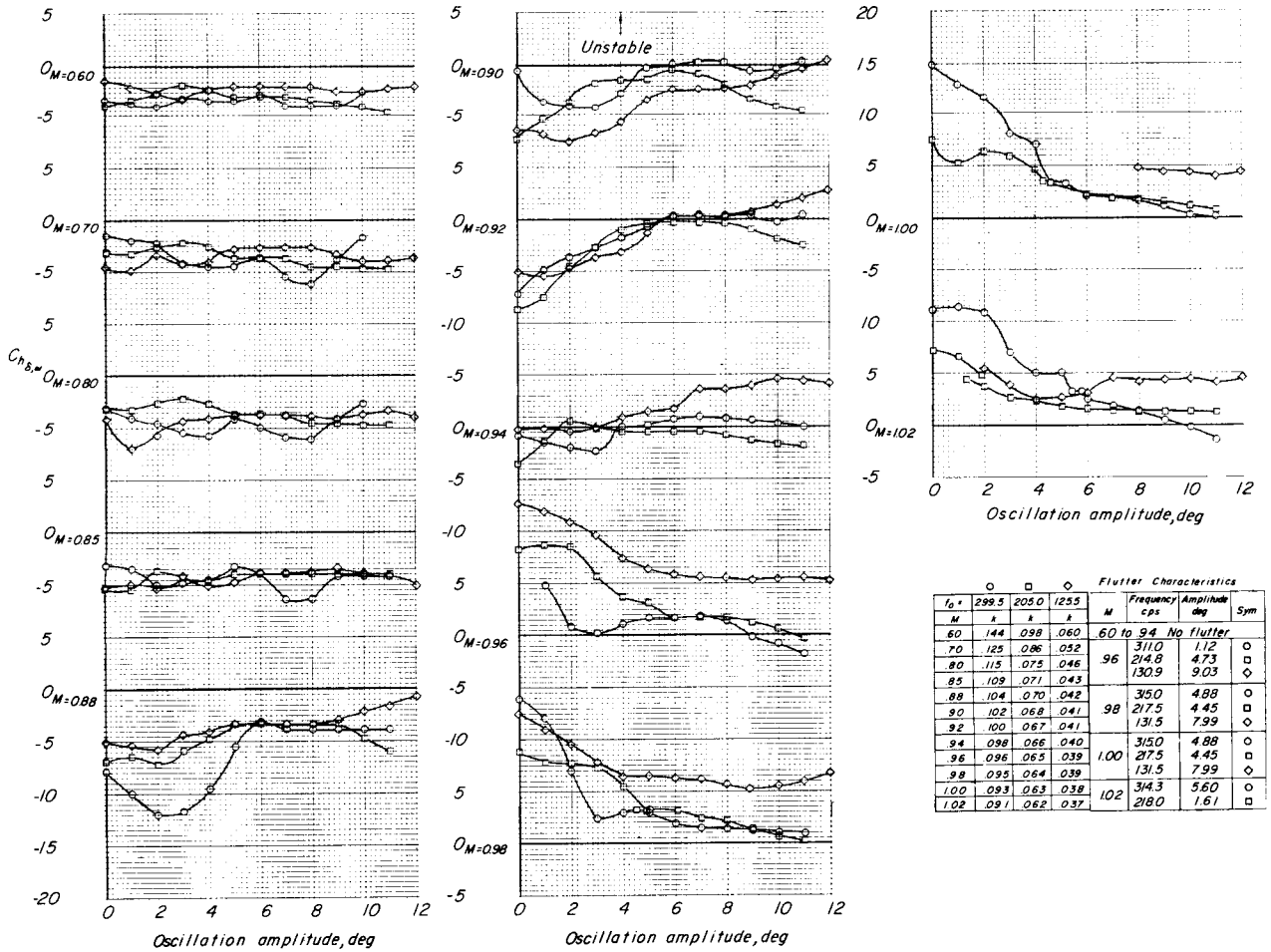

	○	□	◇	Flutter Characteristics			
f_o =	299.5	205.0	125.5	M	Frequency cps	Amplitude deg	Sym
M	k	k	k				
.60	.144	.098	.060	.60 to .94 No flutter			
.70	.125	.086	.052	.96	311.0	1.12	○
.80	.115	.075	.046		214.8	4.73	□
.85	.109	.071	.043		130.9	9.03	◇
.88	.104	.070	.042	.98	315.0	4.88	○
.90	.102	.068	.041		217.5	4.45	□
.92	.100	.067	.041		131.5	7.99	◇
.94	.098	.066	.040	1.00	315.0	4.88	○
.96	.096	.065	.039		217.5	4.45	□
.98	.095	.064	.039		131.5	7.99	◇
1.00	.093	.063	.038	1.02	314.3	5.60	○
1.02	.091	.062	.037		218.0	1.61	□

(a) $t/c = 0.06$; $t_s = 0.013$.

Figure 9.- Variation of damping derivative with oscillation amplitude for various Mach numbers and reduced frequencies. Splitter-plate-control models.

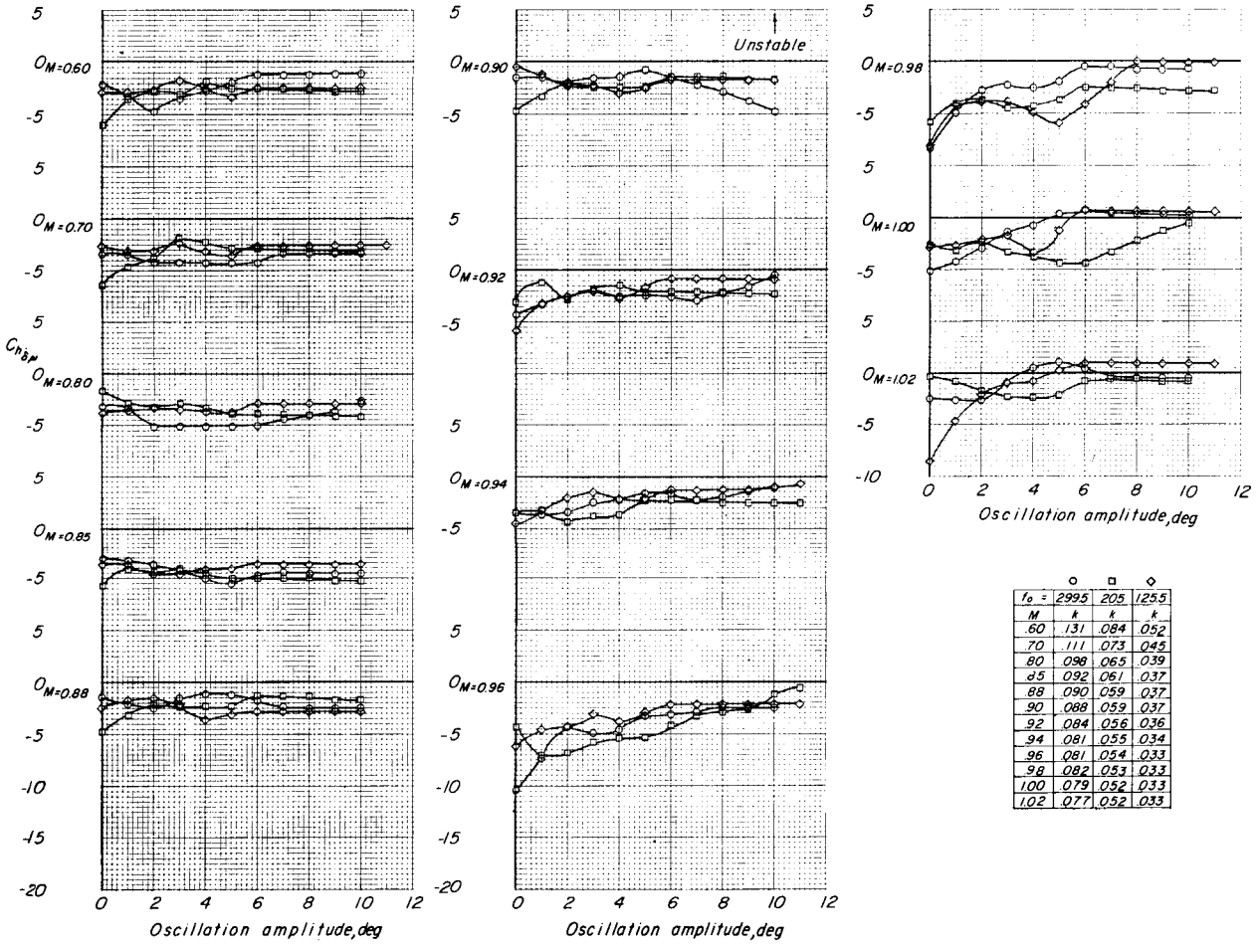

	○	□	◇
f_o =	2995	205	1255
M	k	k	k
.60	.131	.084	.052
.70	.111	.073	.045
.80	.098	.065	.039
.85	.092	.061	.037
.88	.090	.059	.037
.90	.088	.059	.037
.92	.084	.056	.036
.94	.081	.055	.034
.96	.081	.054	.033
.98	.082	.053	.033
1.00	.079	.052	.033
1.02	.077	.052	.033

(b) $t/c = 0.10$; $t_s = 0.013$.

Figure 9.- Continued.

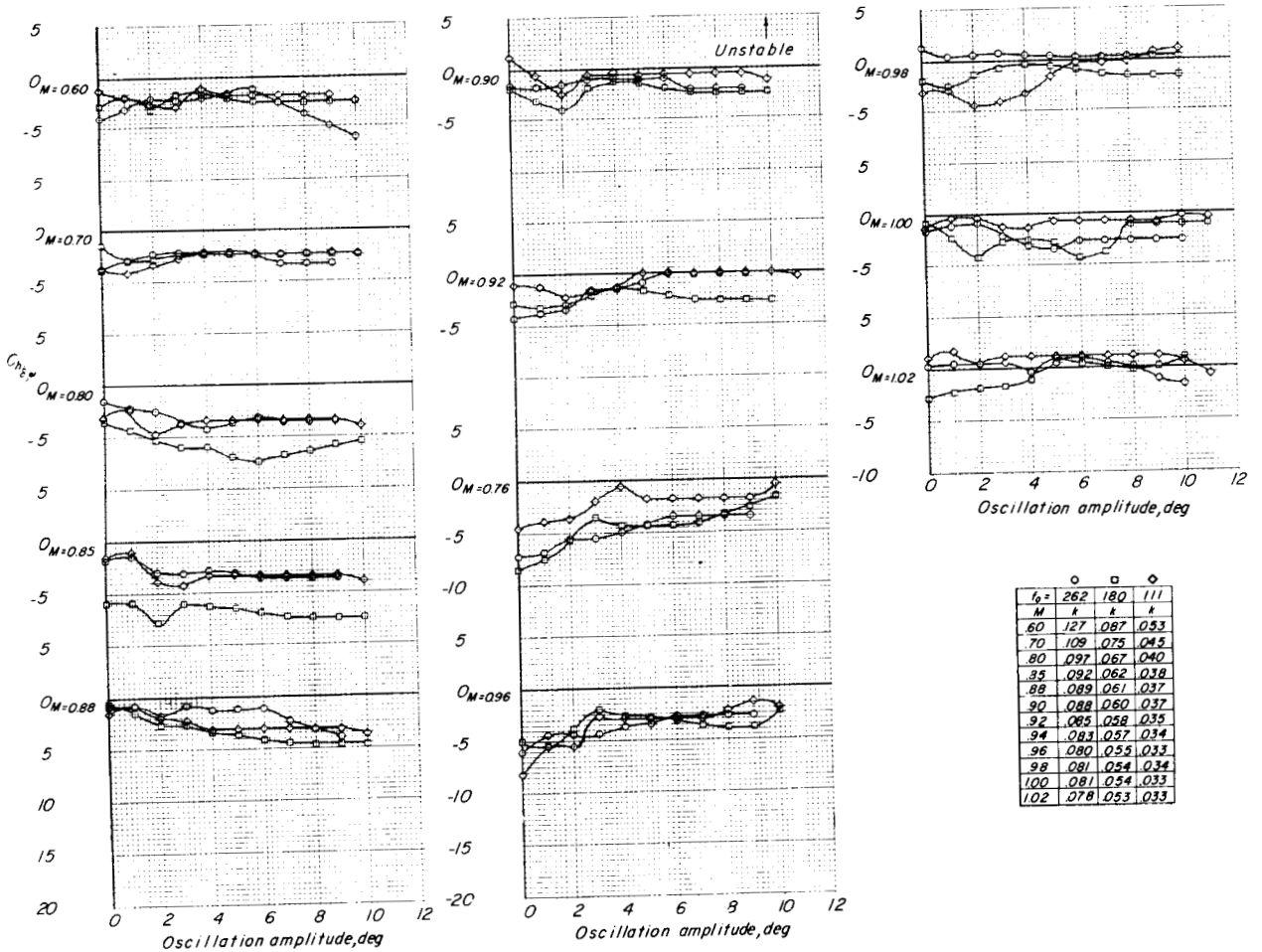

	○	□	◇
f_0 =	262	180	111
M	k	k	k
.60	.127	.087	.053
.70	.109	.075	.045
.80	.097	.067	.040
.85	.092	.062	.038
.88	.089	.061	.037
.90	.088	.060	.037
.92	.085	.058	.035
.94	.083	.057	.034
.96	.080	.055	.033
.98	.081	.054	.034
1.00	.081	.054	.033
1.02	.078	.053	.033

(c) $t/c = 0.10$; $t_s = 0.031$.

Figure 9.- Concluded.

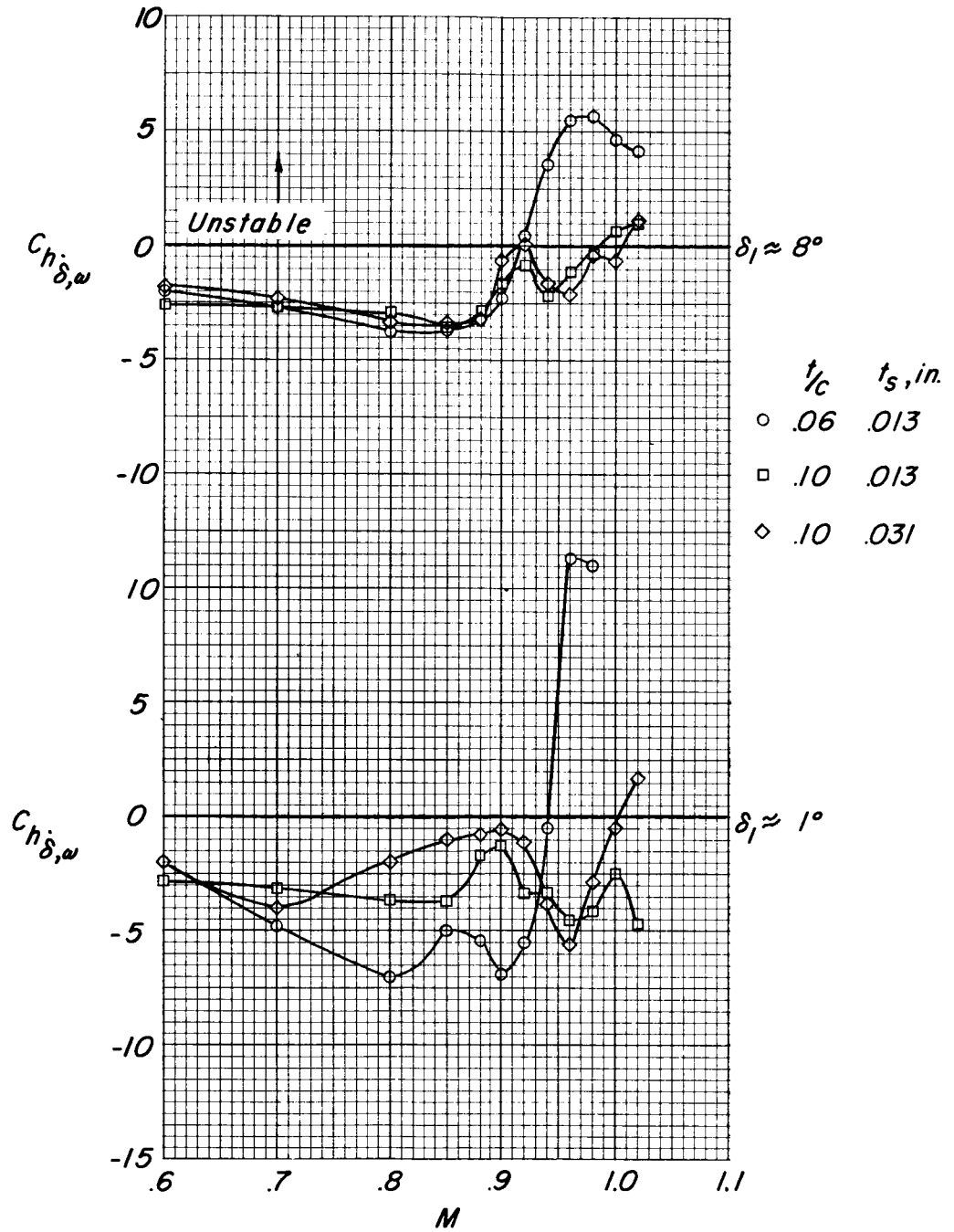

(a) $k \approx 0.04$.

Figure 10.- Variation of damping derivative with Mach number for oscillation amplitudes of approximately 1° and 8°. Splitter-plate-control models.

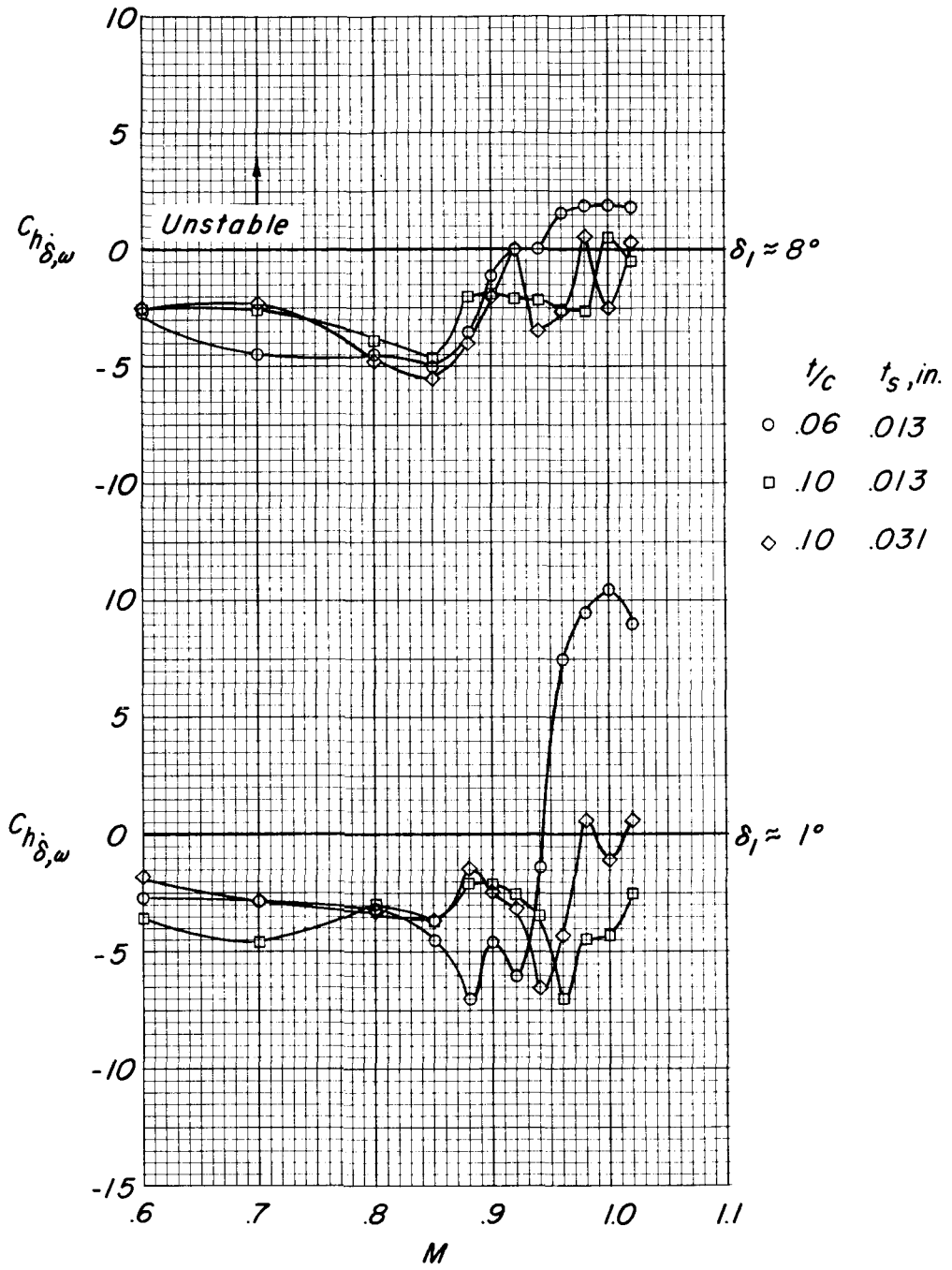

(b) $k \approx 0.08$.

Figure 10.- Concluded.

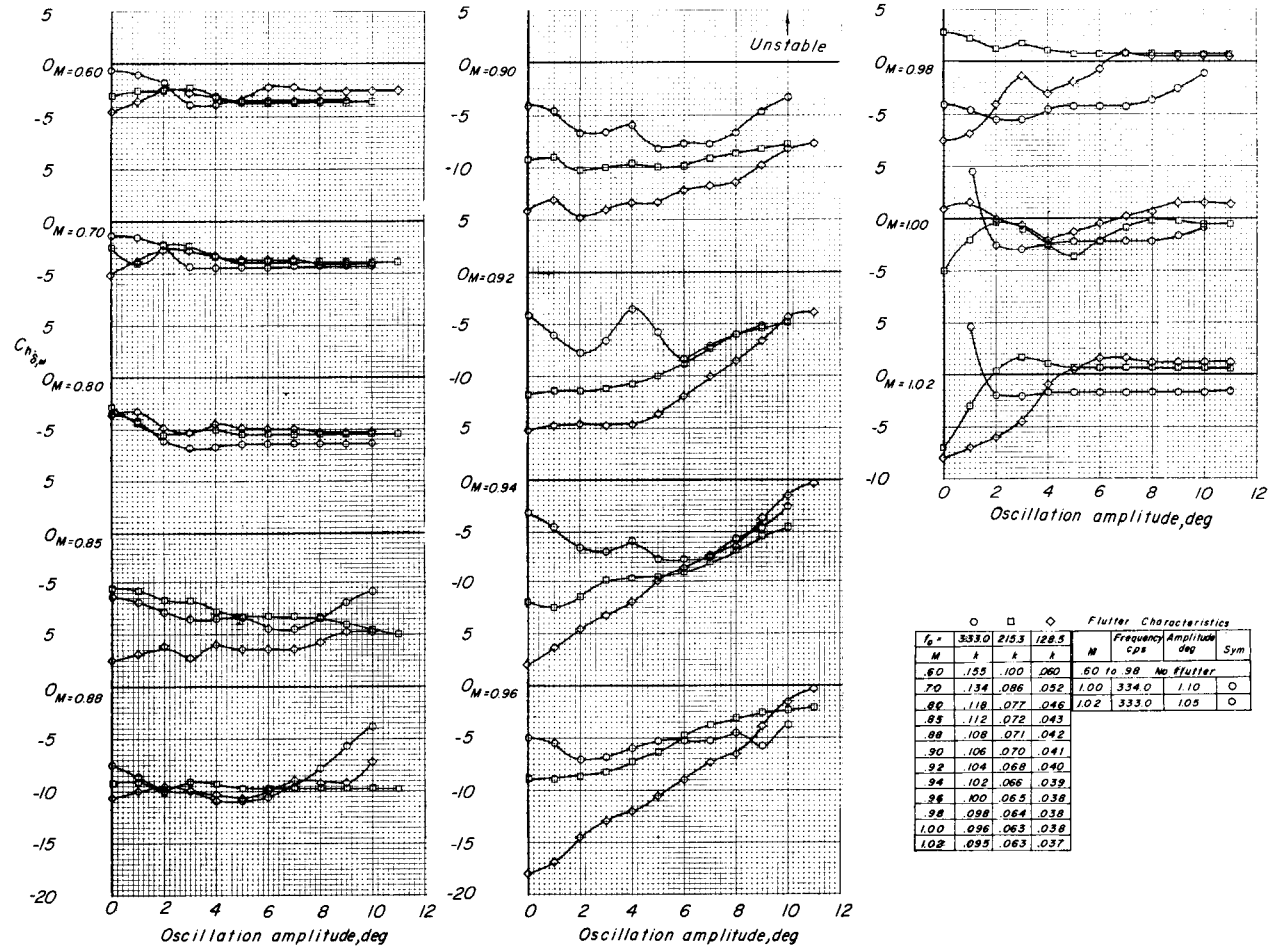

	○		□		◇	
f_o =	333.0		215.3		128.5	
M	k		k		k	
.60	.155		.100		.060	
.70	.134		.086		.052	
.80	.118		.077		.046	
.85	.112		.072		.043	
.88	.108		.071		.042	
.90	.106		.070		.041	
.92	.104		.068		.040	
.94	.102		.066		.039	
.96	.100		.065		.038	
.98	.098		.064		.038	
1.00	.096		.063		.038	
1.02	.095		.063		.037	

Flutter Characteristics

M	Frequency cps	Amplitude deg	Sym
.60 to .98	No flutter		
1.00	334.0	1.10	○
1.02	333.0	1.05	○

(a) Serrated wedge.

Figure 11.- Variation of damping derivative with oscillation amplitude for various Mach numbers and reduced frequencies. Wedge-control models.

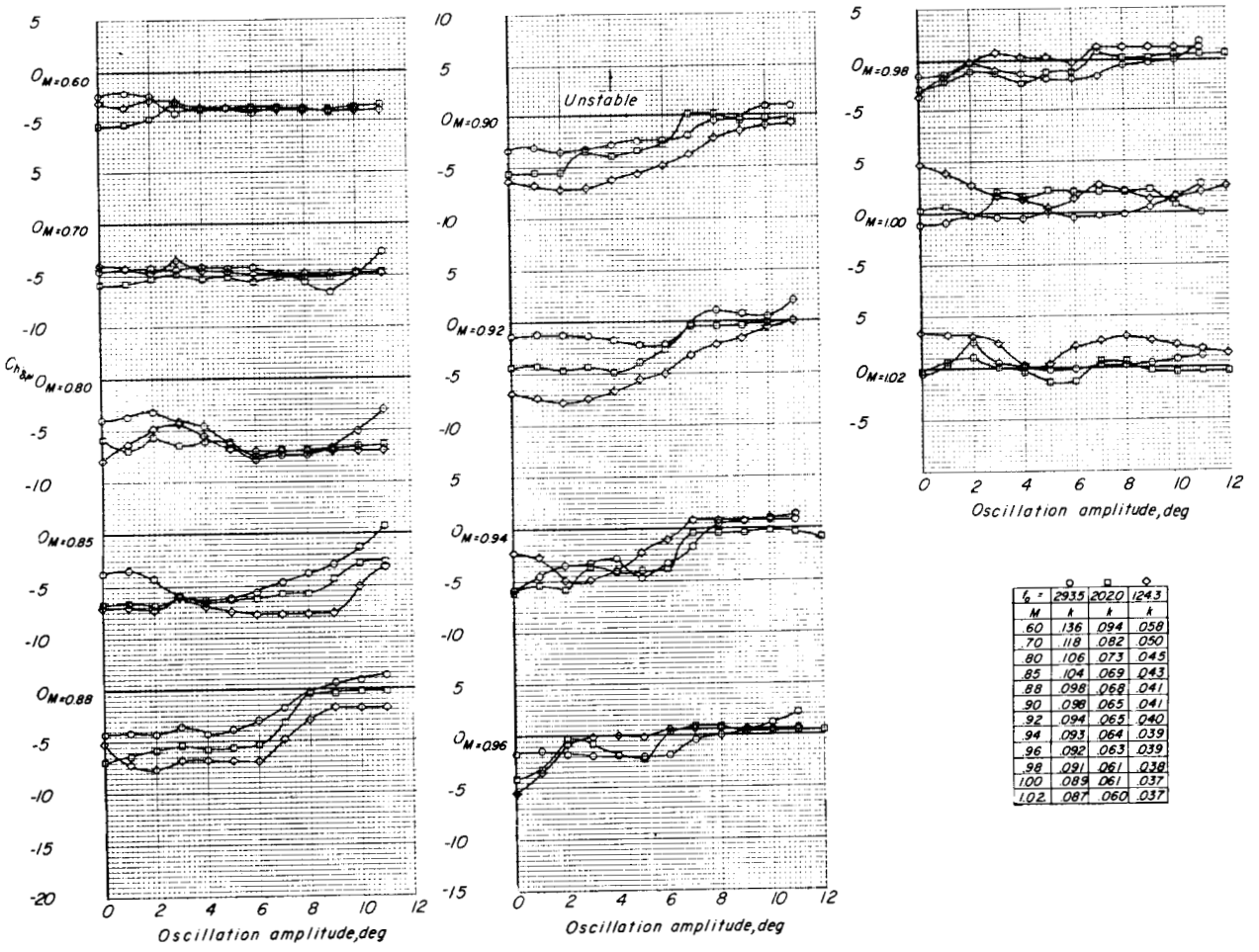

ζ_e =	○ 2935	□ 2020	◇ 1243
M	k	k	k
.60	.136	.094	.058
.70	.118	.082	.050
.80	.106	.073	.045
.85	.104	.069	.043
.88	.098	.068	.041
.90	.098	.065	.041
.92	.094	.065	.040
.94	.093	.064	.039
.96	.092	.063	.039
.98	.091	.061	.038
1.00	.089	.061	.037
1.02	.087	.060	.037

(b) Full wedge.

Figure 11.- Concluded.

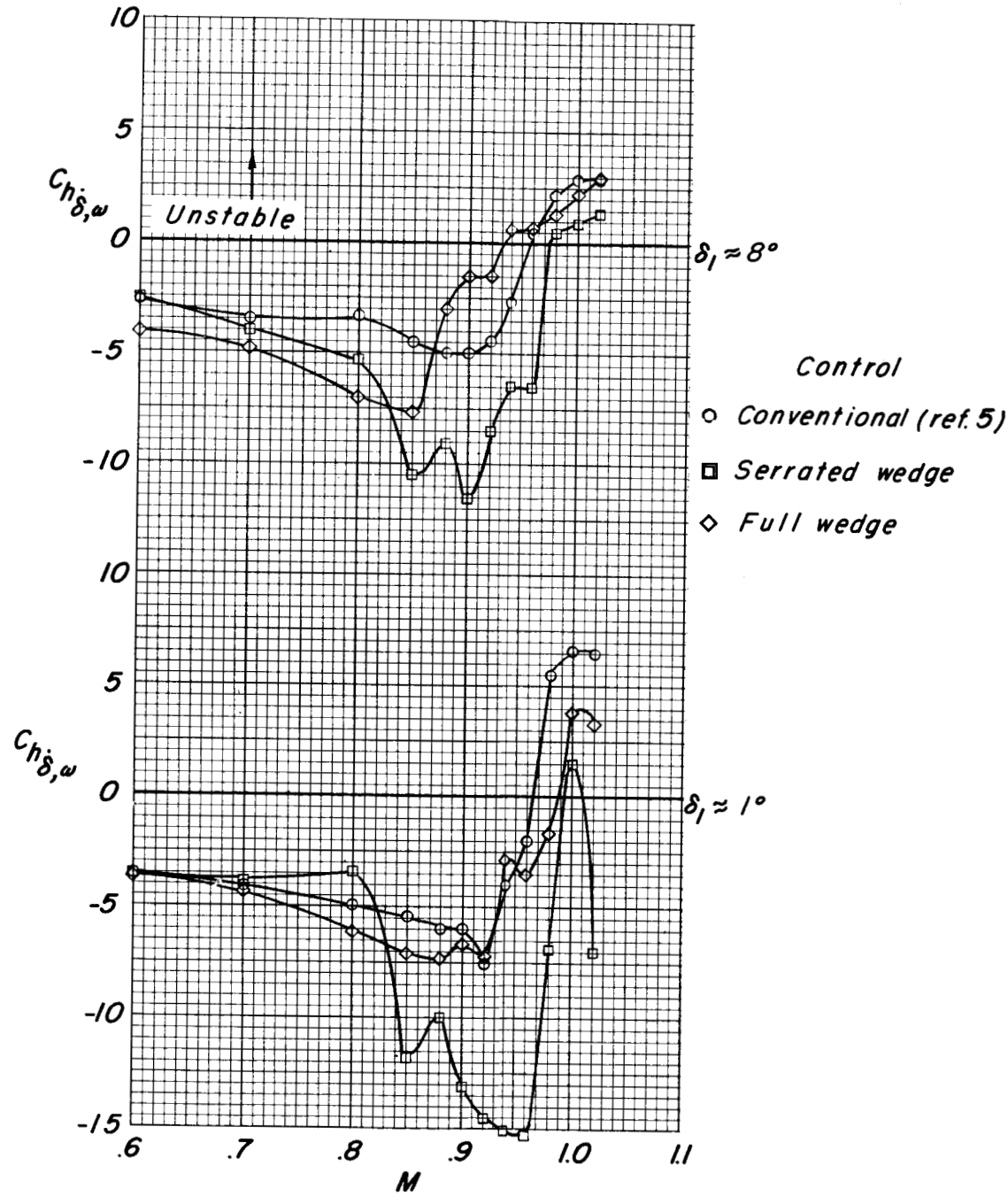

(a) $k \approx 0.04$.

Figure 12.- Variation of damping derivative with Mach number for oscillation amplitudes of approximately 1° and 8°. Wedge-control models.

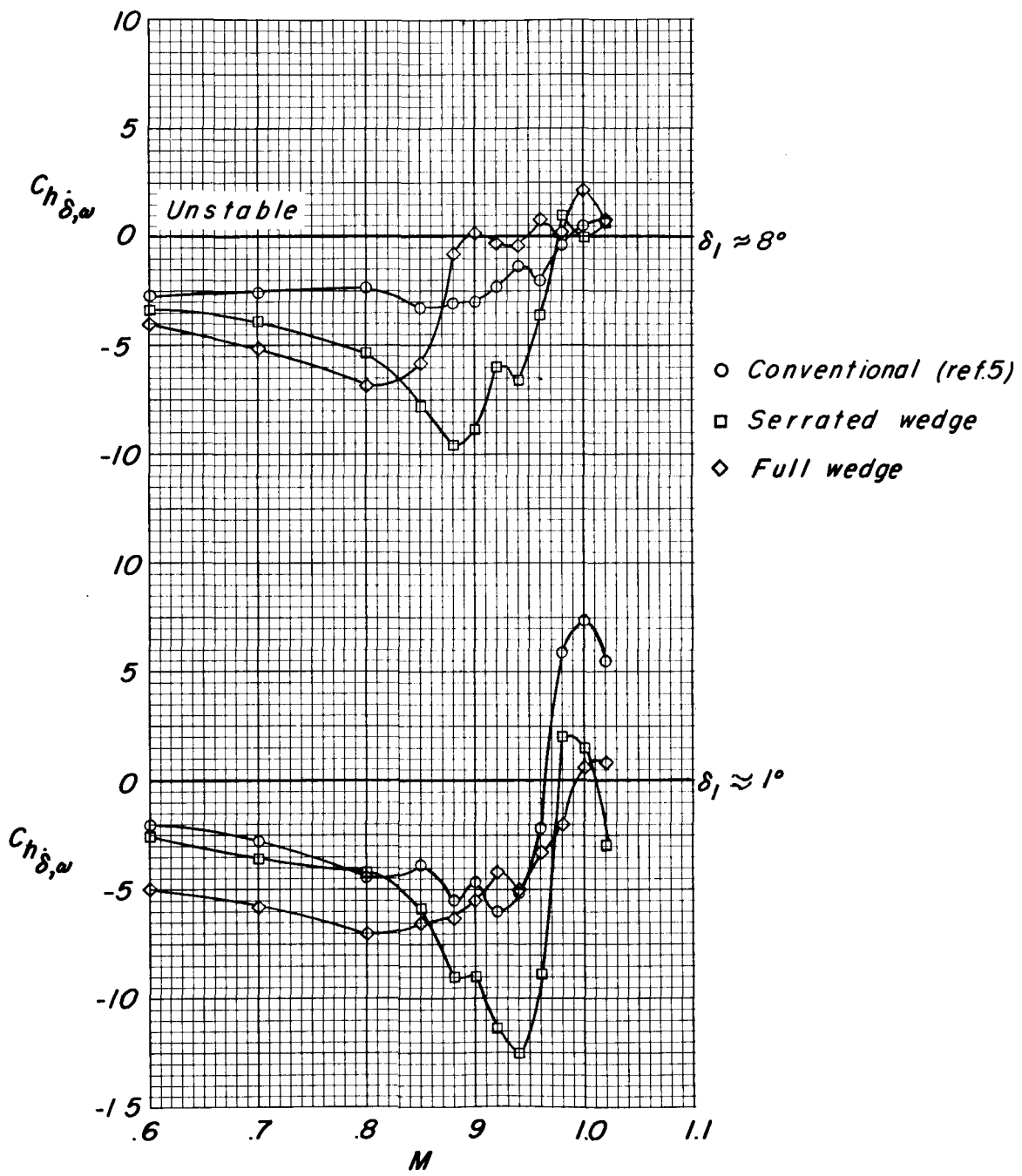

(b) k ≈ 0.08.

Figure 12.- Concluded.

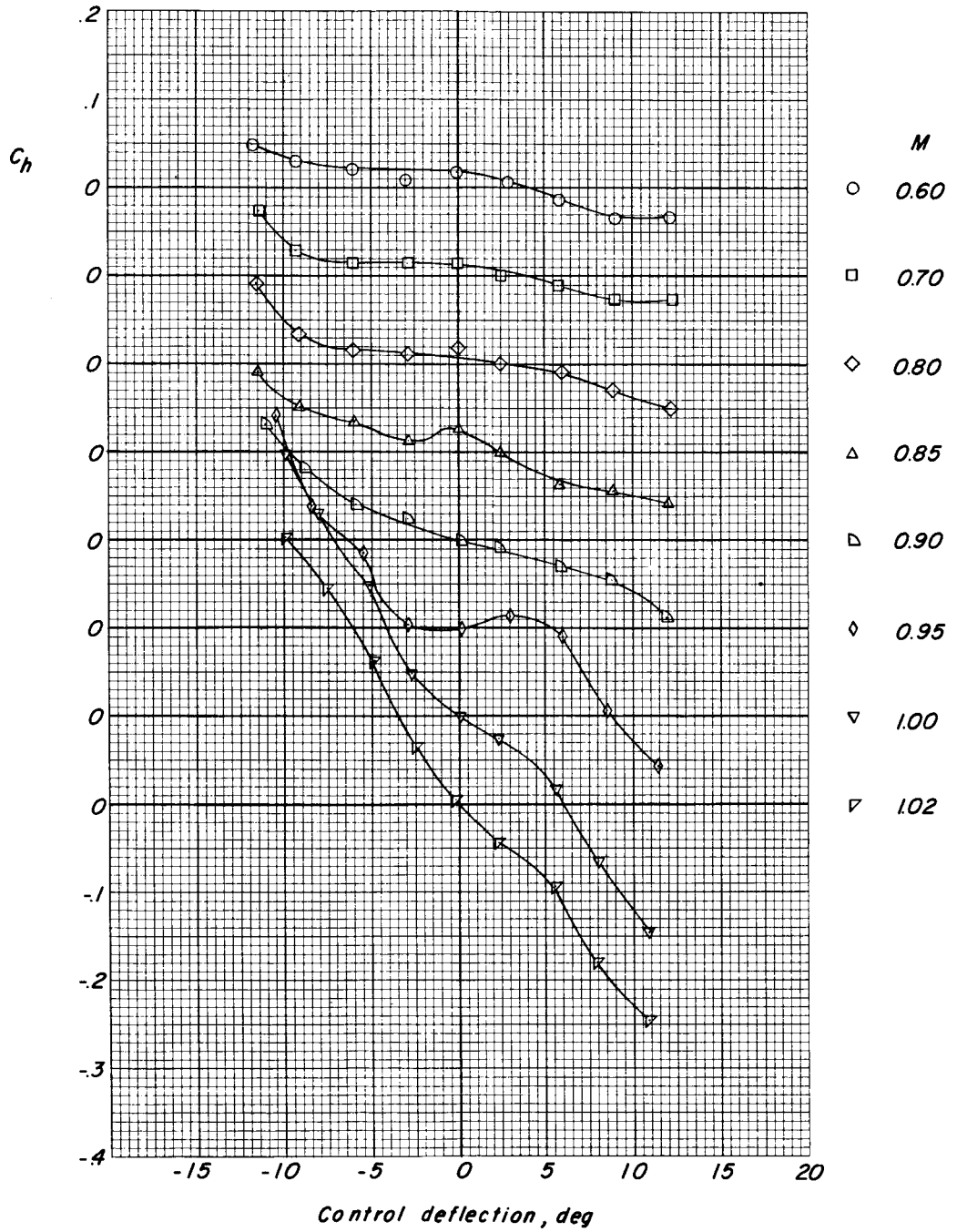

(a) t/c = 0.04.

Figure 13.- Variation of static hinge-moment coefficient with control deflection for the model with ϕ = 13.33° control at various Mach numbers.

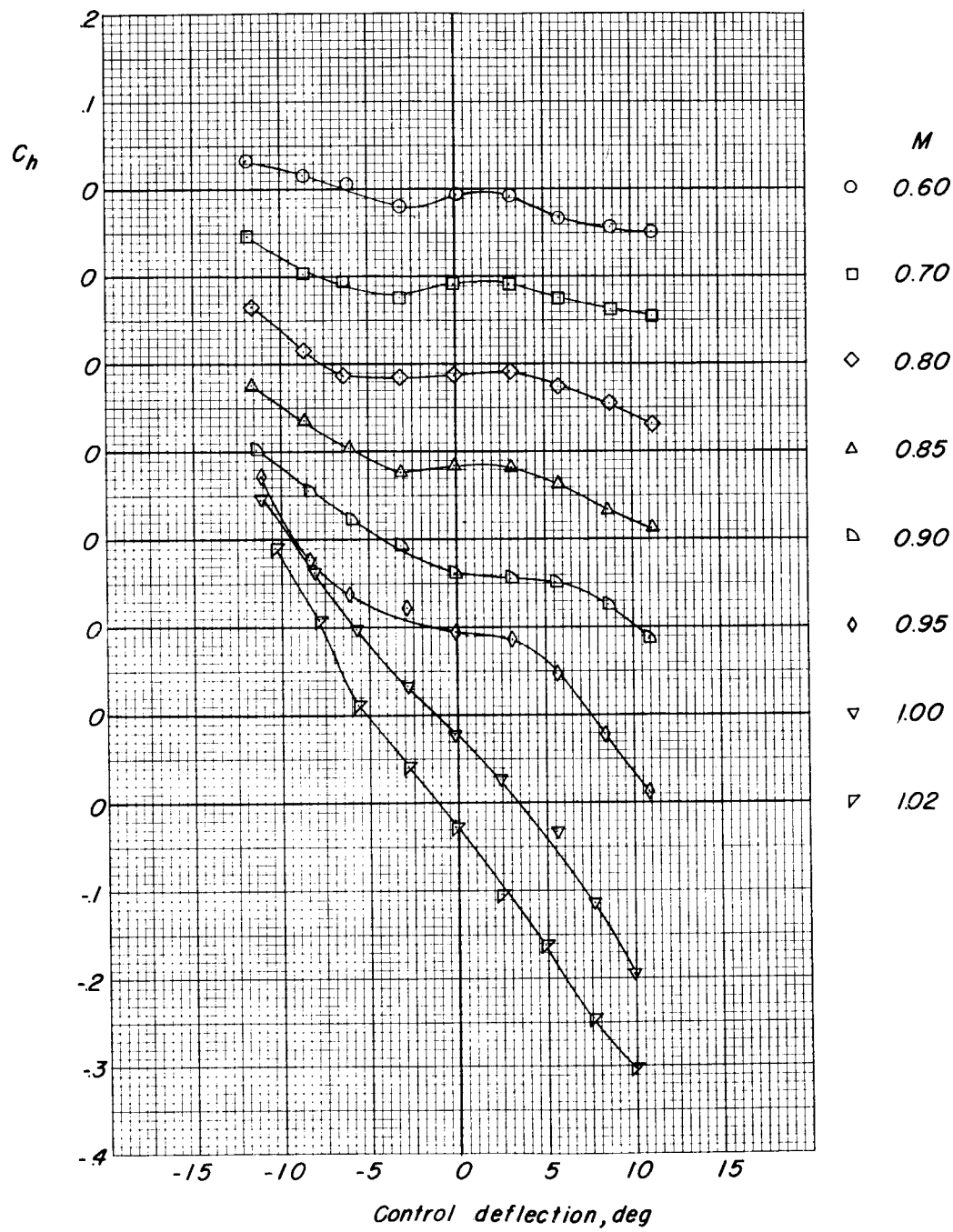

(b) t/c = 0.06.

Figure 13.- Continued.

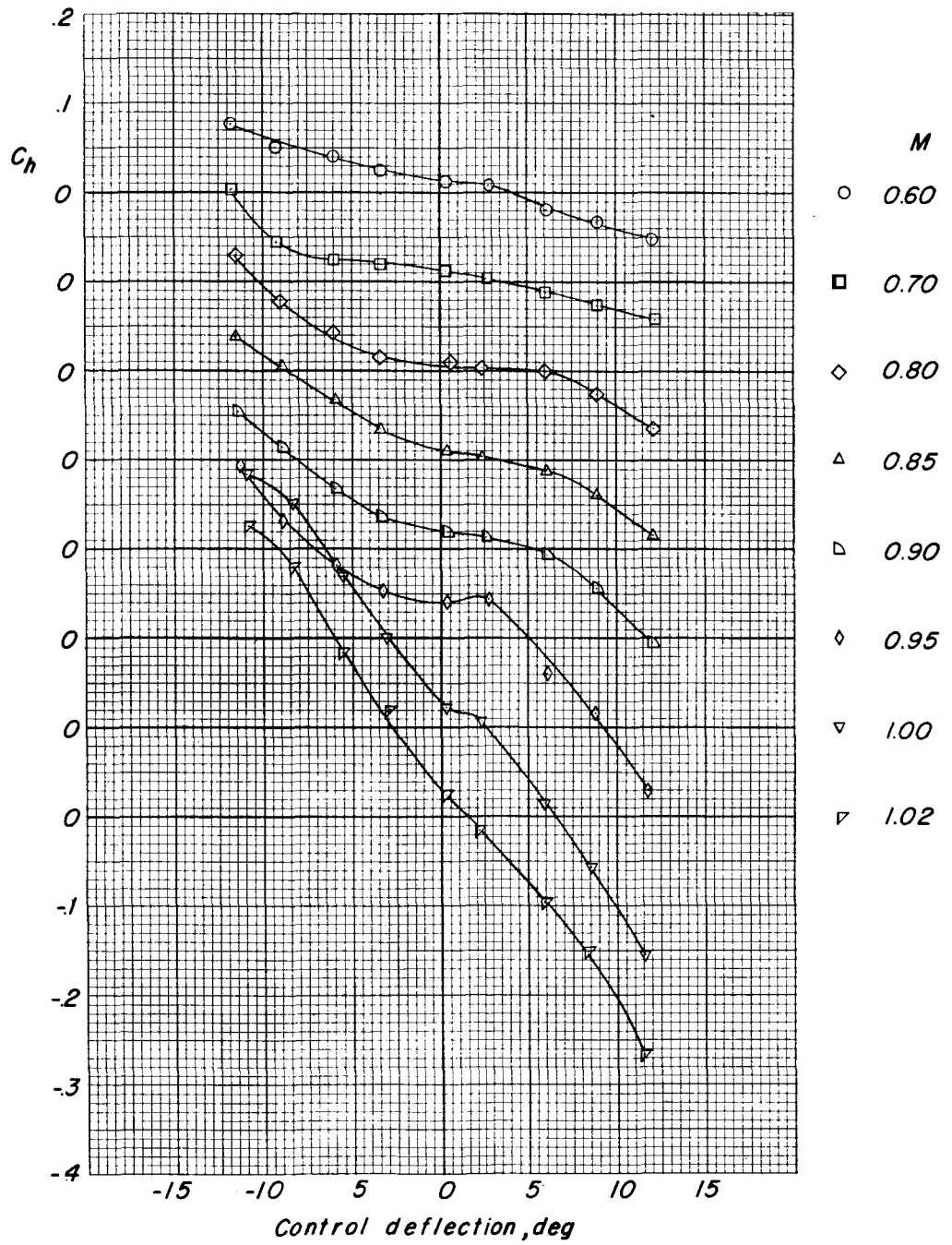

(c) t/c = 0.08.

Figure 13.- Concluded.

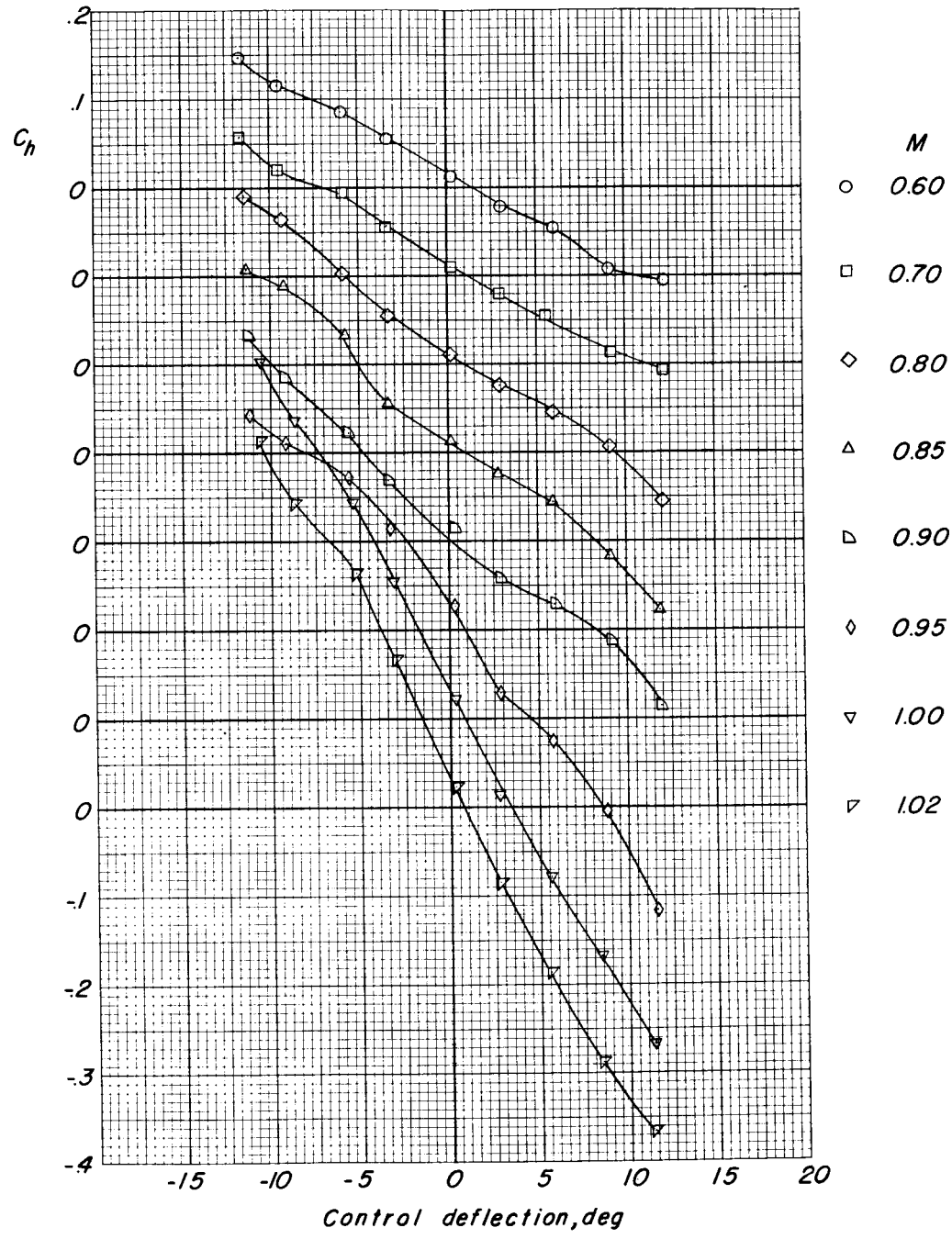

(a) $\phi = 5.25^{\circ}$.

Figure 14.- Variation of static hinge-moment coefficient with control deflection for t/c = 0.10 wing-control model at various Mach numbers.

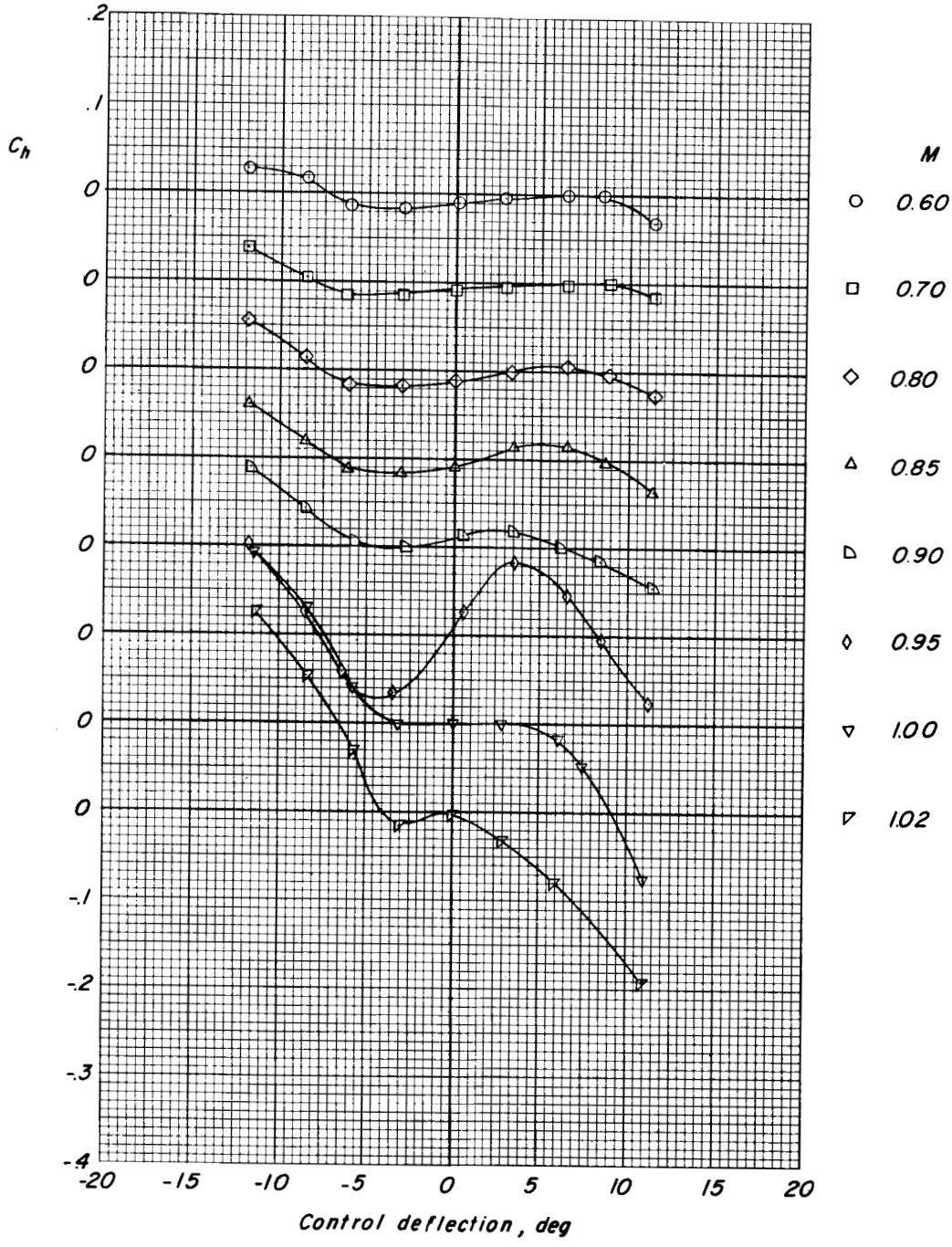

(b) $\phi = 19.75^{\circ}$.

Figure 14.- Concluded.

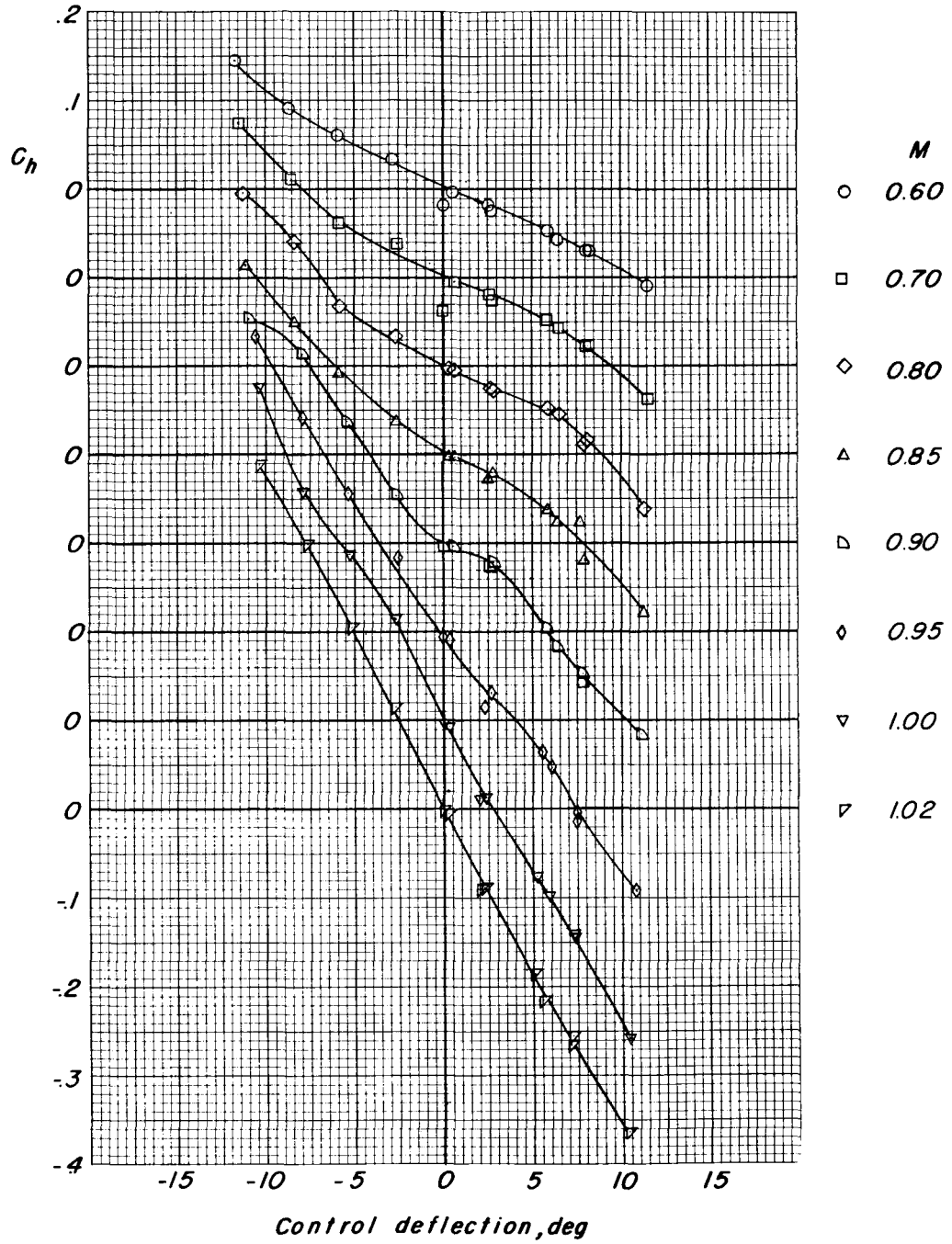

(a) $t/c = 0.06$; $t_s = 0.013$.

Figure 15.- Variation of static hinge-moment coefficients with control deflection for the splitter-plate-control models at various Mach numbers.

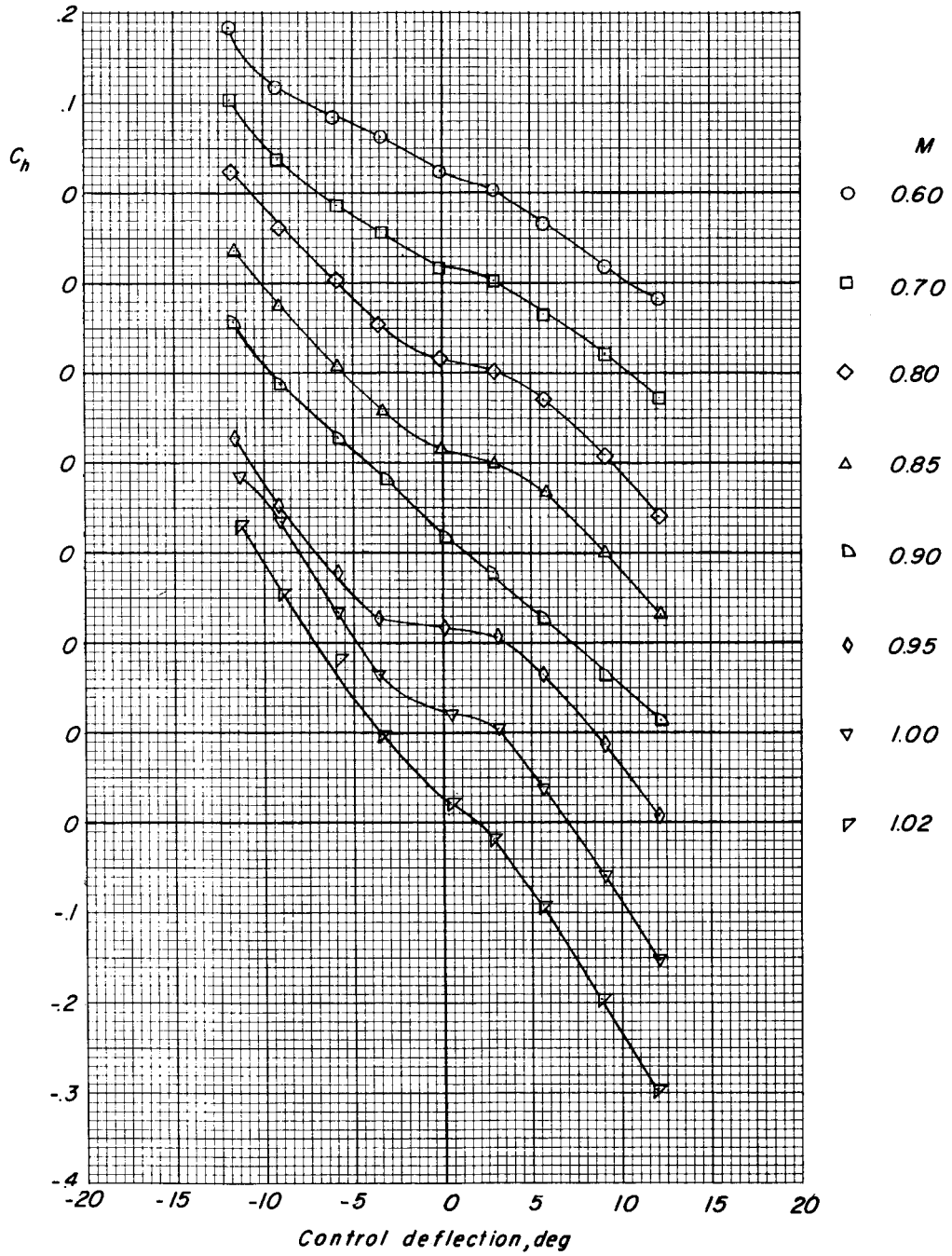

(b) $t/c = 0.10$; $t_s = 0.013$.

Figure 15.- Continued.

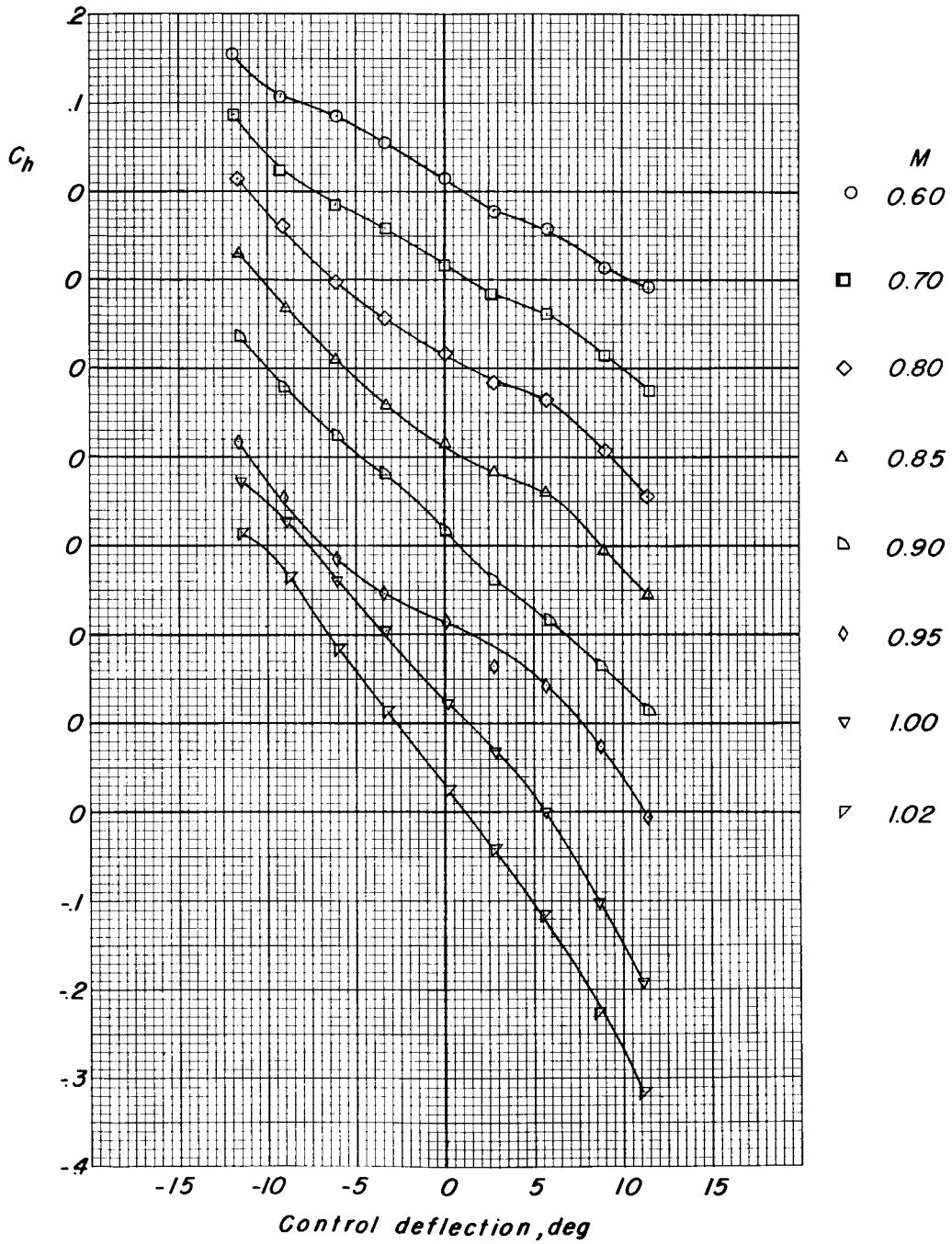

(c) $t/c = 0.10$; $t_s = 0.031$.

Figure 15.- Concluded.

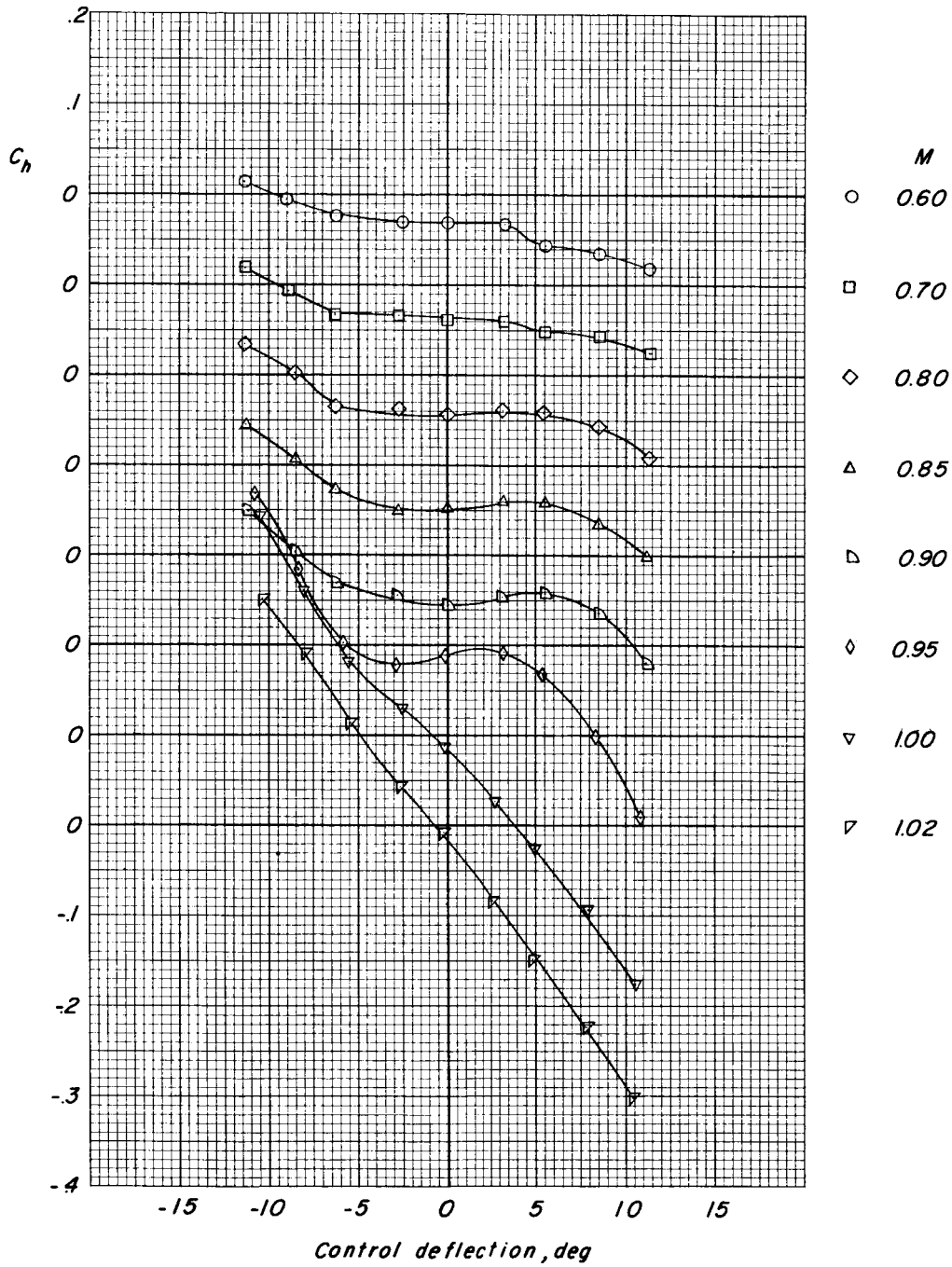

(a) Serrated-wedge control.

Figure 16.- Variation of static hinge-moment coefficients with control deflection for the wedge-control models at various Mach numbers.

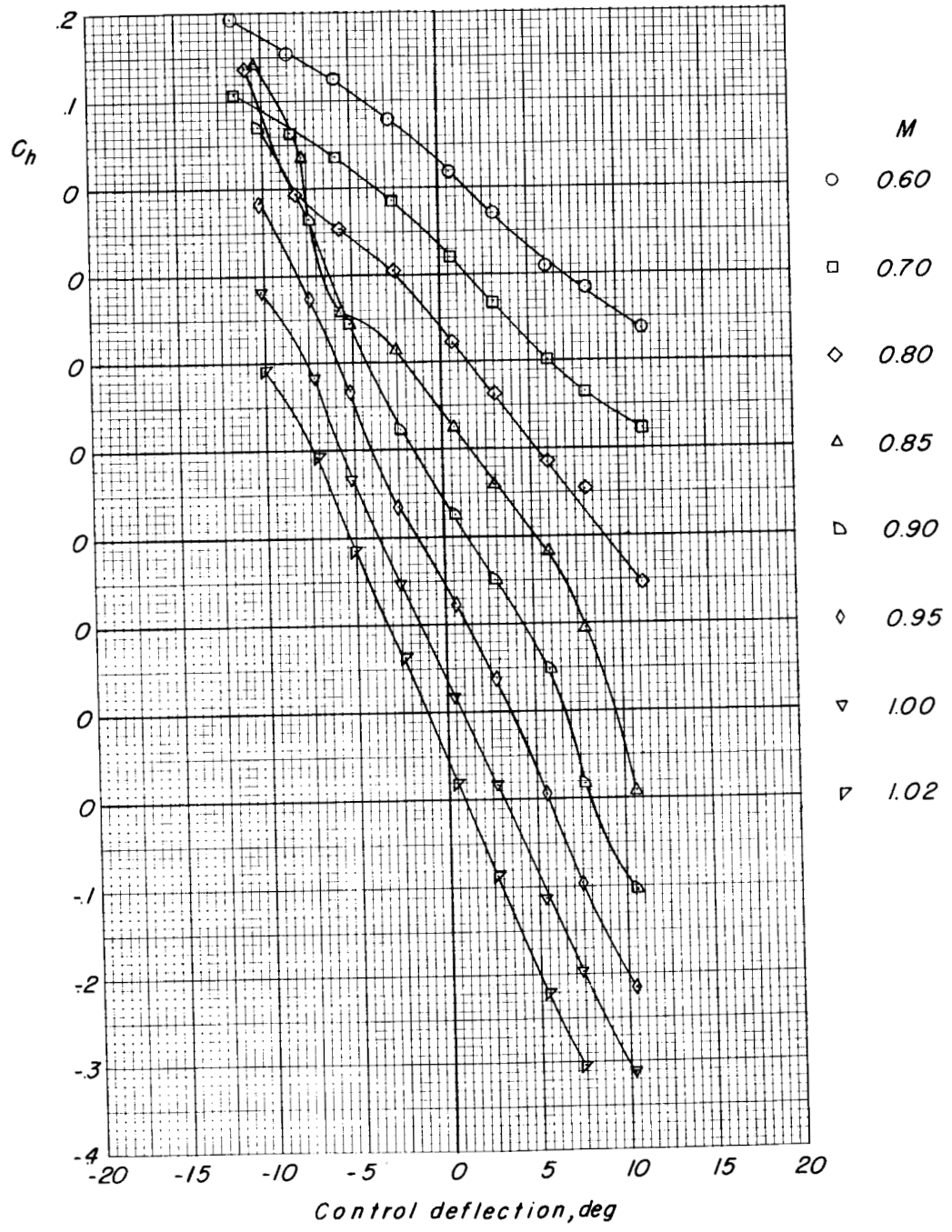

(b) Full-wedge control.

Figure 16.- Concluded.

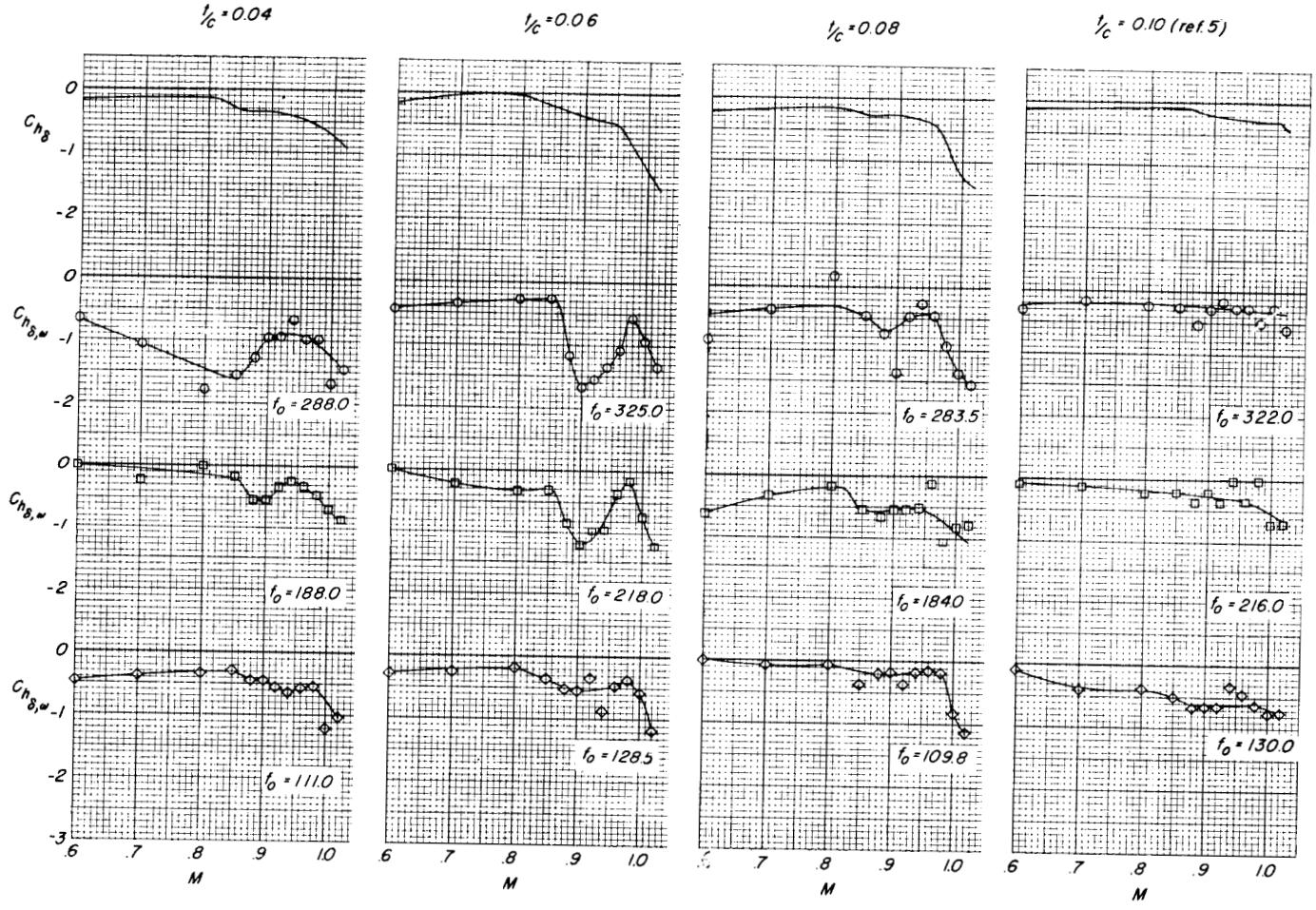

(a) Models with $\phi = 13.33^\circ$ control.

Figure 17.- Variation of C_{h_δ} and $C_{n_{\delta,\omega}}$ with Mach number.

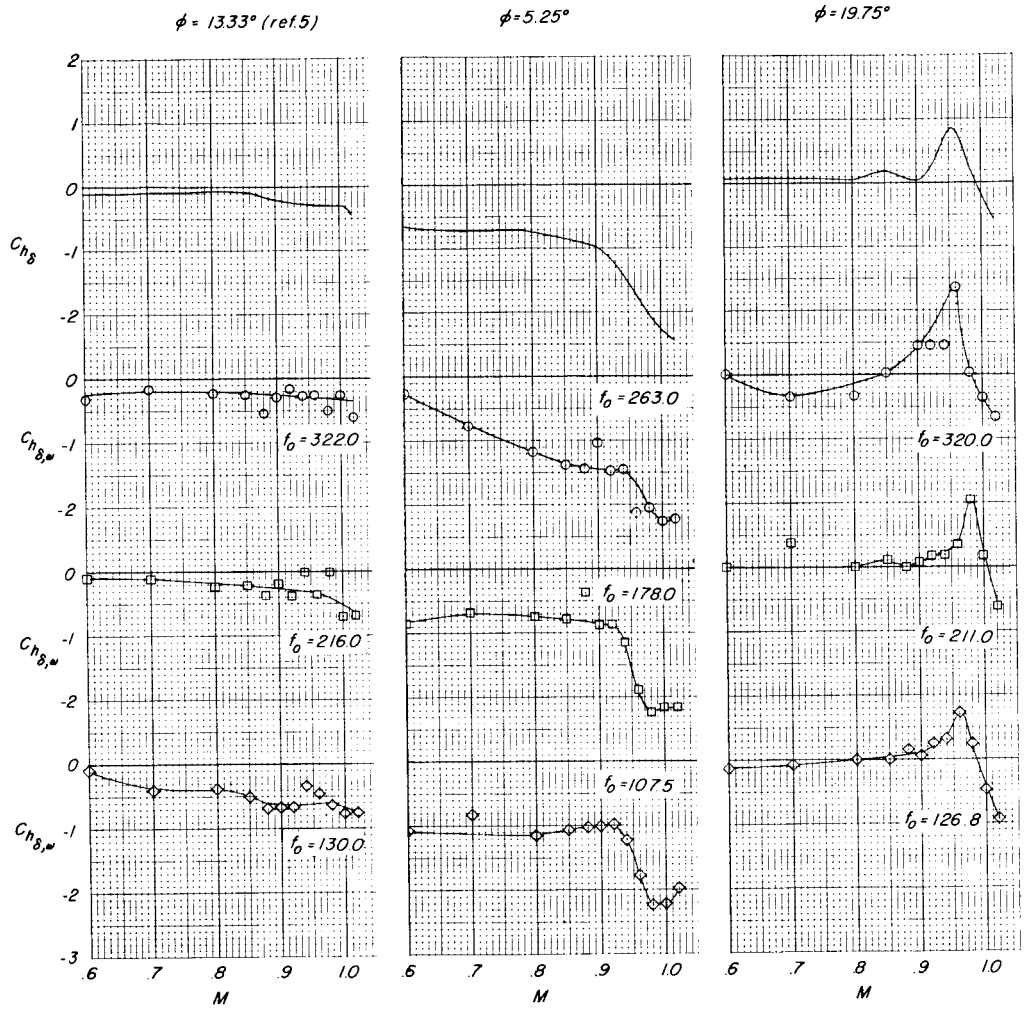

(b) Models with ϕ = 5.25° and ϕ = 19.75° control.

Figure 17.- Continued.

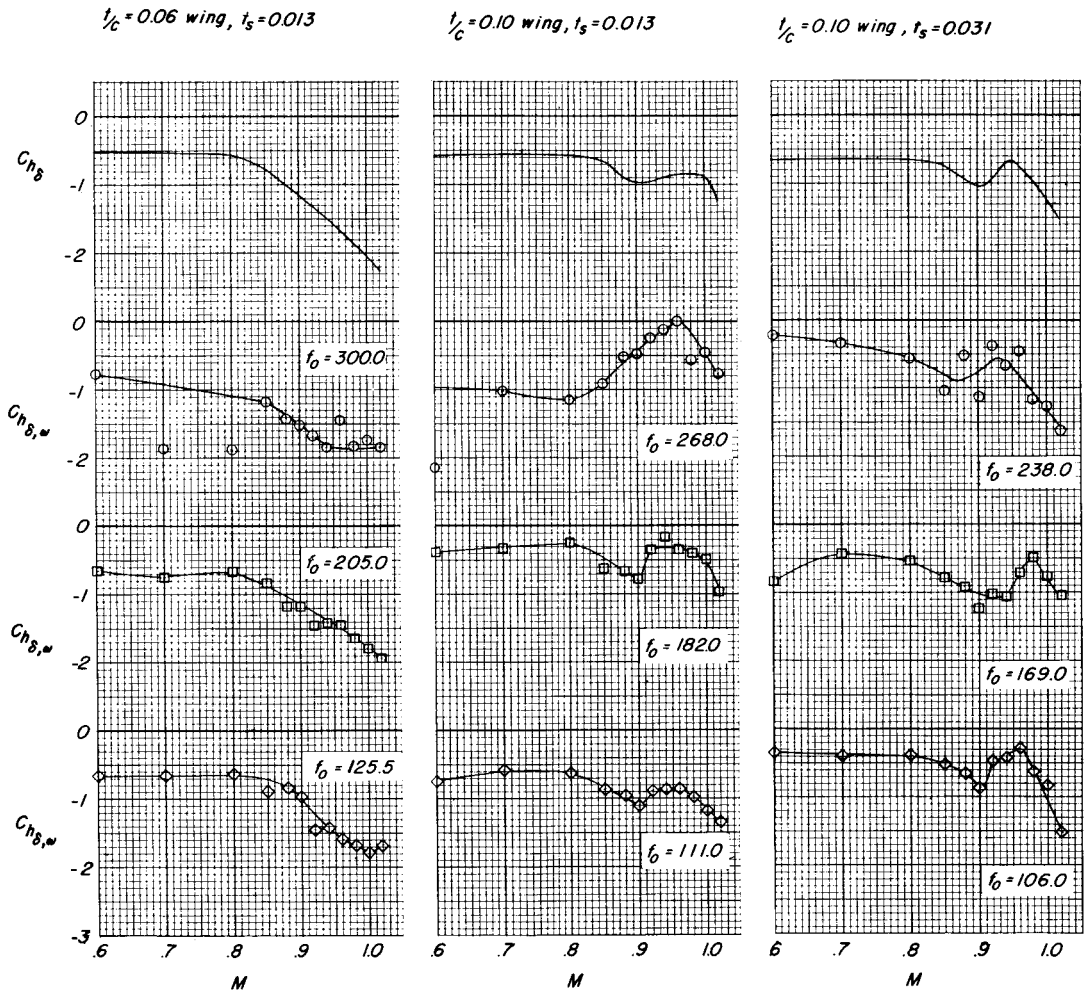

(c) Splitter-plate-control models.

Figure 17.- Continued.

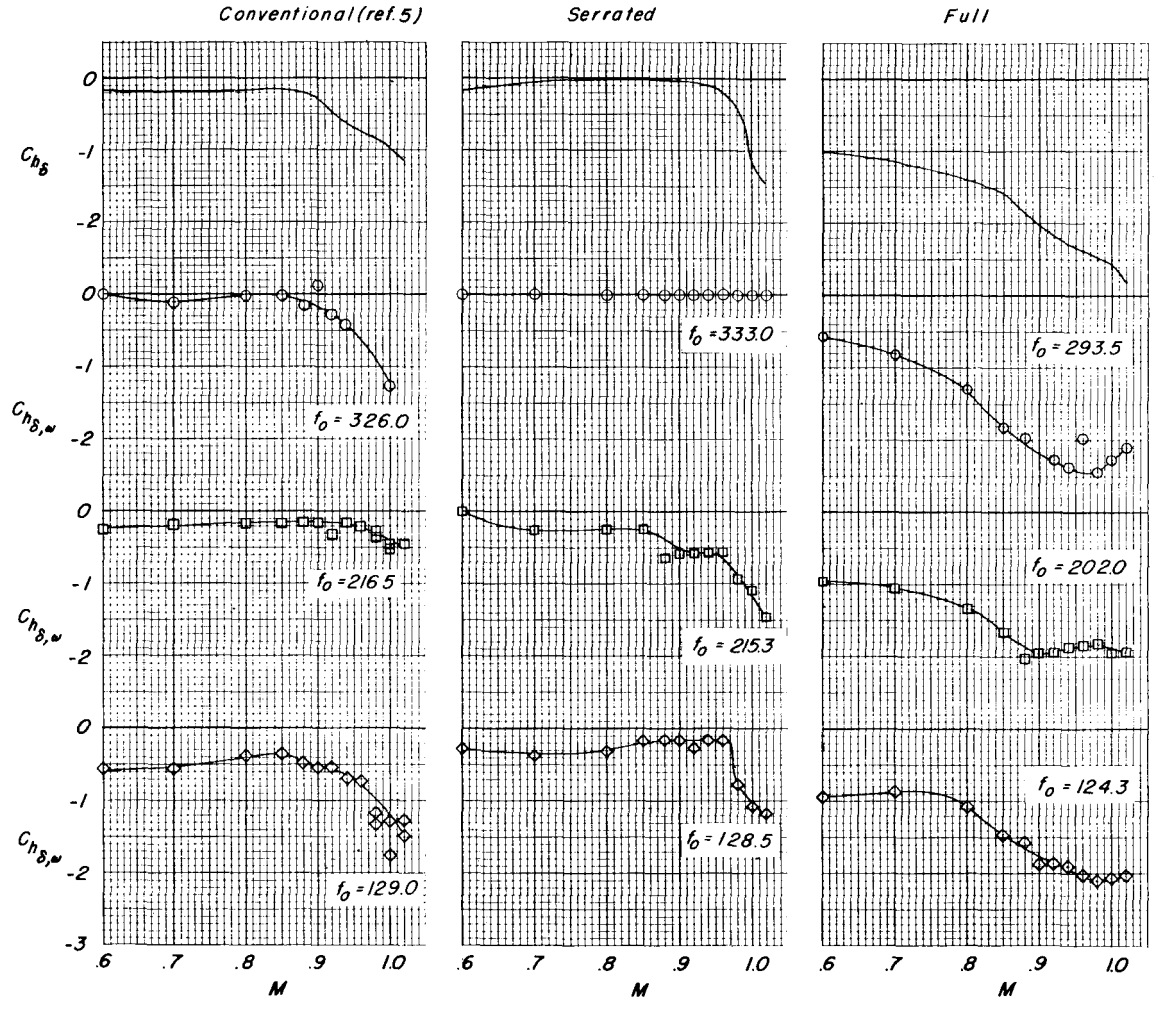

(d) Wedge-control models.

Figure 17.- Concluded.

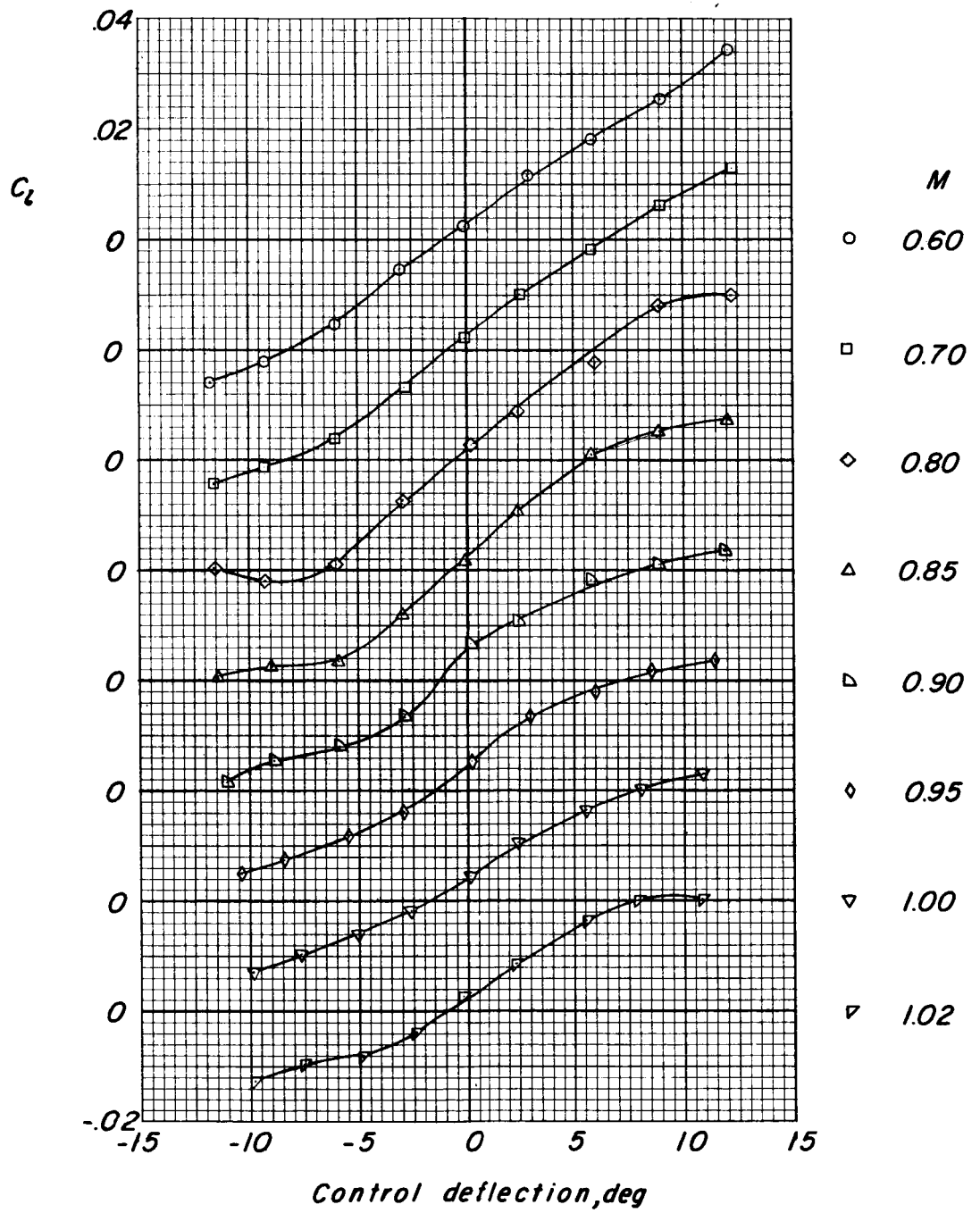

(a) t/c = 0.04.

Figure 18.- Variation of rolling-moment coefficient with control deflection for the models with $\phi = 13.33^{\circ}$ control at various Mach numbers. (Left-wing model.)

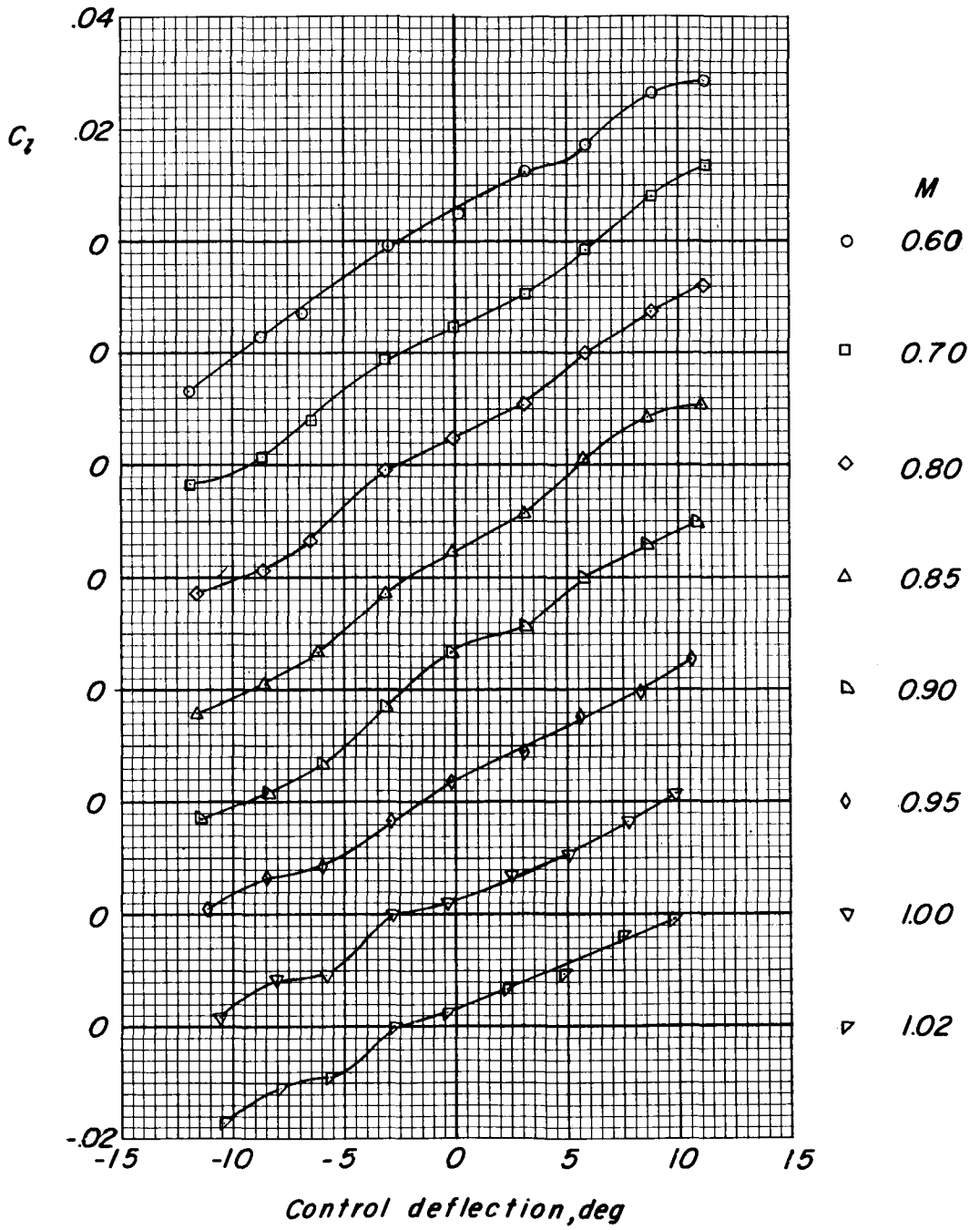

(b) t/c = 0.06.

Figure 18.- Continued.

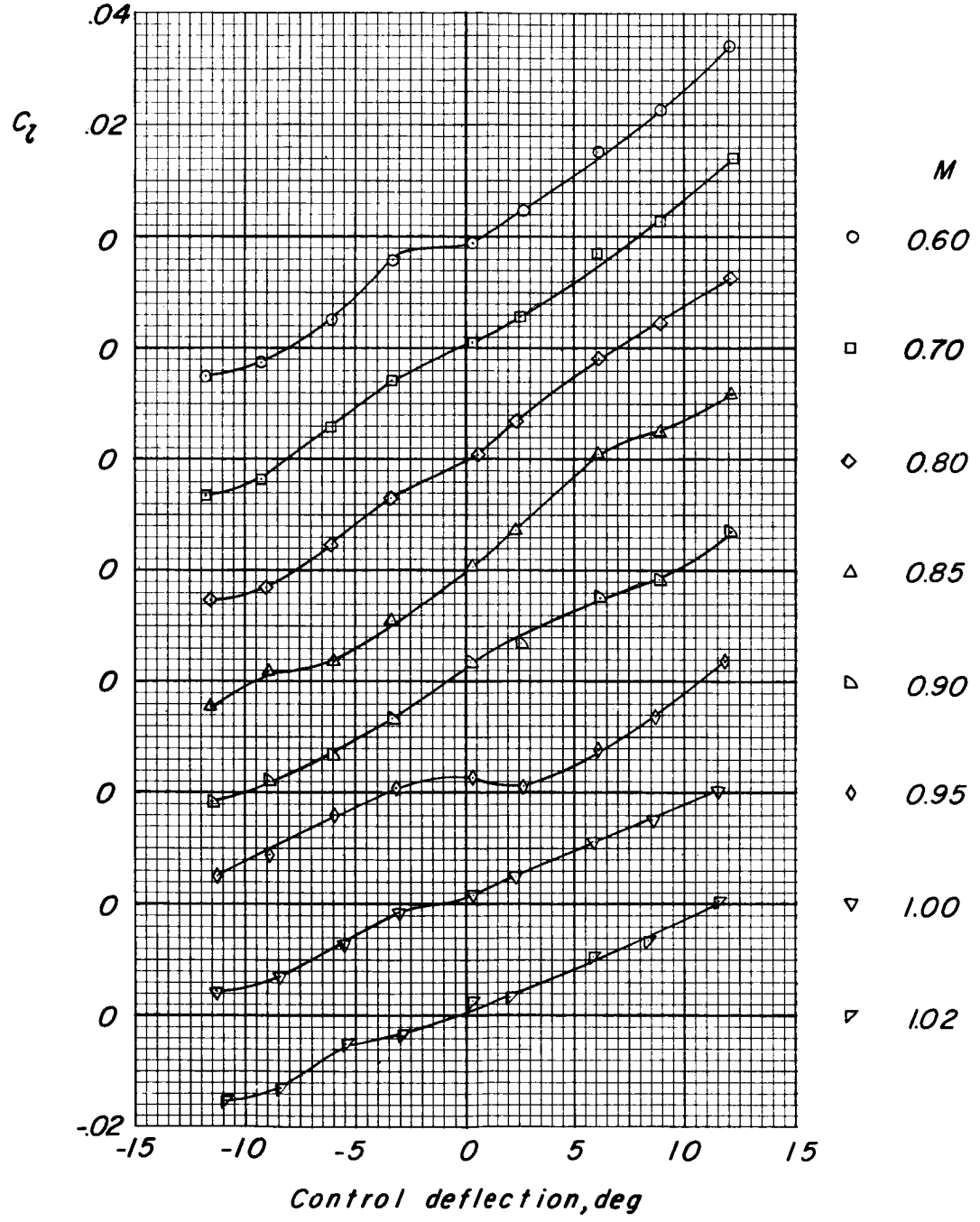

(c) t/c = 0.08.

Figure 18.- Concluded.

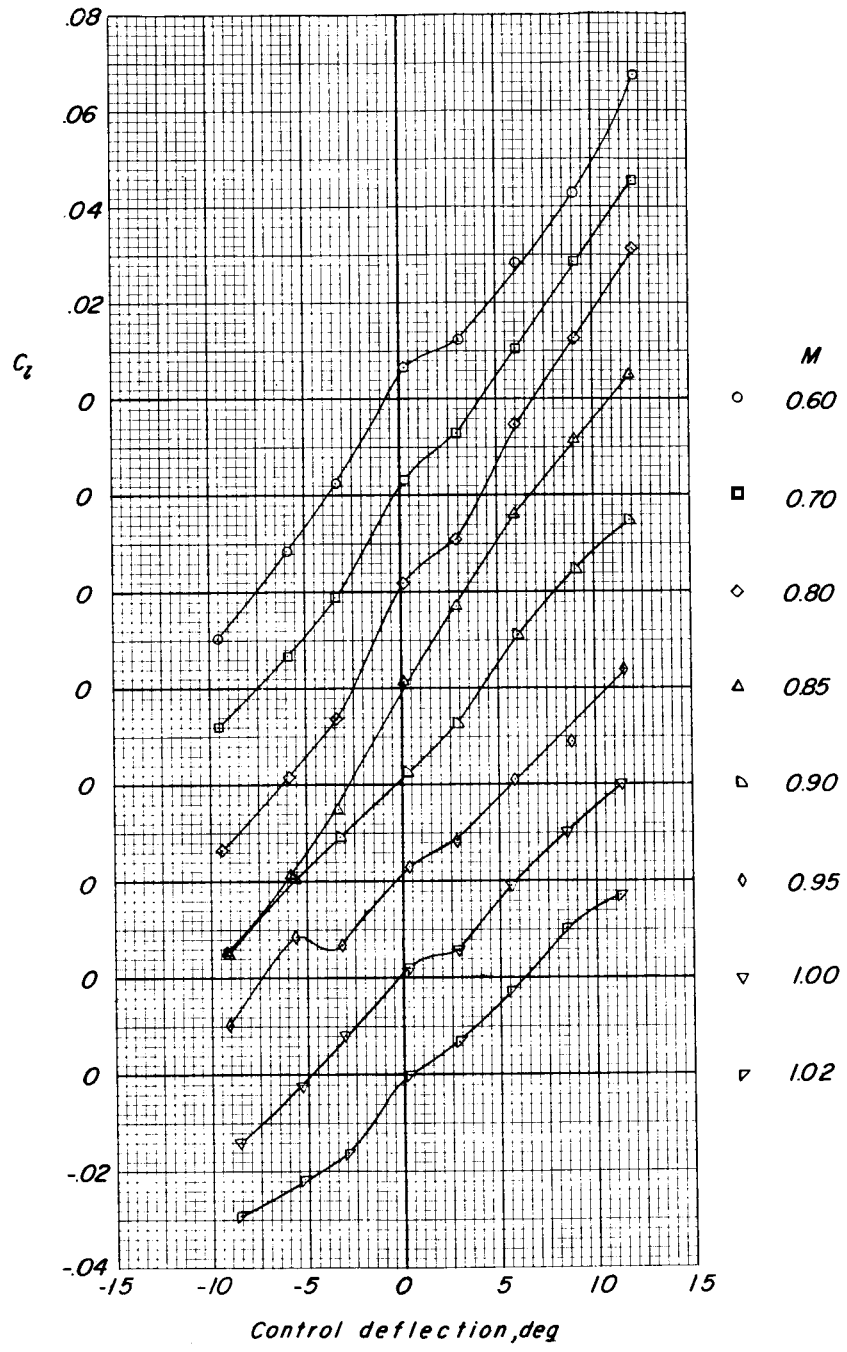

(a) $\phi = 5.25^{\circ}$ control.

Figure 19.- Variation of rolling-moment coefficient with control deflection for the t/c = 0.10 wing-control combinations at various Mach numbers.

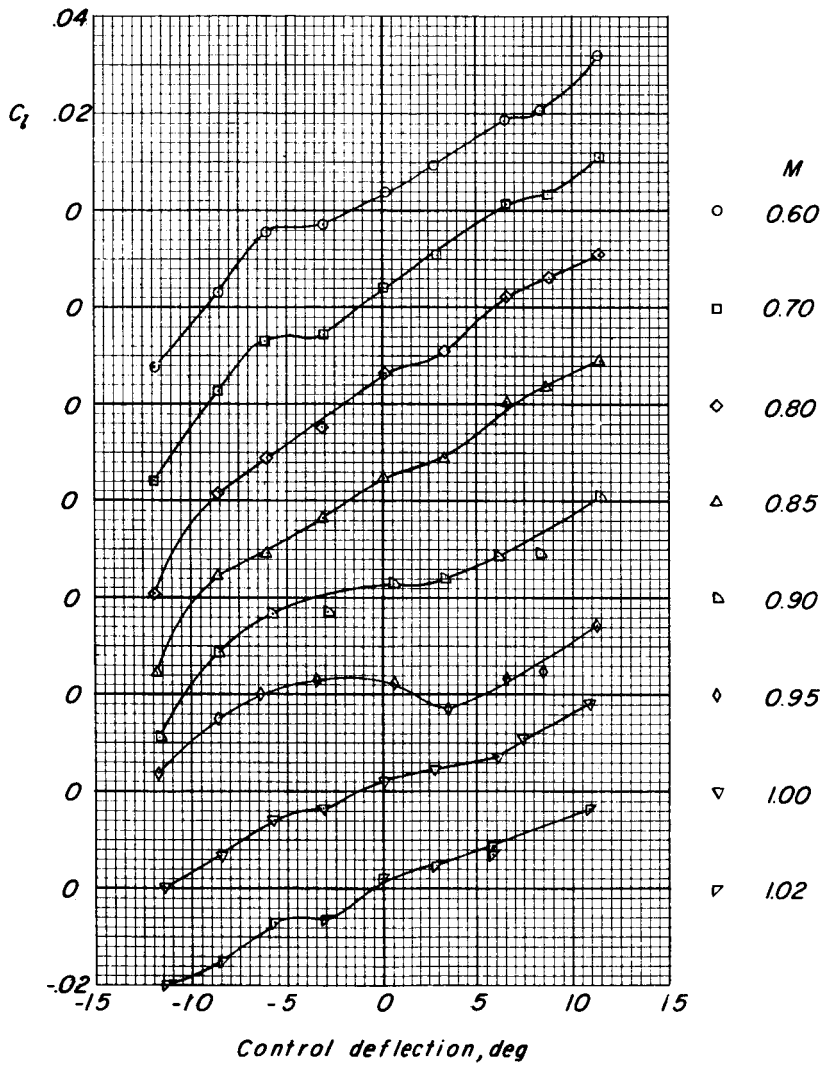

(b) $\phi = 19.75^{\circ}$ control.

Figure 19.- Concluded.

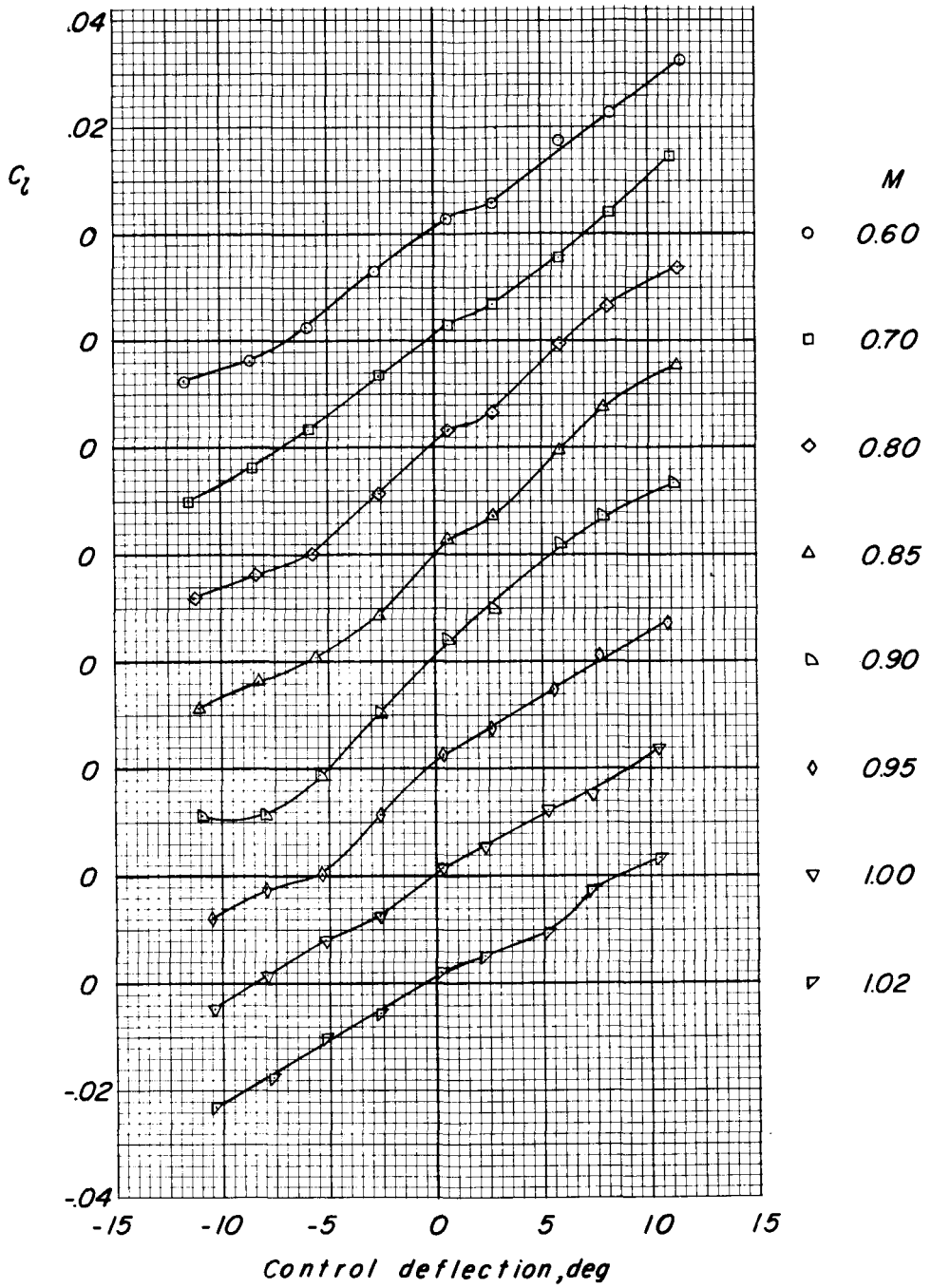

(a) $t/c = 0.06$; $t_s = 0.013$.

Figure 20.- Variation of rolling-moment coefficient with control deflection for the splitter-plate-control models at various Mach numbers.

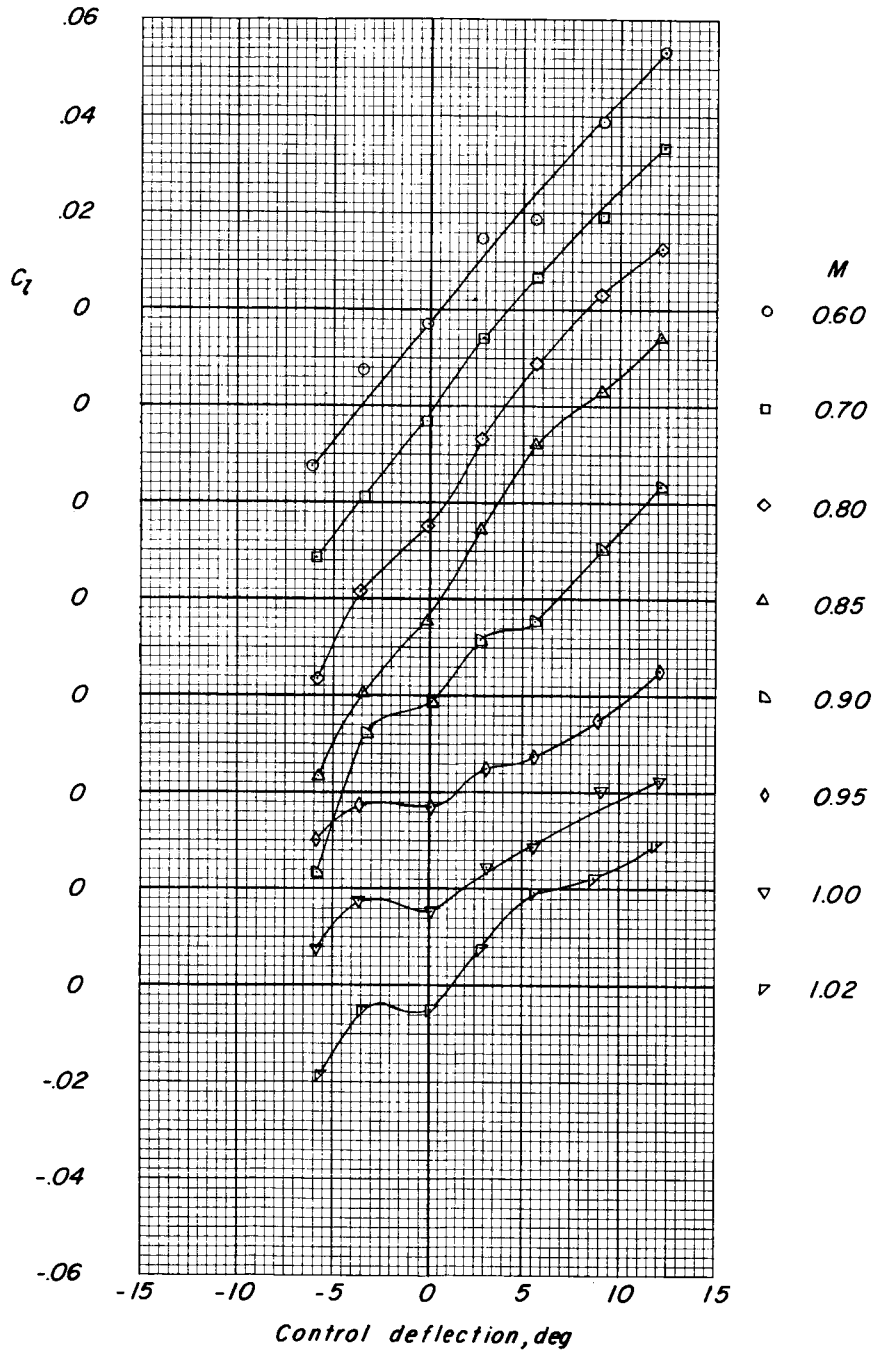

(b) $t/c = 0.10$; $t_s = 0.013$.

Figure 20.- Continued.

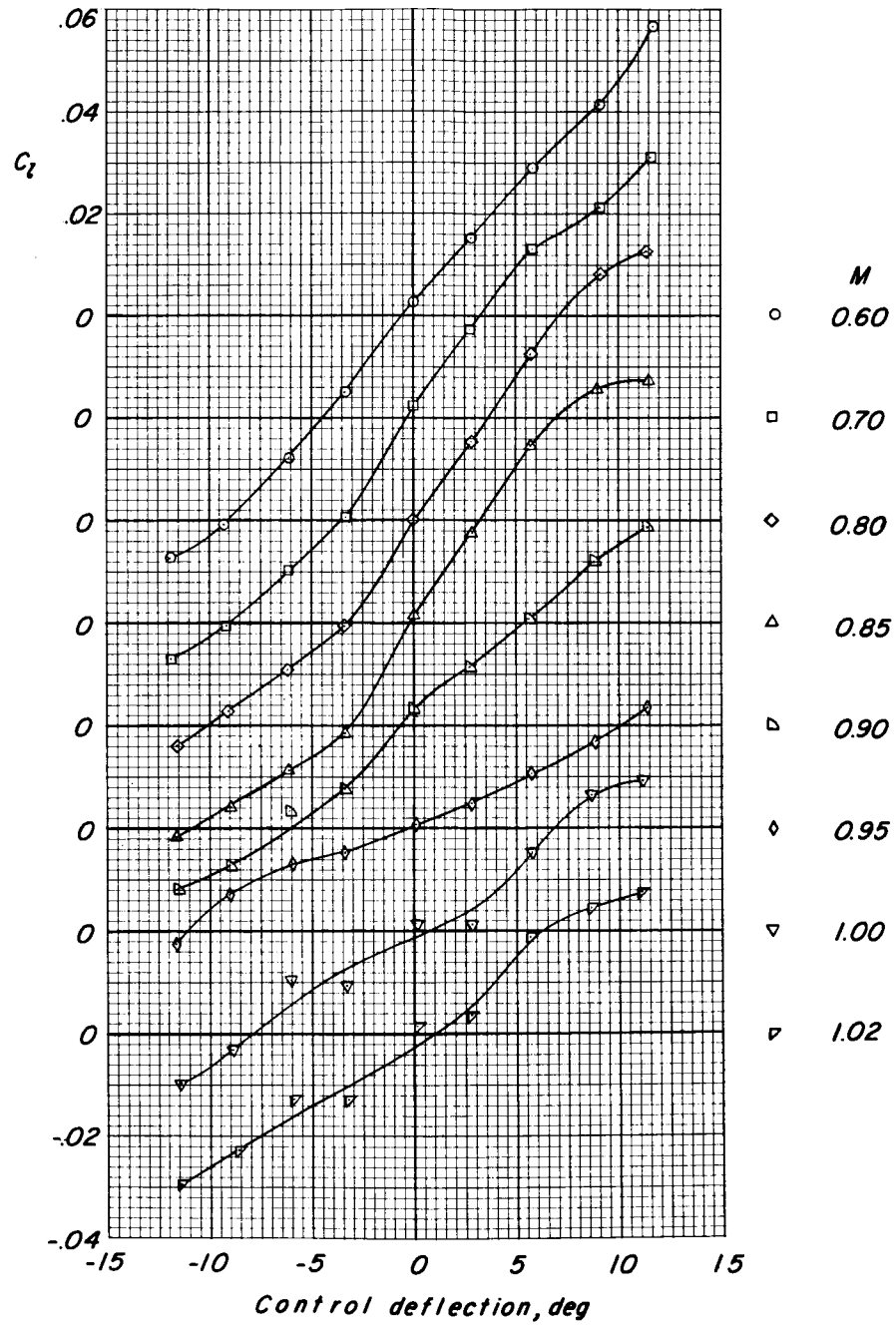

(c) $t/c = 0.10$; $t_s = 0.031$.

Figure 20.- Concluded.

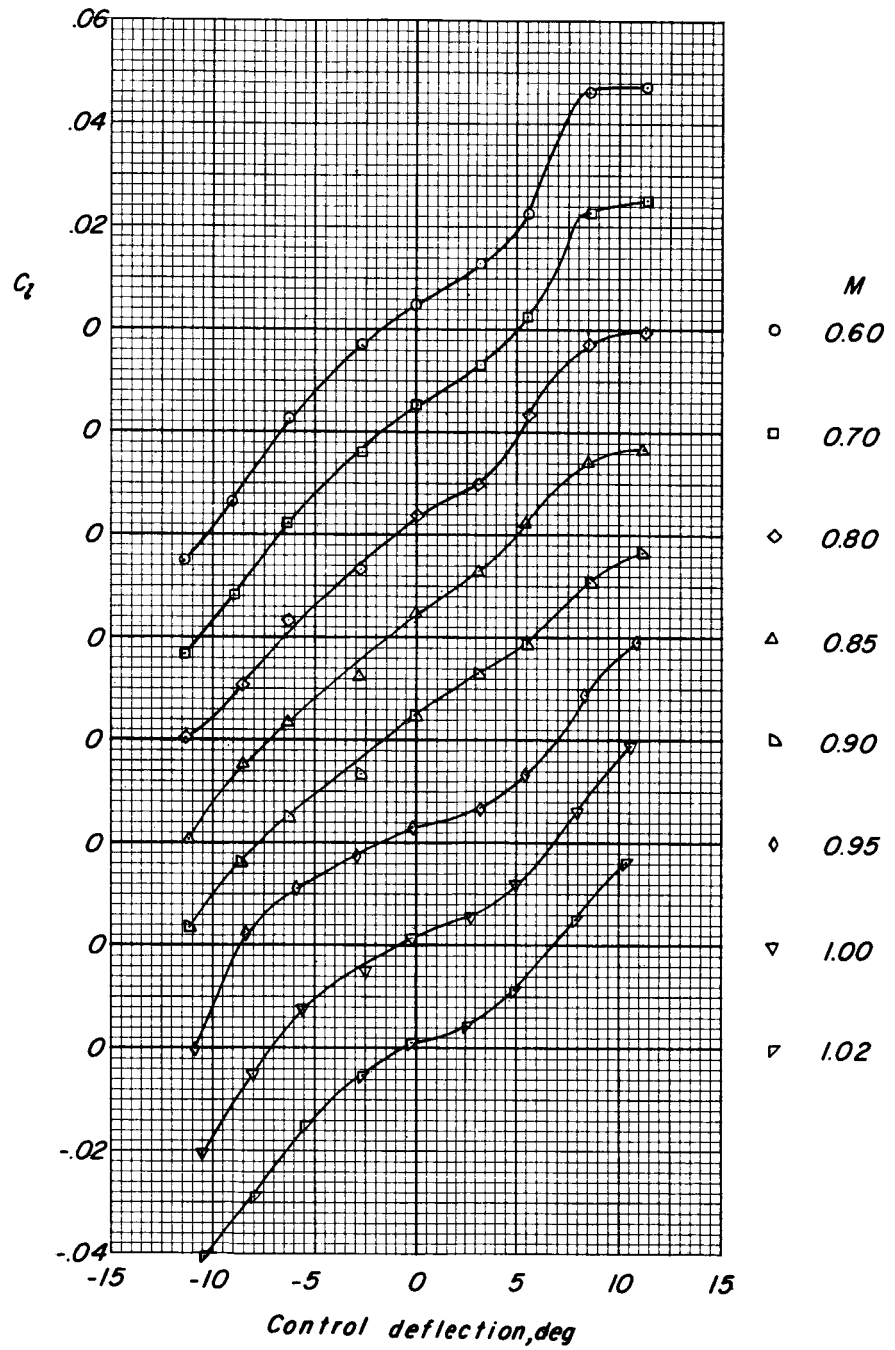

(a) Serrated-wedge control.

Figure 21.- Variation of rolling-moment coefficient with control deflection for the wedge-control models at various Mach numbers.

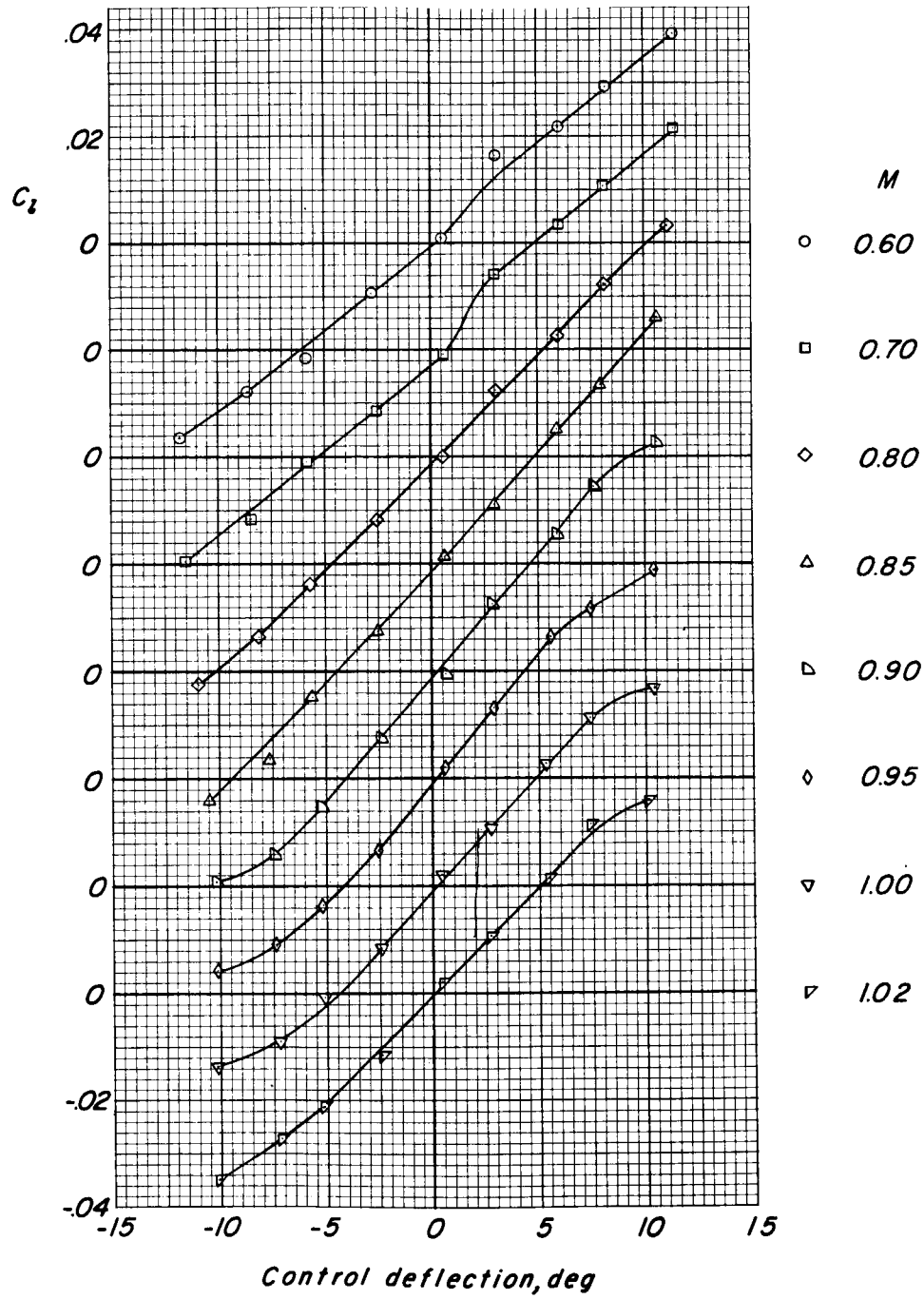

(b) Full-wedge control.

Figure 21.- Concluded.

L-579